Osteochondrale Läsionen am Talus: Anatomische, biomechanische und klinische Analyse

Inauguraldissertation

zur

Erlangung der Würde eines Doktors der Philosophie

vorgelegt der

Medizinischen Fakultät

der Universität Basel

von

André Georges Leumann

aus Erlen, Kanton Thurgau

Basel, 2014

Genehmigt von der Medizinischen Fakultät
auf Antrag von:

Professor Dr. med. Dr. phil. Victor Valderrabano, Basel (Supervisor)
Professor Dr. med. Magdalena Müller-Gerbl, Basel (Co-Supervisorin)
Professor Dr. med. Stefan Nehrer, Krems (Österreich) (externer Gutachter)
Professor Dr. sci. nat. Jess G. Snedeker, Zürich (externer Gutachter)

Basel, den 8. Januar 2014

Prof. Dr. Christoph Beglinger
Dekan, Universität Basel

Inhaltsverzeichnis

1	**Abstracts**		4
2	**Einleitung**		
	2.1	Osteochondrale Läsionen vom Talus	8
	2.2	„The joint as an Organ“-Konzept	15
3	**Originalartikel**		21
	3.1	Mineral density and penetration strength of the subchondral bone plate of the talar dome: high correlation and specific distribution patterns	22
	3.2	A novel imaging method for osteochondral lesions of the talus - comparison of SPECT-CT with MRI	42
	3.3	Radiographic Evaluation of Frontal Talar Edge Configuration for Osteochondral Plug Transplantation	50
	3.4	Altered cell metabolism in tissues of the knee joint in a rabbit model of Botulinum toxin A-induced quadriceps muscle weakness	56
4	**Zusammenfassung und Ausblick**		63
5	**Literaturverzeichnis**		67
6	**Danksagung**		71
7	**Schriftliche Erklärung der eigenständigen Arbeit**		72
8	**Anhang**		73
	8.1	Auszeichnungen	73
	8.2	Verzeichnis zusätzlicher Originalarbeiten	73
	8.3	Übersichtsarbeiten und Buchkapitel	75

1 Abstracts

Als Resultat dieser PhD-Arbeit sind vier Originalarbeiten entstanden. Sie adressieren jeweils eine einzelne Fragestellung.

(I) Mineral density and penetration strength of the subchondral bone plate of the talar dome: high correlation and specific distribution patterns
Leumann A, Valderrabano V, Hoechel S, Goepfert B, Mueller-Gerbl M
J Foot Ankle Surg, Revision submitted July 22, 2013

Objective. The subchondral bone plate plays an important role in stabilizing the osteochondral joint unit and in the pathomechanism of osteochondral lesions and osteoarthritis. The objective of the study was to measure (I) mineral density distribution and (II) subchondral bone plate penetration strength of the talar dome joint facet in order to display and compare specific distribution patterns. Design: Ten cadaver specimen were used for CT-scans wherefrom densitograms were derived by means of CT-osteoabsorptiometry (CT-OAM), and for mechanical indentation testing wherefrom penetration strenght was obtained. Findings: Two different distribution patterns were found for mineral density and penetration strenght. 6 out of 10 specimens (60%) showed bicentric maxima (anteromedially and anterolaterally), while the other 4 specimens (40%) showed a monocentric maximum (either anteromedially or anterolaterally). Highly significant correlation ($p<0.0001$) of both methods confirmed that mineral density relied on local load characteristics. Conclusion: Biomechanical properties of the subchondral bone plate of the talar dome joint facet showed specific distribution patterns. CT-OAM has shown to be a reliable method to display mineral density distribution non-invasively. We recommend CT-OAM for non-invasive analysis of biomechanical properties of the subchondral bone plate in osteochondral joint reconstruction, as well as in prevention and treatment of osteoarthritis and osteochonral lesions.

(II) A novel imaging method for osteochondral lesions of the talus - comparison of SPECT-CT with MRI

Leumann A, Valderrabano V, Plaass C, Rasch H, Studler U, Hintermann B, Pagenstert GI.

American Journal of Sports Medicine, 2011;39: 1095-1101.

** Dirk Schäfer Forschungspreis 2012 des Departements Chirurgie, Universitätsspital Basel*

Background: Magnetic resonance imaging (MRI) is the current standard in noninvasive diagnostics of osteochondral lesions (OCLs) of the talus. Single-photon emission computed tomography-computed tomography (SPECT-CT) is a new technique that displays different imaging qualities. The influence of the aforementioned diagnostic information on treatment decision making in talar OCLs is not known. Purpose: Thea im of the study was to evaluate SPECT-CT in comparison with MRI for image interpretation and decision making in OCLs of the talus. Study design: Case series; level of evidence, 4. Methods. Magnetic resonance imaging and SPECT-CT of 25 patients (average age, 32 years; range 18-69 years) were analyzed by 3 independent orthopaedic surgeons blinded to the study. Raters had to analyze images for predefined criteria of cartilage, subchondral bone plate, and subchondral bone, including bone marrow edema on MRI and scintigraphic activity on SPECT-CT. For MRI alone, SPECT-CT alone, and their combination, the treatment decision had to be defined. Results: In comparison with MRI alone, treatment decision making changed in 48% of the cases with SPECT-CT alone and 52% with SPECT-CT and MRI combined. While cartilage showed good correlation for interpretation between MRI and SPECT-CT, the subchondral bone plate and subchondral bone showed substantial differences. Poor intrarater correlation highlighted the different information provided by the 2 imaging techniques. Poor interrater correlation showed a high heterogeneity in the treatment decision making of OCLs. Conclusion: Compared with MRI, SPECT-CT provides additional information and influences the decision making of OCL treatment. For thorough diagnostic evaluation in OCLs, performing both MRI and SPECT-CT is recommended. Further clinical investigation is needed to see if SPECT-CT in addition to MRI results in improved treatment outcomes.

(III) Radiographic Evaluation of Frontal Talar Edge Configuration for Osteochondral Plug Transplantation

Leumann A, Wiewiorski M, Egelhof T, Rasch H, Magerkurth O, Candrian C, Schaefer DJ, Martin I, Jakob M, Valderrabano V

Clinical Anatomy; 2009;22:261-266.

** 3. Posterpreis, GOTS Jahreskongress 2008*

For successful reconstruction of osteochondral lesions of the talus, the anatomic configuration of the talar edge must be respected. This study evaluated the radiographic configuration of the talar edge in the anterior-posterior (AP) view by analyzing medial and lateral edge angles and radii in 81 patients with a true AP view and without ankle pathology. The mean lateral talar edge angle was 91.8°, and the mean medial talar edge angle was 110.0°. The medial frontal talar edge radius was 4.8mm and the lateral 3.5 mm, respectively. No correlation between angle and radius was found. These results revealed a significant difference between the medial and lateral talar edge configuration. This may be due to the three-dimensional function of the human ankle joint. No study so far has addresssed these differences radiologically. These differences should be addressed in the reconstruction of osteochondral lesions and be included in the preoperative planning.

(IV) Altered cell metabolism in tissues of the knee joint in a rabbit model of Botulinum toxin A-induced quadriceps muscle weakness

Leumann A, Longino D, Fortuna R, Leonard T, Vaz MA, Hart DA, Herzog W

Scandinavian Journal of Medicine and Science in Sport, 2012;22:776-782.

** Preis für die beste wissenschaftliche Arbeit am SGSM-Jahreskongress 2009.*

Background: Quadriceps muscle weakness is frequently associated with knee injuries in sports. The influence of quadriceps weakness on knee joint homeostasis remains undefined. We hypothesized that quadriceps weakness will lead to tissue-specific alterations in cell metabolism of tissues of the knee. Methods: Quadriceps weakness was induced with repetitive injections of Botulinum toxin A in six one-year old NZW rabbits for six months. Five additional animals served as controls with injections of saline/dextrose. Muscle weakness was assessed by muscle wet mass, isometric knee extensor torque, and histological morphology analysis. Cell metabolism was assessed for patellar tendon, medial and lateral collateral ligament, and medial and lateral meniscus by measuring total RNA levels and specific mRNA levels for Collagen I/III, MMP-1/-3/-13, TGF-β, Biglycan, IL-1, and bFGF by RT-PCR. Results: While total RNA levels did not change, tissue-specific mRNA levels were lower for relevant anabolic and catabolic molecules indicating potential changes in tissue mechanical set points. Conclusion: Quadriceps weakness may lead to adaptations in knee joint tissue cell metabolism by altering a subset of anabolic and catabolic mRNA levels corresponding to a new functional and metabolic set-point for the knee which may contribute to the high injury rate of athletes with muscle weakness

2 Einleitung

2.1 Osteochondrale Läsionen des Talus

Osteochondrale Läsionen (OCL) des Talus sind Verletzungen, welche die funktionelle Einheit von Knochen („osteo“) und Knorpel („chondral“) betreffen (Abb. 1). In weiterführender Konsequenz stellen Sie ein Musterbespiel einer Verletzung dar, welche das gesamte Gelenk betrifft. Die Zusammenhänge werden durch das „Joint as an Organ“ Konzept beschrieben.

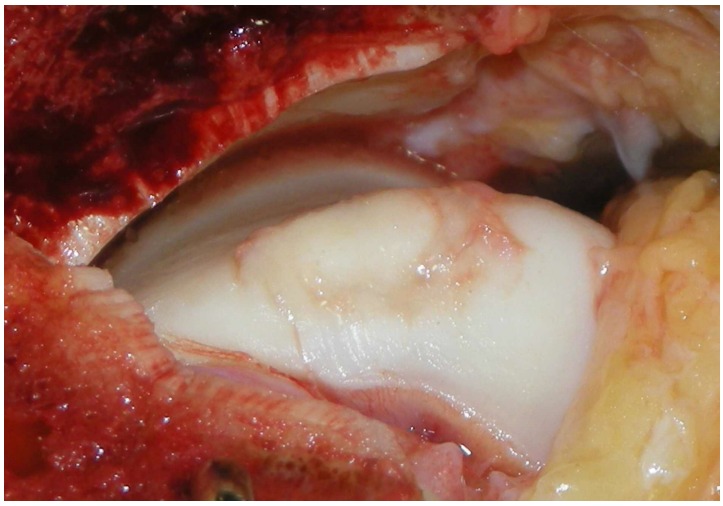

Abbildung 1: Osteochondrale Läsion an der medialen Talusrollen. Intraoperativer Situs mit Zugang über eine Innenknöchelosteotomie.

Osteochondrale Läsionen am Talus betreffen in der Regel junge, sportlich sehr aktive Patienten im Alter von 20 bis 40 Jahren (Verhagen et al., 2003). Sie beklagen Schmerzen, Schwellungszustände und Blockaden des Gelenks. Sehr oft liegt eine traumatische Ursache als Folge einer OSG-Distorsion vor. Am häufigsten liegen diese medial (62%) oder lateral (34%) an der Taluskante (Elias et al., 2006).

Das oberen Sprunggelenk ist gemäss Literatur das am dritthäufigsten betroffene Gelenk nach Kniegelenk und Ellenbogengelenk. Genaue Inzidenzwerte sind jedoch nicht bekannt. Verhagen et al. (2005) berichten, dass bis zu 6,5% aller akuter OSG-Distorsionen zu einer akuten osteochondralen Läsion führen. Wenn man betrachtet, dass die akute OGS-Distorsion die häufigste Verletzung in der Sportorthopädie überhaupt ist, so wäre von einer hohen Rate an osteochondralen Verletzungen auszugehen. Dies entspricht weder der langjährigen Erfahrung noch den bekannten epidemiologischen Daten. So ist von einer hohen Rate an akuten Verletzungen auszugehen, welche jedoch abheilen, bevor sie je als

symptomatisch wurden. Es ist weitgehend unklar, welche pathomechanistischen Ursachen zu einer besseren Abheilung oder bei unvorteilhaftem Verlauf zu einer Chronifizierung und damit Symptomatik des Patienten führen können.

Die anatomische Grundlage der osteochondralen Läsion ist in Abbildung 2 dargestellt: die osteochondrale Einheit, der Verbund von hyalinem Gelenkknorpel, dem darunterliegenden subchondralen Knochen und den verknüpfenden Strukturen (Madry et al., 2010). Dabei kommt der subchondralen Platte eine Schlüsselfunktion zu. Sie verbindet den Knorpel mit dem darunterliegenden subchondralen Knochen und ist damit für den Krafttransfer vom Gelenk auf den Knochen zuständig. Die subchondrale Platte hat jedoch auch nutritive und regulative Funktionen, da der Knorpel bis zur Tidemark über Diffusion von Gefässen aus dem subchondralen Knochen versorgt wird (Pan et al., 2009). Der Knorpel ist in verschiedene nicht-kalzifizierte und eine kalzifizierte Schicht gegliedert. Dass die Knorpeldicke des Talus nicht über die gesamte Gelenksoberfläche symmetrisch und identisch verteilt ist, konnten Millington et al. (2007) zeigen. In Arbeit 1 der vorliegenden Dissertation wurde die biomechanische Funktion und die Mineralisationsdichteverteilung der subchondralen Platte untersucht. Dabei konnte gezeigt werden, dass es typische Verteilungsmuster gibt. Diese ergeben ein Abbild der lokalen biomechanischen Langzeitbelastung. Interessanterweise finden sich die höchsten Dichtemaxima (und damit stabilsten Zonen) in den Bereichen, in denen auch der Knorpel am dicksten ist – und in denen osteochondrale Läsionen am häufigsten gefunden werden (siehe Kapitel 3.1).

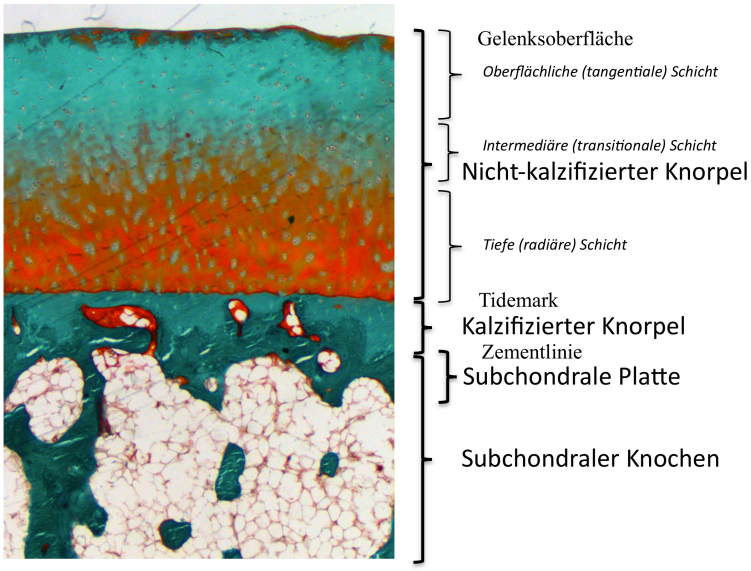

Abbildung 2: Die osteochondrale Einheit am Talus. Humanes Präparat, Goldnerfärbung. Im Rahmen der Dissertation im Labor von Frau Prof. Müller-Gerbl hergestellt.

In der Diagnostik muss auf nicht-invasive Bildgebungsmethoden der Radiologie oder auf die invasive Diagnostik der OSG-Arthroskopie zurückgegriffen werden. Radiologisch steht an erster Stelle das konventionelle Röntgenbild. Dieses kann jedoch nicht alle Formen der OCL zur Darstellung bringen. Weitere, und genauere Aufklärung bringen hier das MRI, das Arthro-CT oder das SPECT-CT (Verhagen et al., 2005; Leumann et al., 2011b). Währenddem das MRI entsprechende Begleitverletzungen (z.B. der Ligamente, der Muskeln oder der Sehnen) zeigen kann, wird allgemein angenommen, dass die osteochondrale Läsion im MRI von der Grösse her eher überschätzt wird (Abb. 3). Deshalb wurde früher das Arthro-CT als zusätzliche Diagnostik verwendet. In Arbeit 2 der vorliegenden Dissertation haben wir die Relevanz des neuen diagnostischen Verfahrens des SPECT-CTs auf die Therapiewahl bei OCL am Talus untersucht (Abb. 4). Das SPECT-CT ist ein digitales Fusionsprinzip, das zwei unterschiedliche Bildgebungen überlagert. Damit ist es möglich, die biologischen Informationen der Osteoblastenaktivität, welche durch die Szintigraphie angezeigt wird, auf der Basis einer Computertomographie (CT) anatomisch exakt einer morphologischen Struktur zuzuordnen.

Hierbei hat sich gezeigt, dass auch durch erfahrene Fusschirurgen eine Änderung der Therapiewahl in 52% vorgenommen wurde, wenn das SPECT-CT als zusätzliches Diagnostikum zum MRI verwendet wurde. Detaillierte Analysen zeigten, dass dies vor allem aufgrund einer anderen Interpretation der subchondralen Platte und des subchondralen Knochens vorgenommen wurde (siehe Kapitel 3.2). Dort wird auch der Ursprung des Schmerzes lokalisiert.

Abb. 3 (Seite 9). MRI bei osteochondraler Läsion des Talus. Folgende Gewebe sind mitbeteiligt: Knorpel mit einem Knorpelfragment und Unterbrechung der Grenzlamelle (Kreis), Knochen mit subchondralem Bone Bruise (°), Synovia mit Erguss und Synovitis (*), Ligamente mit Insuffizienz und Avulsionsverletzung (Pfeile). Abbildung aus Leumann et al. (2011a).

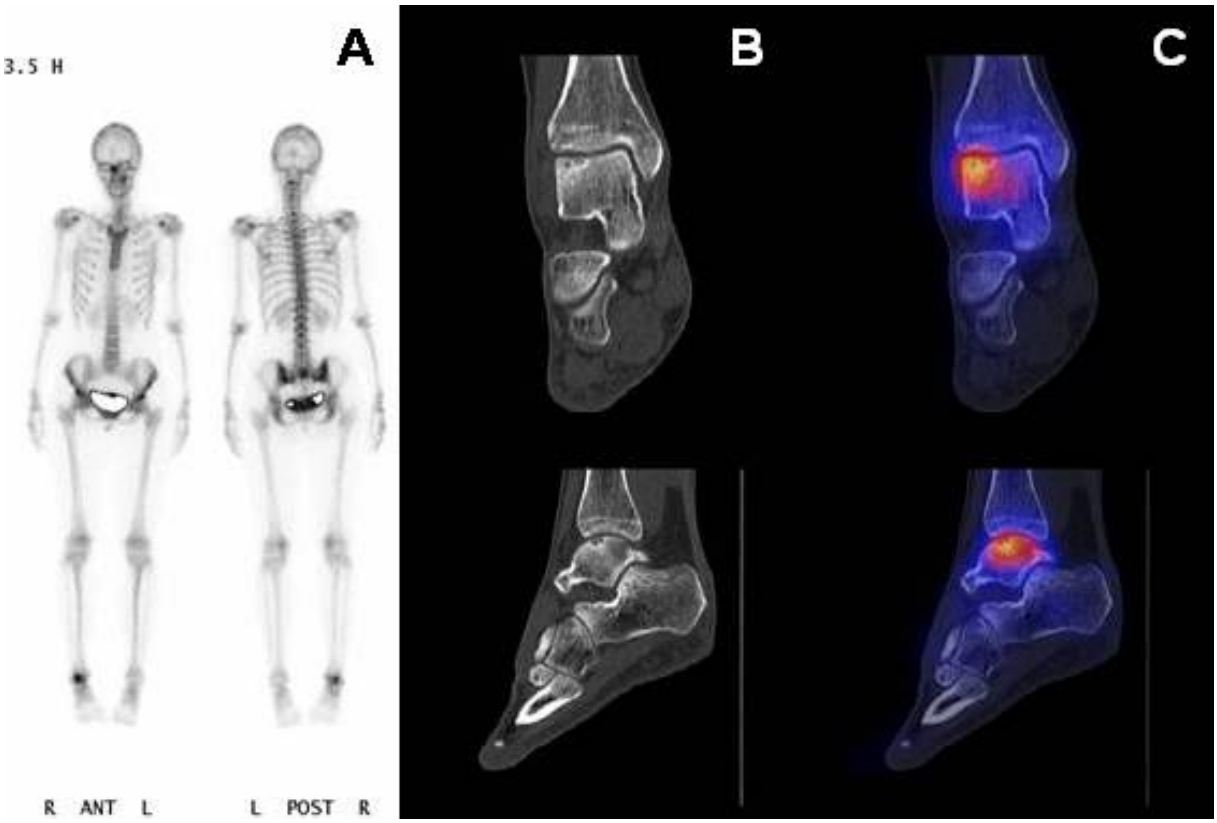

Abb. 4: SPECT-CT. Ein SPECT-CT wird als digitale Fusion (C) einer dreidimensionalen Szintigraphie (A) und einer Computertomographie (B) hergestellt.

	Berndt et Harty	**Anderson et al.**	**Ferkel et al.**	**Dipaola et al.**	**Taranow et al.**	**Hepple et al.**
	1959	1989/2012	1990/2008	1991	1999	1999
	Röntgen	MRT	CT	MRT	MRT	MRT
I	Subchondrale Kompression	Subchondrale Kompression und Knochenmarksödem	Zystische Läsion ohne Gelenkszugang	Knorpelverdickung und Signalveränderunge, aber nicht Ablösung	Subchondrale Kompression / Bone Bruise auf T2 Bildern	Isolierter Knorpelschaden
II	Fragment, aber nicht vollständig abgelöst	Subchondrale Zysten (a) oder inkomplett abgelöstes Fragment (b)	Zystische Läsion (a) mit Zugang zum Gelenk oder (b) offen zum Gelenk hin mit nicht disloziertem Fragment	Unterbrechung des Knorpels, Signalalteraltionen die darauf hinweisen, dass das Fragment fibrös verbunden ist.	Subchondrale Zysten	Knorpelschaden mit (a) oder ohne (b) darunterliegender Frakturzeichen oder Knochenödem
III	Abgelöstes Fragment, aber nicht dislozíert	Abgelöstes, nicht dislozíertes Fragment, von Synovialflüssigkeit umgeben	Undislozíertes Fragment mit Zeichen der Entkalkung	Unterbrechung des Knorpels, Signalveränderungen, die das Eindringen von Synovialflüssigkeit unter das Fragment nachweisen	Partiell oder vollständig abgelöste Fragmente in situ	Abgelöstes aber nicht dislozíertes Fragment
IV	Abgelöstes und disolziertes Fragment	Dislozíertes Fragment	Dislozíertes Fragment	Freie Gelenkskörper	Dislozierte Fragmente	Abgelöstes und dislozíertes Fragment
V	Subchondrale Zysten *					Subchondrale Zysten
	* Grad V ergänzt von Loomer et al. (1994)					

Tabelle 1: Zusammenstellung verschiedener osteochondraler Läsionen (Leumann et al., 2013)

Verschiedene Klassifikationen geben Auskunft über die Einteilung der osteochondralen Läsionen (Tabelle 1). Am häufigsten werden die Klassifikationen nach Berndt und Harty (1959) für das konventionelle Röntgen und nach Taranow et al. (1999) für das MRI verwendet. Abbildung 5 zeigt die beiden Klassifikationen. Diese haben auch eine Therapierelevanz (Tabelle 2 und 3). Dabei fällt auf, dass Stadium 5 nach Berndt et Harty dem Stadium 2 nach Taranow entspricht. Bei dieser Unterschiedlichkeit muss eine chronologische Abfolge, wie dies von Berndt und Harty in ihrer Publikation postuliert wurde, in Frage gestellt werden. Interessant ist diese Überlegung vor allem in Bezug auf die subchondrale Platte (Grenzlamelle). Ihr scheint für das Fortschreiten einer OCL eine Schlüsselrolle zuzukommen. Besonders häufig findet man das Stadium II nach Taranow mit zystischen Veränderungen im subchondralen Knochen. Diese entstehen wahrscheinlich dadurch, dass Gelenksflüssigkeit durch kleine Knorpelrisse und Risse in der subchondralen Platte in den subchondralen Knochen mit jeder Bewegung und jedem Schritt gepumpt werden (Valderrabano, Leumann et al., 2009). Bei Fortschreiten dieser Zysten kann es dann auch zur Ablösung oder zum Herausbrechen von Fragmenten oder Dissektaten kommen. In diesen Stadien stellt das SPECT-CT zweifelsohne einen grossen Mehrwert dar.

Klassifikation nach Berndt/Harty und Loomer et al. (Konventionelles Röntgen):

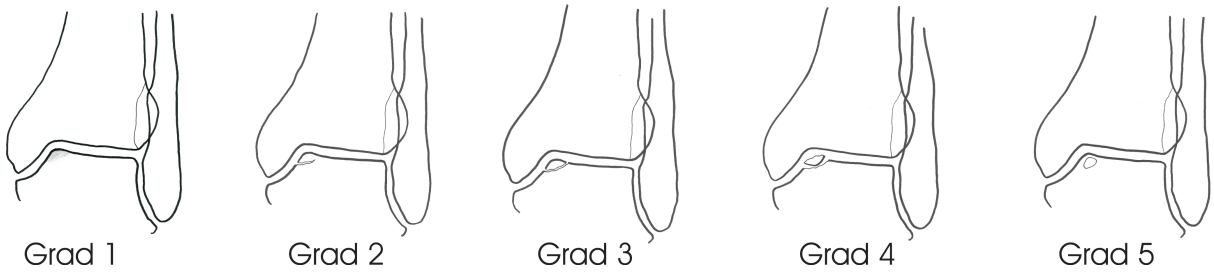

Klassifikation nach Taranow et al. (MRI):

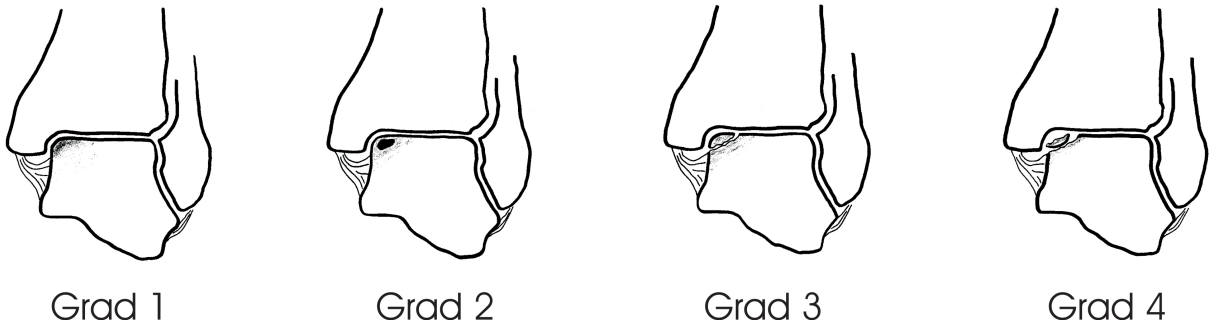

Abbildung 5: Zeigt die typischen Befunde der osteochondralen Läsionen nach Berndt/Harty und Loomer für das konventionelle Röntgen (Grad 1-5) und nach Taranow für das MRI (Grad 1-4).

Technik	Knorpel	Knochen
Débridement / Curettage	+	+
Mikrofrakturierung	+	+
Anbohrung / Drilling	+	++
Osteochondral Autologous Transplantation System (OATS) / Mosaikplastik	++	++
Autologe Chrondrozyten Implantation (ACI)	++	-
Matrix assozierte autologe Chrondrozyten Implantation (MACI)	++	-
Autologe Matrix-induzierte Chondrozytogenese (AMIC)	++	-
Autologe Spongiosplastik	-	++
Retrograde Anbohrung / Drilling	-	++

Tabelle 2: Chirurgische Techniken zur Therapie von osteochondralen Läsionen (Leumann et al., 2008). Die Wahl der OP-Technik erfolgt nach Einschätzung des Operateurs, basierend auf den vier unten aufgeführten Faktoren in Berücksichtigung von Patientenalter, Grösse der Läsion und anderen Co-Faktoren (z.B. sportlicher Anspruch, Begleitverletzungen, Nikotinabusus etc.). Es ist auch die Kombination von verschiedenen Methoden möglich, z.B. zeigt die Kombination von AMIC und autologer Spongiosaplastik exzellente Resultate (Valderrabano, Leumann et al., 2013).

Grad (Berndt et Harty)	***I und II***	***III und IV***
	Retrograde Anbohrung Mikrofrakturierung Chondrale Rekonstruktion (ACI, MACI, AMIC)	OATS/Mosaikplastik Kombinierte ossäre und chondrale Rekonstruktion (ACI, MACI oder AMIC mit Spongiosaplastik)
Grösse	***<1.5cm2***	***>1.5cm2***
	Retrograde Anbohrung Mikrofrakturierung Debridement	OATS/Mosaikplastik Kombinierte ossäre und chondrale Rekonstruktion (ACI, MACI oder AMIC mit Spongiosaplastik)
Patientenalter	***<50 Jahre***	***> 50 Jahre***
	Chondrale Rekonstruktion (ACI, MACI, AMIC)	Retrograde Anbohrung Mikrofrakturierung Endoprothetik oder Arthrodese

Tabelle 3: Typischer Behandlungsalgorithmus als Guideline zur Wahl der OP-Technik (Giannini et Vannini, 2004; Valderrabano et Leumann, 2008).

Therapeutisch ist in der Mehrzahl der Fälle ein chirurgisches Vorgehen nicht zu vermeiden. Eine Übersicht über verschiedene Therapieoptionen gibt Tabelle 2. Hierbei kann sowohl die chondrale als auch die ossäre Ebene therapeutisch adressiert werden. Bei grossen und schweren osteochondralen Läsionen ist es sicherlich sinnvoll, sogar beide Ebenen kombiniert anzugehen. Verschiedene Faktoren sind für die therapeutischen Überlegungen wichtig:

(I) ***Stabilität***; die Rekonstruktion muss stabil sein, um einen Krafttransfer zu ermöglichen. Insbesondere auch darum, weil die Läsionen an den Orten der höchsten biomechanischen Belastung liegen. Eine Analyse zur Belastungsverteilung erfolgte in Kapitel 3.1.

(II) ***Vitalität***; alle avitalen und sklerotischen Areal müssen entfernt und ersetzt werden. Wichtige biologische Informationen zur Vitalität gibt uns das SPECT-CT (Kapitel 3.2).

(III) ***Anatomie***; das OSG ist das kongruenteste der grossen Gelenke des Menschen. Um ein perfektes Gleiten der beiden Gelenksflächen zu ermöglichen, ist eine optimale anatomische Rekonstruktion notwendig. Eine radiologische Analyse zur Talusdomanatomie zeigt Kapitel 3.3.

(IV) ***Biomechanik*** des gesamten Gelenks; Um eine möglichst normale Biomechanik des Gelenks wiederherzustellen ist das Adressieren möglicher Co-Faktoren wichtig: Muskeln – Atrophie; Ligamente – Instabilität; Sehnen – Tendinopathie; Gelenk – Synovitis. Deshalb sind in vielen Operationen Zusatzeingriffe notwendig wie Osteotomien (supramalleolär, calcanear, etc.), Ligamentrekonstruktionen, Sehnenrevisionen, -raffungen, und –transfers, und Gelenkdebridements. Das Gelenk ist ein Organ, das über eine Homöostase in einer fein regulierten Balance gehalten wird. Dieser Faktor wurde in einem Modell adressiert, welches den Einfluss einer Muskelatrophie auf andere für die Gelenkhomöostase wichtige Gewebe untersuchte, und das Zusammenspiel und die Abhängigkeit der einzelnen biomechanischen Faktoren aufzeigen konnte (Kapitel 3.4).

2.2 The joint as an Organ – Konzept

(Adaptiert nach Leumann et al. 2011a)

Für das Verständnis und die Therapie von Gelenkspathologien ist es wichtig, nicht das einzelne Gewebe (z.B. ein Knorpelschaden) isoliert zu betrachten, sondern das Gelenk als Funktionseinheit. Dieses Konzept wird als „Joint as an Organ"-Konzept bezeichnet. Dies gilt genauso für akute Verletzungen (z.B. VKB-Ruptur) wie chronische Pathologien (z.B. posttraumatische Arthrose). Es gibt jedoch keine Gelenkspathologie, die das „Joint as an Organ"-Konzept besser verkörpert als die osteochondrale Läsion. Wie auf dem MRI (Abbildung 3) ersichtlich, sind neben Knorpel (lokal, joint-wide) und Knochen (subchondral, bone bruise) auch die Synovia (Erguss, Synovitis) und die Ligamente (chronische Rotationsinstabilität) mitbetroffen. Durch die OSG-Instabilität kommt es auch zu einer Mitbeteiligung der Muskel-Sehneneinheit (v.a. Peronealmuskulatur und -sehne). Somit erscheint es naheliegend, dass ein erfolgreicher Therapieansatz nicht alleine auf einer Knorpeltherapie beruhen kann. Das „The joint as an Organ"-Konzept hat massgeblich dazu beigetragen, das Verständnis für die Komplexität der osteochondralen Läsionen zu verbessern. Jedoch sind weiterhin einige Aspekte dieses Konzepts noch nie untersucht worden. Eine dieser Lücke schliesst die vierte hier vorliegende Arbeit, indem sie die chronischen Effekte einer Muskelatrophie auf ein Gelenk gemessen hat (Kapitel 3.4).

Gelenkshomöostase

Aus der Physiologie kennen wir den Begriff der Homöostase seit langem. Homöotase ist die Tendenz eines Organismus oder Systems (z.B. ein Organ), einen ausgeglichenen und konstanten inneren Zustand aufrechtzuerhalten. Befindet sich ein System im Gleichgewicht, so spricht man vom Steady state. Der Ist-Wert und der Soll-Wert sind dann identisch. Kommt es zu einer Divergenz beider Werte, gleicht sich das Regelsystem dem Sollwert an. Auch das Gelenk befindet sich in einer Homöostase. Die Regelgrösse für den Steady state ist dabei der Krafttransfer, welchem das Gelenk ausgesetzt ist. Zum Gelenk zählen dabei im engeren Sinne folgende Gewebe: Knorpel, Knochen, Sehnen, Ligamente, Synovia und die Muskulatur (Abbildung 6). Die Anpassung an einen Steady state erfolgt dabei durch Adaptationen in Form und Funktion der einzelnen Gewebe: Hypertrophie – Atrophie, Hyperplasie – Hypoplasie, sowie spezifische Reaktionen einzelner Gewebe (Knochen: Sklerose – Osteopenie; Muskel: Zunahme des kontraktilen Materials – fettige Degeneration; Sehne/Ligamente: Zunahme an Kollagenfasern und Cross-link der Kollagenfasern – hyaline Degeneration). Somit gibt die lokale Beanspruchung (und damit die Biomechanik oder die Funktion) die morphologische Ausgestaltung der Form (im Detail) vor. Die einzelnen Gewebe

passen sich im Sinne der Gelenkshomöostase der Beanspruchung an. Damit kann man das Gelenk als Organ bezeichnen.

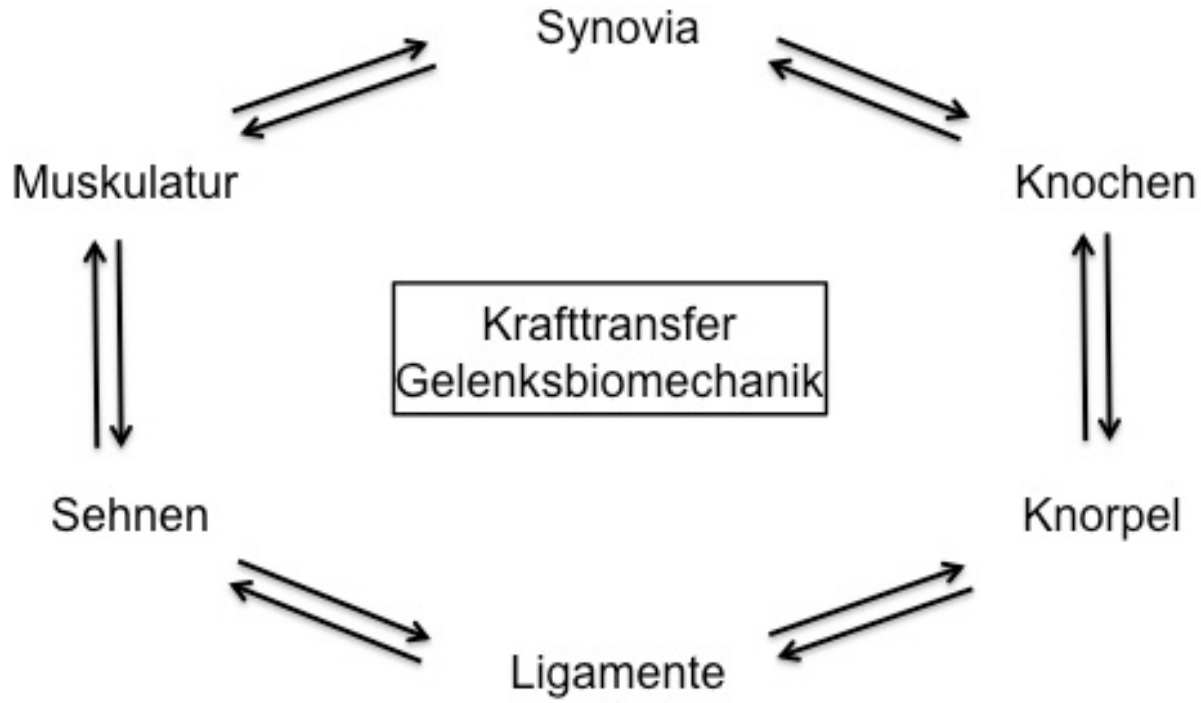

Abbildung 6: Muskuloskelettale Gewebe: Es besteht eine Interaktion zwischen allen muskuloskelettalen Gewebe. Die Gelenksbiomechanik stellt dabei in der Gelenkshomöostase die Regelgrösse dar. Die osteochondrale Läsion kann alle diese Faktoren betreffen.

Adaptationskaskade

Die Adaptationskaskade bei gestörtem Steady state beginnt bei intrazellulären Rezeptoren, welche einen mechanischen Reiz (Druck, Zug) in ein chemisches Signal umsetzen. So konnte eine ganz aktuelle Studie nachweisen, dass bei Kompression von Knorpelzellen intrazelluläre Calcium Sparks ausgelöst werden (Han et al., 2011). Ca^{2+}-Ionen sind eines der wichtigsten intrazellulären Signalmoleküle, ein anderes ist das c-AMP second messenger System. Die intrazellulären Signale führen zu einer veränderten Transkription (DNA->RNA) und Translation (RNA->Proteinprodukt) und somit zu einer erhöhten oder verringerten Produktion der relevanten Endprodukte (Proteine, Matrix), die zur Adaptation an die neue biomechanische Belastung und das Erreichen eines neuen Steady state notwendig sind. Letztendlich führt dies zu einer veränderten biomechanischen Qualität des Gewebes. Dabei wird bei den meisten Studien die mRNA einzelner Enzyme gemessen, also der Anteil der RNA, welcher tatsächlich in einer Proteinproduktion resultiert. Es werden dabei anabole und

katabole Faktoren unterschieden (Tabelle 4). Und um den gesamten Ablauf noch komplizierter zu gestalten, sind viele synergistische und antagonistische Effekte der einzelnen Faktoren miteinander bekannt. Selbstverständlich finden sich gewebetypische Adaptationsmuster, jedoch sind die Grundgerüste und Hauptfaktoren erstaunlich konstant. Eine der wichtigsten Erkenntnisse für den Sportorthopäden ist die Tatsache, dass diese Prozesse in den einzelnen Gewebe unterschiedlich schnell ablaufen. Während sich die Muskulatur innerhalb von Tagen bis wenigen Wochen anpassen kann, braucht Sehnen- oder Knorpelgewebe Wochen bis Monate für die Adaptation.

Anabole Enzyme	Katabole Enzyme
Collagen-1/3	Matrix Metalloproteinase-1/3/13 (MMP-1/3/13)
TIMP's (Tissue inhibitors of MMP)	COX-2
TGF-β	Cathepsin K (CATH K)
Biglycan	Interleukin-1
Fibular GF	TNF-α
Bone Morphogenic Protein-2/-7 (BMP-2/-7)	
Platelet derived Growth Factor (PDGF)	

Tabelle 4: Ein Auszug über wichtige anabole und katabole Enzyme im Bewegungsapparat.

Adaptationsprozesse

Die Adaptation des Knochens an die Belastung wurde bereits im 19. Jahrhundert von Wolff beschrieben (*Das Gesetz der Transformation des Knochens*, 1892). Bei anderen Geweben kommt man diesen Prozessen erst in den letzten Jahren auf die Spur. Eine entscheidende Tatsache ist, dass man diese Anpassungsprozesse für jedes Gewebe nachweisen kann, auch Knorpel, Meniskus oder Sehnen, obwohl diese noch bis vor kurzem als avital beschrieben wurden. Bei diesen Geweben ist die Prävention von Verletzungen und Spätschäden (Arthrose, Tendinopathien etc.) schwierig und vielleicht gerade deshalb besonders wichtig.

Die Muskulatur ist der Hauptakteur am Gelenk. Durch eine Muskelkontraktion (konzentrisch, exzentrisch, oder isometrisch) erfolgt ein Kraft- und Druckaufbau im Gelenk (Herzog et al., 2003). Diese physiologische Kraftbelastung des Gelenks muss abgegrenzt werden von pathologischen Kraftbelastungen wie z.B. ein Trauma oder eine Belastung durch Schläge (Impact Loading).

Als Beispiel dieser Adaptationsprozesse soll hier der Zusammenhang von Muskelaktivität und Sehnengewebe ausgeführt werden (Abbildung 7). Dabei müssen die zellulären Mechanismen nach einmaliger Belastung, mehrmals repetitiver Belastung und chronischer Belastung unterschieden werden. Wobei letzte einen neuen Steady state darstellt und damit den Endpunkt eines Adaptationsprozesses. Bei einmaliger Belastung mit Knieextensionstraining (70% der Maximalkraft) fanden Sullivan et al. (2009) eine Reduktion der mRNA der Patellarsehne von anabolen (Collagen-1, Collagen3) und katabolen (z.B. Matrix Metalloproteinase-3 (MMP-3), TNF alpha) Enzymen (Hart et Achari, 2011). 4h nach dem Training waren diese Werte bereits wieder normalisiert. Im längeren Verlauf nach einem ähnlichen Training fanden Miller et al. (2005), dass es 24h nach dem Training zur höchsten Konzentration an anabolen Faktoren kam, während dem sich die katabolen Faktoren reduziert hatten. Ohne weiteren Trainings-Input reduzieren sich danach die mRNA-Level wieder auf die Ausgangsnormwerte. In dieser Phase kommt es also bei repetitiven biomechanischen Reizen zu einer zwischenzeitlichen Netto-Synthese von Sehnenmaterial. Das Gewebe passt sich der neuen Belastungssituation an, indem ein neuer Steady-state hergestellt wird. Ist dieser erreicht, pendelt sich Synthese und Abbau von Gewebe neu ein. Bei vermehrtem Training ist sind dabei sowohl die mRNA Level der anabolen wie auch katabolen Faktoren erhöht. Dies konnte Archambault et al. (2001) zeigen, der die Wadenmuskulatur von Kaninchen täglich während 11 Wochen stimulierte und in der Achillessehne erhöhte mRNA Expression von anabolen (Collagen III) und katabolen (MMPs) nachwies. Die Anpassungsreaktion findet natürlich nicht nur in der Sehne, sondern auch im trainierten Muskel und den anderen am Gelenk beteiligten Geweben statt. Heinemeier et al. (2007) konnten nachweisen, dass die Veränderung der mRNA Level in der Muskulatur deutlich schneller und ausgeprägter auftreten.

Kaum erstaunlich ist, auch wenn deutlich weniger gut erforscht, dass der Effekt umgekehrt in ähnlicher Weise auftritt. Durch eine Reduktion der Muskelaktivität kommt es zu einer Down-Regulation der mRNA Expression. Wir konnten in einer eigenen Studie an Kaninchen zeigen, dass durch eine Quadriceps-Muskelschwächung, hervorgerufen durch repetitive Botulinum Toxin A-Injektionen (Botox), es nach 6 Monaten zu einer Down-Regulation von anabolen und katabolen Faktoren kam und sich ein neuer , tieferer Steady-state eingependelt hat (Leumann et al. 2012). Interessanterweise fand sich dabei kein Unterschied in der Anpassung an den neuen Steady-state zwischen der Patellarsehne, die direkt mit dem Quadricepsmuskel eine Muskel-Sehneeinheit bildet, und anderen Geweben, wie Innen- und Aussenmeniskus, oder Innen- und Aussenband. Dies unterstützt das „Joint as an Organ"-Konzept, welches die gesamte Gelenks-Homöostase in den Mittelpunkt rückt.

Auch wenn viele dieser Erkenntnisse am Tiermodell gewonnen wurden, so finden sich gerade im Sport viele Beispiele, wo eine Adaptation von Gewebe auf die Belastung

beschrieben wurde. Couppé et al. (2008) konnte bei Elite-Badminton-Spielern zeigen, dass die Patellarsehne des führenden Beines signifikant dicker ist, als das Bein, welches hinten positioniert ist.

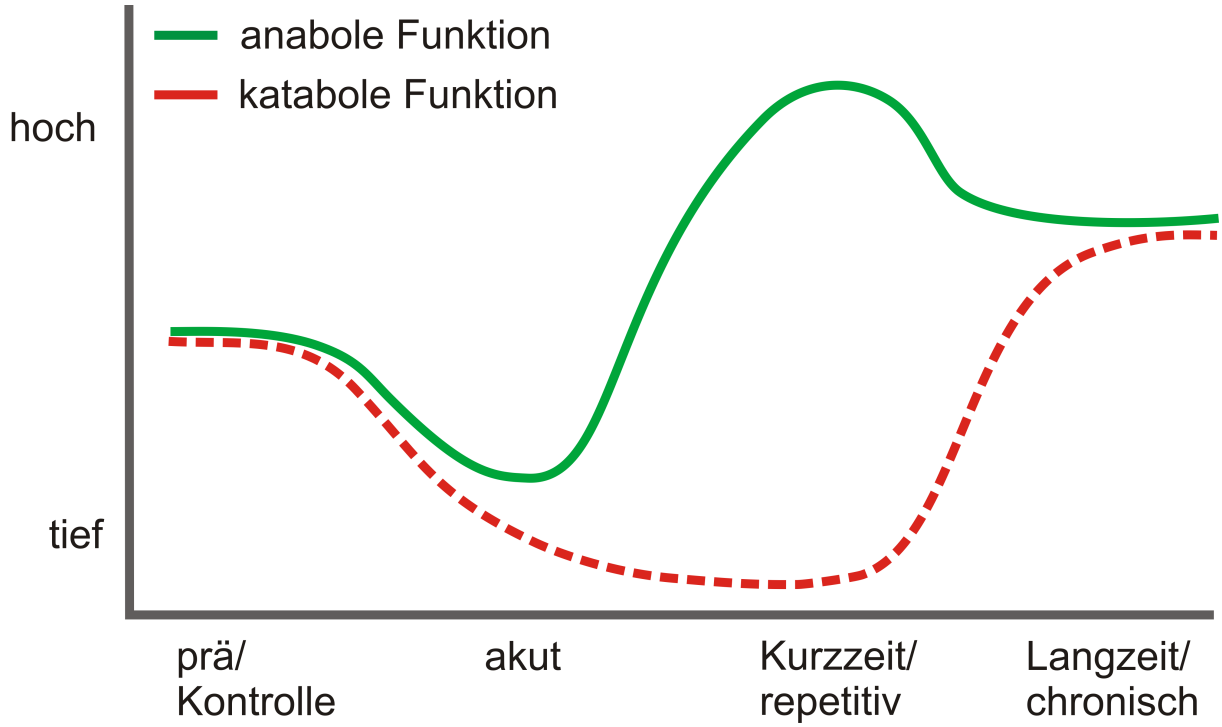

Abbildung 7: Verhältnis von anabolen zu katabolen Faktoren bei Sehnengewebe auf Be- und Entlastung. Zum Abschluss der Anpassung wurde ein neuer Steady State erreicht. Im gezeigten Fall ein höherer Steady State aufgrund einer vermehrte Belastung. Bei vermehrter Entlastung wird ein niedrigerer Steady State erreicht.

Intensiv untersucht wurde das Verhalten von Knorpel bei Langstreckenläufern. Nach einer Laufbelastung fanden sich sowohl reduzierte Knorpelvolumina (minus 2,5-6%), als auch veränderte funktionelle Knorpelwerte (in T2 mapping und dGEMRIC) (Boocock et al. 2009). Nach einem Marathonlauf bleiben diese Werte bis über 3 Monate verändert, bevor sie sich normalisieren (Luke et al. 2011). Trotzdem konnte Krampla et al. (2008) auch in einer 10 Jahresverlaufsstudie kein erhöhtes Risiko für Knorpelschäden nachweisen. Viel mehr konnte Racunica et al. (2007) nachweisen, dass sportlich aktive Personen ein grösseres Knorpelvolumen im Kniegelenk haben als inaktive. Auch die intensiven Bemühungen und die klinische Anwendung um die Knorpelzelltransplantation bestätigen die zwar limitierte, aber vorhandene Anpassungsfähigkeit des Knorpels. Trotzdem wird dem Knorpel weiterhin fehlende regenerative Kapazität zugesagt.

Der Zusammenhang von Biomechanik, Muskelaktivität und Knorpel wird noch spannender, wenn wir die Langzeiteffekte bei Arthrose betrachten. Eine Gelenksdegeneration führt zu einer Muskelatrophie, zu einem Kraftverlust, aber auch zu einer veränderten Muskelfunktion (z.B. veränderte EMG-Aktivitätsmuster) (Valderrabano et al., 2007). Umgekehrt wissen wir aus dem Kaninchenmodell, dass eine alleinige Muskelatrophie die Ursache für eine Knorpeldegeneration sein kann. Youssouf-Reehan et al. (2009) hat dies histologisch am Kniegelenk nachgewiesen.

3 Originalarbeiten

3.1	Mineral density and penetration strength of the subchondral bone plate of the talar dome: high correlation and specific distribution patterns	21
3.2	A novel imaging method for osteochondral lesions of the talus - comparison of SPECT-CT with MRI	41
3.3	Radiographic Evaluation of Frontal Talar Edge Configuration for Osteochondral Plug Transplantation	49
3.4	Altered cell metabolism in tissues of the knee joint in a rabbit model of Botulinum toxin A-induced quadriceps muscle weakness	55

Mineral density and penetration strength of the subchondral bone plate of the talar dome: high correlation and specific distribution patterns

Running title: Biomechanics of subchondral bone plate

Leumann André 1,2
Valderrabano Victor 2
Hoechel Sebastian 1
Göpfert Beat 3
Müller-Gerbl Magdalena 1
1 Institute of Anatomy, University of Basel, Switzerland
2 Orthopaedic Department, University Hospital of Basel, Switzerland
3 Laboratory of Biomechanics & Biocalorimetry, CMBE, University of Basel, Switzerland

Revisions Submitted to:
J Foot Ankle Surgery
July 22, 2013

Correspondence:
Dr. André Leumann
Orthopaedic Department, University Hospital of Basel
Spitalstr. 21, 4031 Basel, Switzerland
aleumann@uhbs.ch, Tel: +4161 265 2525, Fax: +4161 265 7829

Abstract

The subchondral bone plate plays an important role in stabilizing the osteochondral joint unit and in the pathomechanism of osteochondral lesions and osteoarthritis. The objective of the study was to measure (I) mineral density distribution and (II) subchondral bone plate penetration strength of the talar dome joint facet in order to display and compare specific distribution patterns. Therefore, ten cadaver specimen were used for CT-scans wherefrom densitograms were derived by means of CT-osteoabsorptiometry (CT-OAM), and for mechanical indentation testing from where penetration strength was obtained. As results, two different distribution patterns were found for mineral density and penetration strength. Six out of 10 specimens (60%) showed bicentric maxima (anteromedially and anterolaterally), while the other 4 specimens (40%) showed a monocentric maximum (either anteromedially or anterolaterally). Highly significant correlation ($p<0.0001$) of both methods confirmed that mineral density relied on local load characteristics. In conclusion, biomechanical properties of the subchondral bone plate of the talar dome joint facet showed specific distribution patterns. CT-OAM has shown to be a reliable method to display mineral density distribution non-invasively. We recommend CT-OAM for non-invasive analysis of biomechanical properties of the subchondral bone plate in osteochondral joint reconstruction as well as in prevention and treatment of osteoarthritis and osteochondral lesions.

Clinical Level of Evidence : 5

Key words:

ankle, bone density, cartilage, osteoarthritis, osteochondral lesion, talus, tibia

Introduction

The subchondral bone plate is anatomically located between the calcified cartilage (deepest layer of cartilage) and the subchondral bone. The subchondral bone plate thickness is 0.1 to 1.5 mm and may be seen on the CT-scan as a distinct radio-dense line separating articular cartilage and cancellous bone [1,2]. Its function is to transfer and modulate load from the joint to the subchondral cancellous bone and vice versa [3]. It was suggested by Mente and Lewis that the subchondral bone plate serves as a transitional zone of intermediate stiffness [4].

The subchondral bone plate gathers increasing attention as it was found to be involved in the main joint pathologies like osteoarthritis (OA), osteochondral lesions, osteonecrosis, and osteochondral or intraarticular fractures [1]. In animal models of OA, the subchondral bone plate shows thinning in models of early OA and thickening in late stages of OA [5,6]. Subsequent to cartilage degeneration, load transfer modulation is changed leading to higher local peak forces and changes to the biomechanical properties of tissue. In humans, vascular invasion, microcracks, and multiplication of the tidemark were found in OA [7]. In treating osteochondral lesions (e.g. the talus), restoration of the subchondral bone plate has become an important factor to seal the subchondral bone and to avoid cyst recurrence [8].

As all musculoskeletal tissues (e.g. bone, cartilage, muscle) adapt to mechanical input such as load or strain, the subchondral bone plate is thought to adapt to the load transfer through the joint and therefore pictures the mechanical long-term load: “morphology revealed biomechanics”. CT-osteoabsorptiometry (CT-OAM) is a non-invasive technique that displays mineral density distribution in the subchondral bone plate based on conventional CT scans [9]. Mineral densitograms show consistent patterns for several joints, such as the knee, hip, and shoulder joint [9-12].

The objective of this study were to measure and display mineral density distribution and penetration strength patterns of the subchondral bone plate of the talar dome joint facet of

the ankle joint and to compare the results of these two techniques with each other. The talar dome is a joint facet that is frequently affected by osteoarthritis and osteochondral lesions [13,14]. Biomechanical properties by means of penetration strength and mineral density may help to elucidate mechanical and anatomical subchondral bone plate properties and to understand pathobiomechanical joint disorders.

Method

Specimen

Ten unpaired human cadaver tali were used for this study. At time of death, donors aged 85.4 years in average (range, 72-91yrs.; female, 6; male, 4). The specimen were fixed in formalin. Exclusion criteria were macroscopic cartilage degeneration according to the International Cartilage Repair Society (ICRS) score (≥1) [15], signs of osteoarthritis or osteoporosis in the CT-scans based on the Osteoarthritis Reseach Society International (OARSI) criteria [16], and positive patient history for ankle pathologies. Approval of the local ethical committee to conduct this study was obtained.

CT-Osteoabsorptiometry

Data sets for CT-OAM were acquired by conventional CT scanning (16 row-detector; thickness, 1mm; Siemens Somatom Sensation, Erlangen, Germany) and analyzed with a specific image analyzing system (ANALYZE 7.4, Biomedical Imaging Resource, Mayo Foundation, Rochester, MN). The CT scans were segmented in order to isolate the subchondral bone plate. Maximum intensity projection revealed HU of each pixel. Threshold values were chosen according to previous studies to be < 200 HU to > 1200 HU [17]. In order to display mineral density distribution, these data were false color coded and superimposed on the identically 3D reconstructed talar bone for anatomical localization (Figure 1).

Indentation testing

104 Indentation testing (IT) was performed with a material testing machine (Synergie 100,
105 MTS Systems, Eden Prairie, MN, USA) at predefined measuring points according to a 15
106 point grid scheme, measuring the reactive force with constant speed of penetration [17].
107 Therefore the specimen were fixed in a custom-made frame on a ball joint that allowed to
108 always penetrate the subchondral bone plate perpendicularly to the surface (Figure 2). A
109 custom-made indenter made of stainless steel with a conical tip (radius, 1.25mm; area,
110 4.91mm^2) was used. The distance between the IT measurement points was chosen to be 7mm
111 based on the results of previous studies in order to minimize interference of measurements
112 [9,18].
113 For analysis, the force curve was divided into three relevant parts. The first part with reactive
114 force resembled the cartilage indentation (A-B), the second part the deflection of the
115 subchondral bone plate consisting of a linear slope (B-C), and the third part was defined as
116 the end point of this slope depicting the failure (= fracture) of the subchondral bone plate (C)
117 (Figure 3). At point C, failure load (N) was measured. Penetration strength (MPa) was
118 calculated by dividing failure load through the indenter size (mm^2). The term penetration
119 strength was used throughout the article as this value was independent of indenter size.
120 *Comparison of CT-OAM and IT*
121 The resolution of CT-OAM and the 15 measurement points of IT were largely
122 different. To be able to compare both methods, CT-OAM values were identified at exactly the
123 same measurement points with the same measurement size (indenter siz, 4.91mm^2), where
124 penetration strength was measured. HU were scaled in 8-bit. Both methods were visualized
125 in similar schematic diagrams that visual comparison was possible.
126 Correlation of mineral density and penetration strenght was calculated for
127 corresponding data set points to elucidate correlation of non-invasively measurable
128 densitograms with invasive mechanical strength testing. For statistical analysis, linear

129 regression correlation (Bravais-Pearson correlation coefficients) were calculated using Excel
130 2007. Level of significance was set at $\alpha<0.05$.
131
132 **Results**
133 *Density distribution*
134 Mineral density distribution was not homogenously throughout the entire joint facet,
135 but followed distinct distribution patterns. Two specific patterns of density distribution were
136 identified. In 6 out of 10 samples (60%), bicentric density maxima were found (Figure 4c).
137 The absolute maxima were found anteromedial with an extension along the medial talar edge
138 towards posterior and a second maxima on the anterolateral talar edge. For the other 4
139 samples (40%), monocentric maxima were found (Figure 4a). Out of these 4, two were
140 located anteromedially, and two anterolaterally. All of the described maxima extended
141 towards the center of the medial groove.
142
143 *Penetration strength distribution*
144 Identically to the mineral density distribution patterns, two specific patterns were seen
145 for penetration strength distribution. Bicentric penetration strength distribution patterns were
146 found in the same 6 samples (60%) as for bicentric mineral density distribution (Figure 4d).
147 These maxima were located equally on the anterior to central parts of the medial and lateral
148 talar edge. In the case of the other 4 samples (40%), corresponding to the mineral density
149 distribution patterns, monocentric maxima were seen. Out of these 4, two samples showing its
150 maxima anteromedially and two samples anterolaterally (Figure 4a).
151
152 *Correlation*
153 Mineral density and penetration strength do not only correlate visually, but showed
154 highly significant correlations for values measured at the same points (Table 1). r^2 correlation

ranged from 0.59 to 0.96 (median, 0.88), correlation coefficent of Bravais-Pearson from 0.77 to 0.99 (median, 0.92) (Figure 5).

Discussion

This study analyzed biomechanical properties of the subchondral bone plate of the talar dome joint facet with two different methods. CT-OAM displayed mineral density as a measure of local long-term loading conditions. Indentation testing determined penetration strength of the subchondral bone plate. Both methods showed that the distribution throughout the entire joint is not homogenous at all. Moreover, distribution was identical and correlated significantly ($p<0.0001$) for both methods and followed two specific patterns: in 60% of specimens, a bicentric distribution was found, in 40% a monocentric distribution. Based on these findings, biomechanical penetration strength of the subchondral bone plate may be imaged non-invasively in an intact joint by CT-OAM. And this could be usefull in understanding pathologies and treatment of talar disorders, such as osteochondral lesions or ankle osteoarthritis.

The understanding of the physiologic bone plate and its pathologic conditions of the talar dome is of major importance for Orthopaedic surgeons. Beside many other conditions, osteochondral lesions have a high impact on patients, as young, sports active patients are affected. OCL may lead to sports invalidity as the foot does no longer tolerate any load, or in long-term may lead to ankle osteoarthritis needing ankle fusion or total ankle replacement as final treatment options [19].

Osteochondral lesions were found most frequently on the medial talar edge and on the lateral talar edge [20]. At the same localization the cartilage was found to be thickest [21]. Furthermore, as shown in our study, the subchondral bone plate is strongest at the same localization. Two hypothesis may explain this consistency: (A) These two localizations seem to be the two areas that are loaded more then the surroundings. Higher load could turn the

area more vulnerable for OCL; (B) Thicker and harder tissues may have less regenerative potential (e.g. due to impaired vascular supply), what could impair healing of cartilage impacts or injuries. It is one of the most accepted hypothesis of the basically unknown natural history on OCL that crack initiation of the subchondral bone plate may lead to a mechanism where joint fluids may be pumped into the subchondral bone through these cracks [22]. Thus leading to intraosseous cyst formation and detachment of fragments. CT-OAM has the advantage of being non-invasive. First pilot experiments in humans showed that CT-OAM may help to objectify regeneration of the subchondral bone plate (as a very sensitive marker of the osteochondral joint unit) after surgical treatment of a pathobiomechanical joint condition (e.g. osteochondral lesion, asymmetric ankle osteoarthritis) (so far unpublished data).

While measurement of penetration strength through indentation testing in the subchondral bone has been used for decades [23], measurement of penetration strength of the subchondral bone plate and also the CT-OAM technique are relatively new. Although inter-individual comparison is difficult due to several factors, such as patient age, gender, body weight, physical activity, nutrition, and others, distribution patterns showed to be very consistent. They seemed to mostly rely on joint biomechanics and joint morphology (e.g. load transfer, range of motion, joint axis). Knowing this, it is interesting to take into account the structure of the opposite joint facet, the distal tibial plafond. Mühlhofer et al. [17] found in the distal tibial joint facet also a bicentric mineral density distribution pattern where the absolute maxima were located anteromedially and a second maxima was located anterocentrally to anterolaterally. Comparing our results with the results of the study of Mühlhofer et al. [17] we see that the maxima of the distal tibial plafond correspond anatomically to the maxima of the talar dome joint facet.

Understanding penetration strength as the fracture level load, we can calculate the load that can be transferred through the ankle joint. By calculating the average penetration

strength, (39.2MPa) and estimating the area of the talar dome joint facet (110mm^2), the total joint load that may be transferred through the ankle joint is about 3500N. That is around 5 times body weight for a person weigthing 70kg. Walking leads to a load of around 3 times body weight.

This study has to be seen within its limitation. The specimens had an average age of 85.4 years. This is higher than patients with osteoarthritis (40-80 yrs.) as well as with osteochondral lesions (20-50 yrs.). So far, no studies are available that discuss the influence of age on the subchondral bone plate. However, specimens with signs of osteoarthritis were excluded from the study.

Calculations of Houndsfield units by CT-scans have to rely on predefined control measurement on CT phantom. This was not done in this study as earlier published validation results showed minimal interference of ±4HU for subchondral bone plates [9]. Four HU correspond to 0,3-1% of measured HU values. Most of all, the key function of CT-OAM is the description of mineral density distribution in order to show its local variability.

A conical indentation tip was used to measure the penetration strength based on the work of Hvid [23] and Müller-Gerbl [9]. A conical indenter has the advantage of minimized friction during penetration, so that compaction of bone does not falsify the measured data [23]. However, this method does only allow to measure penetration strength, but not axial compression strength. Axial compression strength may be calculated based on an empirical formula by Hvid and Hansen [18].

Finally, formalin fixed specimens were used. In comparison to fresh specimens, no statistically significant differences were found in terms of penetration strength and mineral density [24,25]. Currey et al. [26] reported of changes of mechanical strength by up to 10%. This has to be differentiated to measurements of torsional properties (e.g. in the spine and long diaphyseal bones) where changes up to 96% were reported [27]. Torsional properties were not measured in our study. CT-OAM measurements in patients or fresh specimens

showed identical mineral density distributions and identical location of bicentrical density maxima. Therefore we might conclude that relative distribution of penetration strength is not affected by formalin fixation.

In conclusion, this study showed biomechanical properties of the subchondral bone plate of the talar dome facet in terms of penetration strength and mineral density distribution measured by CT-OAM. Based on the highly significant correlation ($p<0.0001$) of penetration strength and mineral density distribution, one may conclude that mineral density distribution imaged the local biomechanical long-term loading history. For the talar dome joint facet, in both methods, two specific distribution patterns were found. In 60% of specimens, a bicentric distribution pattern was recognized with two maxima located anteromedially and anterolaterally, and a monocentric distribution pattern in 40% of specimens having the maximum located either on the medial or lateral taral edge. Based on the significant correlation of CT-OAM and indentation testing, CT-OAM seemed to be an accurate and reproducible method to describe mineral density distribution and local joint loading conditions.

The understanding of biomechanics and function of the subchondral bone plate is important as it plays a major role in different joint pathologies. Future studies will have to show how biomechanical joint load and mineral density distribution do change in different pathologic conditions and whether these changes might be reversible with adequate treatment and restoration of a normal biomechanical joint function.

Funding

No funding was received for this study.

Competing Interests

None of the authors have anything to declare in relation to this article.

References

1. Madry H, Van Dijk CN, Müller-Gerbl M. The basic science of the subchondral bone. Knee Surg Sports Traumatol Arthrosc 18:419-33, 2010.
2. Milz S, Putz R. Quantitative morphology of the subchondral plate of the tibial plateau. J Anat 185 :103-10, 1994.
3. Pan J, Zhou X, Li W, Novotny JE, Doty SB, Wang L. In situ measurement of transport between subchondral bone and articular cartilage. J Orthop Res 27:1347-52, 2009.
4. Mente PL, Lewis JL. Elastic modulus of calcified cartilage is an order of magnitude less than that of subchondral bone. J Orthop Res 12;637-47, 1994.
5. Intema F, Hazewinkel HAW, Gouwens D, Bijlsma JWJ, Weinans H, Lafeber FPJG et al. In early OA, thinning of the subchondral plate is directly related to cartilage damage: result from a canine ACLT-meniscectomy model. Osteoarthritis Cartilage 18:691-8, 2010.
6. Botter SM, Van Osch GJVM, Waarsing JH, Van der Linden JC, Verhaar JAN, Pols HAP et al.Cartilage damage pattern in relation to subchondral plate thickness in a collagenase-induced model of osteoarthritis. Osteoarthritis Cartilage 16:506-14, 2008.
7. Hulth A. Does osteoarthrosis depend on growth of the mineralized layer of cartilage? Clin Orthop Relat Res 287:19-24, 1993.
8. Valderrabano V, Leumann A, Rasch H, Egelhof T, Hintermann B, Pagenstert G. Knee-to-ankle mosaicplasty for the treatment of osteochondral lesions of the ankle. Am J Sports Med 37;105S-11S, 2009.
9. Müller-Gerbl M. The subchondral bone plate. Adv Anat Embryol Cell Biol 141:1-134, 1998.

285 10. Schulz CU, Pfahler M, Anetzberger HM, Becker CR, Müller-Gerbl M, Refior HJ. The
286 mineraliziation patterns at the subchondral bone plate of the glenoid cavity in healthy
287 shoulders J Shoulder Elbow Surg 11:174-81, 2002.
288 11. Von Eisenhart R, Adam C, Steinlechner M, Müller-Gerbl M, Eckstein F. Quantitative
289 determination of joint incongruity and pressure distribution during simulated gait and
290 cartilage thickness in the human hip joint. J Orthop Res 17:532-39, 2008.
291 12. Zumstein V, Krajlevic M, Wirz D, Hügli R, Müller-Gerbl M. Correlation between
292 mineralization and mechanical strength of the subchondral bone plate of the humeral
293 head. J Shoulder Elbow Surg 2012. Epub ahead of print.
294 13. Valderrabano V, Hintermann B, Horisberger M, Fung TS. Ligamentous posttraumatic
295 ankle osteoarthritis. Am J Sports Med 34 :612-20, 2006.
296 14. Verhagen RA, Maas M, Dijkgraaf MG, Tol JL, Krips R, Van Dijk CN. Prospective
297 study on diagnostic strategies in osteochondral lesions of the talus. Is MRI superior to
298 helical CT? J Bone Joint Br 87:41-6, 2005.
299 15. Brittberg M, Aglietti P, Gambardella R, Hangody L, Hauselmann HJ, Jakob RP, et al.
300 The ICRS clinical cartilage injury evaluation system – 2000. In: 3rd ICRS Meeting in
301 Göteborg, Sweden, April 28–29, 2000.
302 16. Altman RD, Gold GE. Atlas of individual radiogrphaic features in osteoarthritis,
303 revised. Osteoarthritis Cartilage 15:A1-56, 2007.
304 17. Mühlhofer H, Ercan Y, Drews S, Matsuura M, Meissner J, Linsenmaier U et al.
305 Mineralization and mechanical strength of the subchondral bone plate of the inferior
306 tibial facies. Surg Radiol Anat 31:237-43, 2009.
307 18. Hvid I, Hansen SL. Trabecular bone strength patterns at the proximal tibial epiphysis.
308 J Orthop Res 3:464-72, 1985.

19. Haddad SL, Coetzee JC, Estok R, Fahrbach K, Banel D, Nalysnyk L. Intermediate and long-term outcomes of total ankle arthroplasty and ankle arthrodesis. A systematic review of the literature. J Bone Joint Surg Am 89:1899-905, 2007.
20. Elias I, Zoga AC, Morrison WB, Besser MP, Schweitzer ME, Raikin SM. Osteochondral lesions of the talus: localization and morphologic data from 424 patients using a novel anatomical grid scheme. Foot Ankle Int 28:154-61, 2007.
21. Millington SA, Grabner M, Wozelka R, Anderson DD, Hurwitz SR, Crandall JR. Quantification of ankle articular cartilage topography and thickness using a high resolution stereophotography system. Osteoarthritis Cartilage 15:205-11, 2007.
22. Valderrabano V, Horisberger M, Russell I, Dougall H, Hintermann B. Etiology of ankle osteoarthritis. Clin Orthop Relat Res 467:1800-06, 2009.
23. Hvid I. Cancellous bone at the knee: a comparison of two methods of strength measurement. Arch Orthop Trauma Surg 104:211-7, 1985.
24. Burkart KJ, Nowak TE, Blum J, Kuhn S, Welker M, Sternstein W et al. Influence of formalin fixation on the biomechanical properties of human diaphyseal bone. Biomed Tech 55:361-5, 2010.
25. Van Haaren EH, van der Zwaard BC, van der Veen VJ, Heyligers IC, Wuisman PI, Smit TH. Effect of long-term preservation on the menchanical properties of cortical bone in goats. Acta Orthop 79:708-16, 2008.
26. Currey JD, Brear K, Zioupos P, Reilly GC. Effect of formaldehyde fixation on some mechanical properties of bovine bone. Biomaterials 16:1267-71, 1995.
27. Wilke HJ, Krischak S, Claes LE. Formalin fixation strongly influences biomechanical properties of the spine. J Biomech 29:1629-31, 1996.

334 **Tables**

335 **Table 1: Results per specimen.** Mineral density values are 8-bit grey scaled (GS),

336 penetration strength is shown as failure load in Newton (N). Correlation coefficient of

337 Bravais-Pearson (r), coefficient of determination (r^2), and significance (p) were given.

338

Specimen	Mineral Density (GS)		Failure Load (N)				
	Minimum	Maximum	Minimum	Maximum	r	r^2	p
1	148	183	122	215	0,92	0,85	*<0,0001*
2	150	195	117	334	0,98	0,96	*<0,0001*
3	159	187	131	364	0,98	0,96	*<0,0001*
4	122	217	50	344	0,96	0,93	*<0,0001*
5	134	182	60	284	0,99	0,98	*<0,0001*
6	177	231	121	315	0,80	0,63	*<0,0001*
7	146	189	73	241	0,94	0,89	*<0,0001*
8	146	181	91	222	0,92	0,85	*<0,0001*
9	135	231	81	269	0,91	0,83	*<0,0001*
10	155	225	100	638	0,91	0,82	*<0,0001*

339

340

Figure 1: CT-Osteoabsorptiometry of a right talus (specimen 2). Characteristic distribution of subchondral bone plate mineral density. One area of high density is found in the anterior to central parts of the medial curvature and another area of high density is found on the lateral curvature. Color-coded CT-OAM densitogram is superimposed onto the surface of the total talar body to facilitate anatomic orientation.

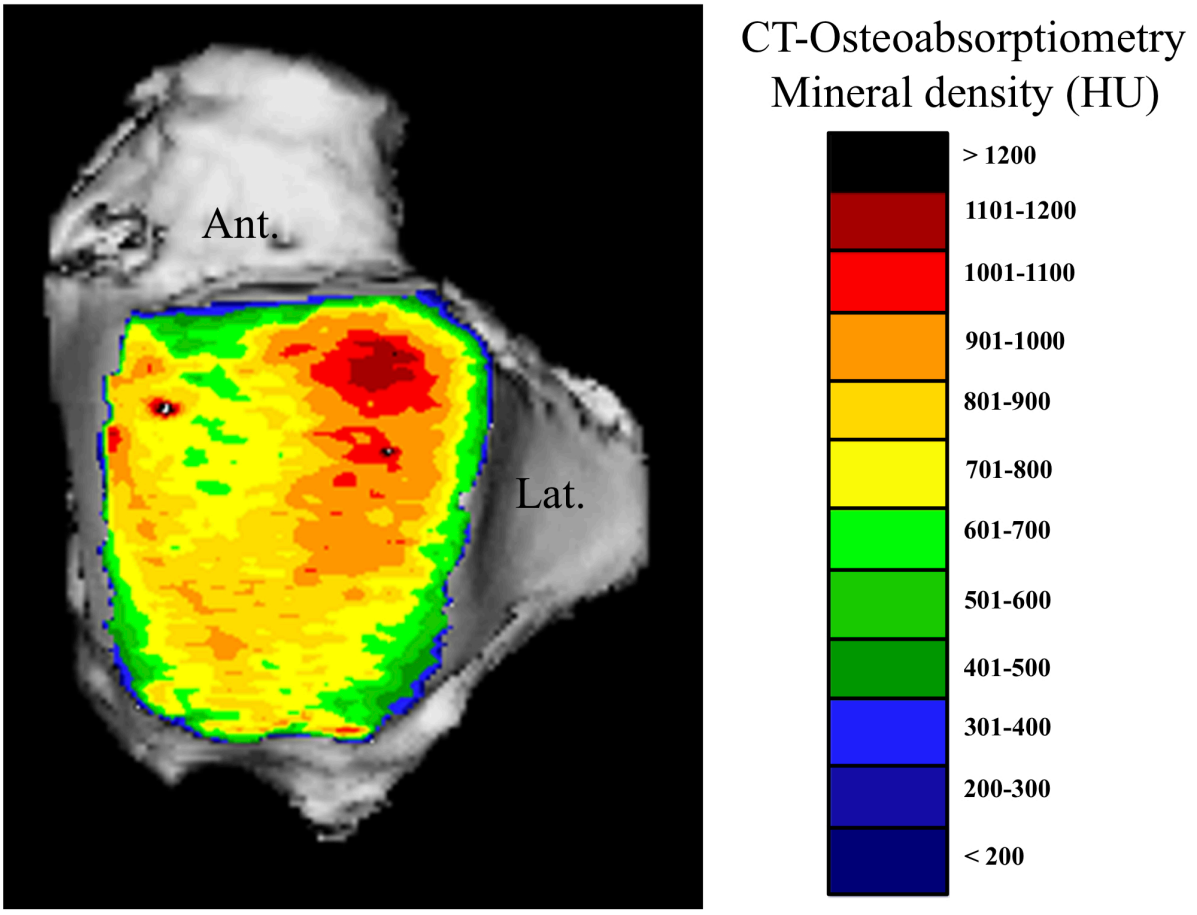

Figure 2: Setup indentation testing. The specimens were fixed in a custom-made frame that allowed three dimensional, step-free positioning so that the MTS machine penetrated the osteochondral unit always perpendicularly.

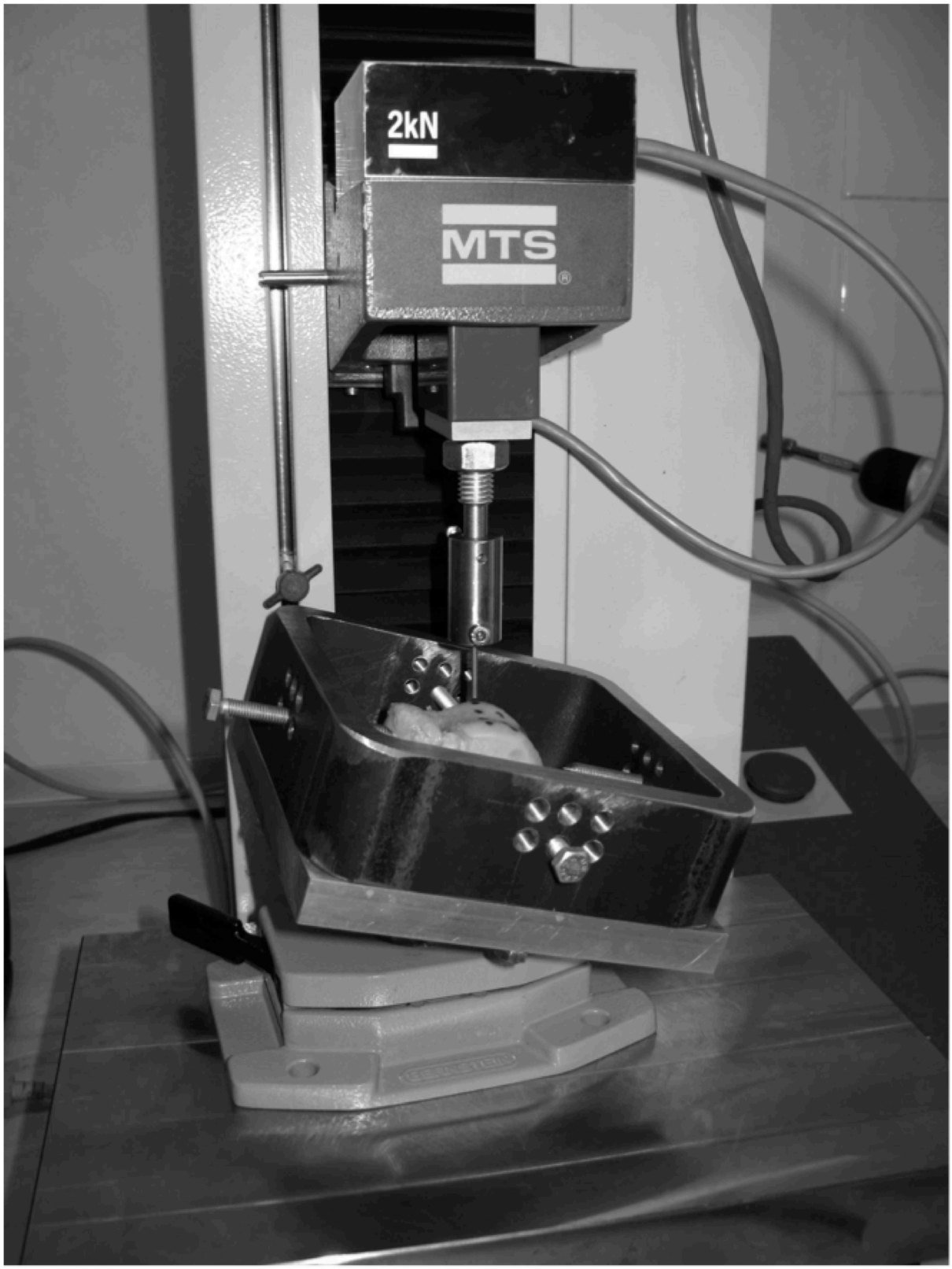

Figure 3: Indentation testing. At point A, indenter set contact with the cartilage. Up to point B, the indenter penetrated the cartilage with low force resistance. At point B, the indenter reached the subchondral bone plate and linear deflection of the subchondral bone plate started until failure of the subchondral bone plate was reached (point C). Penetration strength was calculated from the force at which failure of the subchondral bone plate occurred. The bumpy area following C showed displacement within the subchondral cancellous bone.

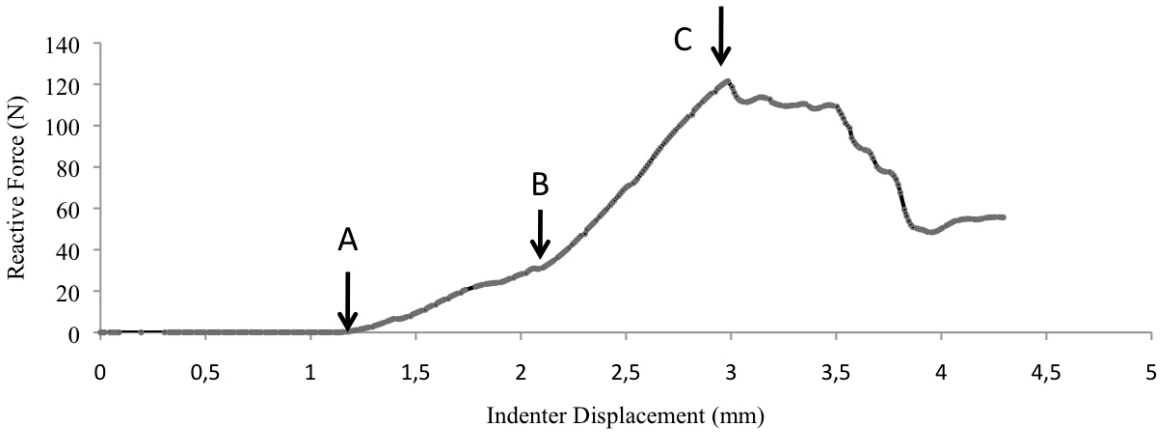

Figure 4: Penetration strength and mineral density of two representative specimen. Monocentric (a-c) and bicentric (d-f) distribution patterns for CT-OAM (HU) (a and d), mineral density transferred to a schematic diagram (HU, 8-bit color code) generated by CT-OAM (b and e), and penetration strength (MPa) (c and f) measured by indentation testing.

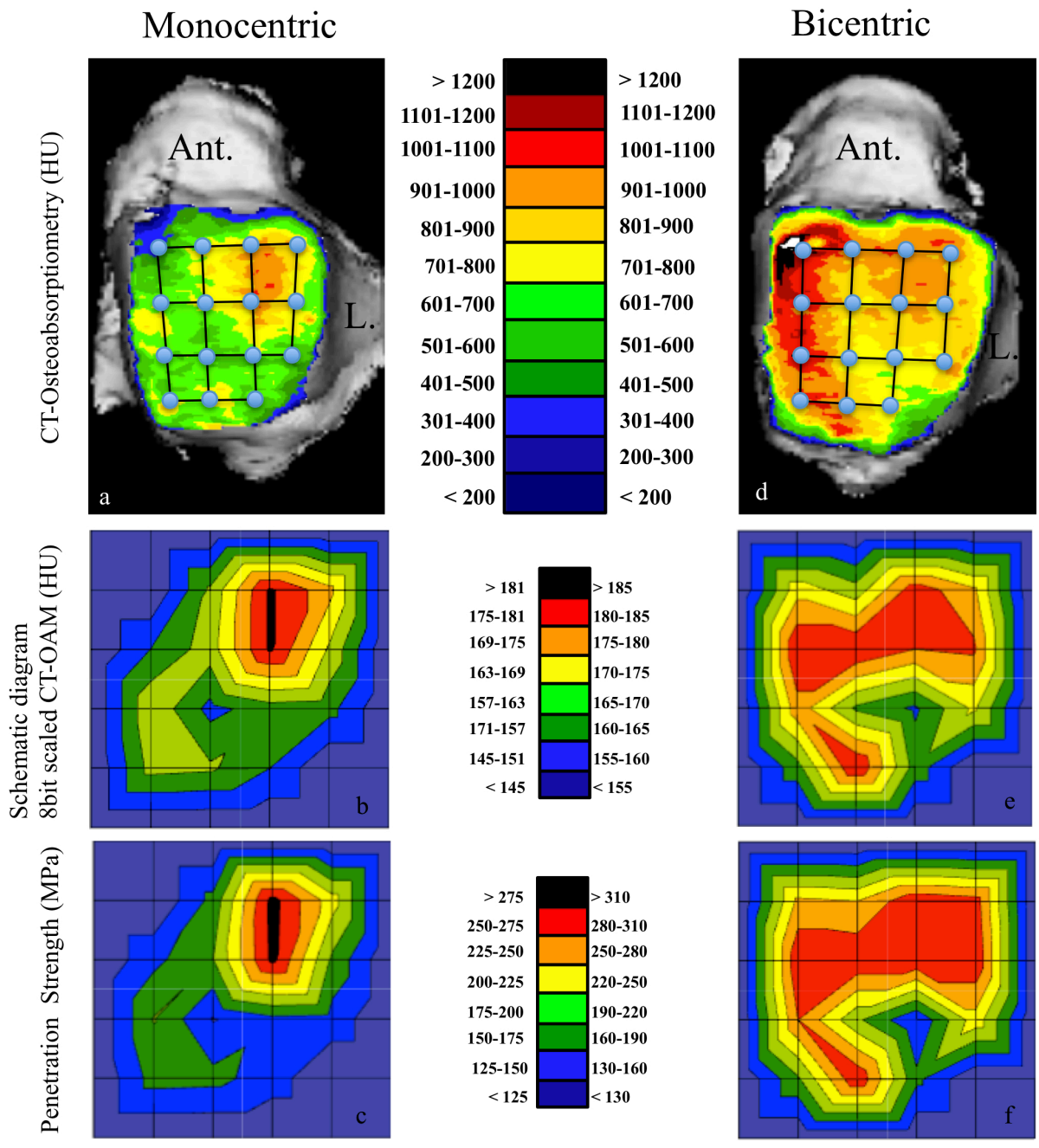

Figure 5: Correlation of mineral density and penetration strength (specimen 2). Highly significant correlation of mineral density generated by CT-OAM and penetration strength measured by indentation testing was found.

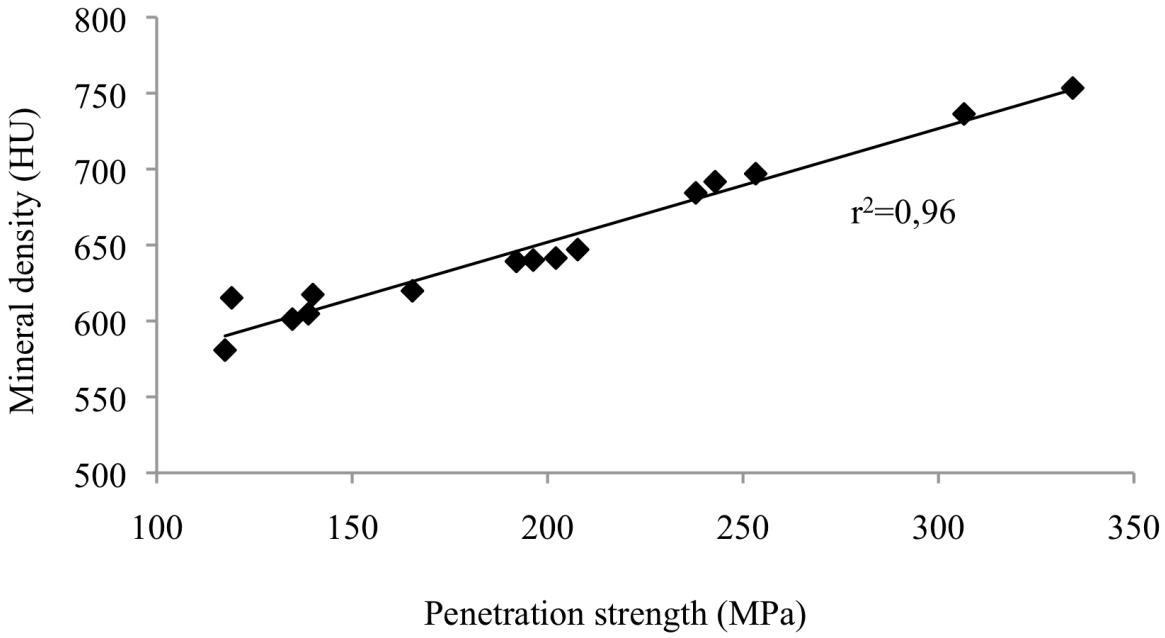

The American Journal of Sports Medicine

http://ajs.sagepub.com/

A Novel Imaging Method for Osteochondral Lesions of the Talus––Comparison of SPECT-CT With MRI

André Leumann, Victor Valderrabano, Christian Plaass, Helmut Rasch, Ueli Studler, Beat Hintermann and Geert I. Pagenstert

Am J Sports Med 2011 39: 1095 originally published online February 7, 2011
DOI: 10.1177/0363546510392709

The online version of this article can be found at:
http://ajs.sagepub.com/content/39/5/1095

Published by:

http://www.sagepublications.com

On behalf of:

American Orthopaedic Society for Sports Medicine

Additional services and information for *The American Journal of Sports Medicine* can be found at:

Email Alerts: http://ajs.sagepub.com/cgi/alerts

Subscriptions: http://ajs.sagepub.com/subscriptions

Reprints: http://www.sagepub.com/journalsReprints.nav

Permissions: http://www.sagepub.com/journalsPermissions.nav

>> Version of Record - May 5, 2011

OnlineFirst Version of Record - Feb 7, 2011

What is This?

Downloaded from ajs.sagepub.com at Medizinbibliothek on April 21, 2013

A Novel Imaging Method for Osteochondral Lesions of the Talus—Comparison of SPECT-CT With MRI

André Leumann,* MD, Victor Valderrabano,*† MD, PhD, Christian Plaass,* MD, Helmut Rasch,‡ MD, Ueli Studler,§ MD, Beat Hintermann,‖ MD, and Geert I. Pagenstert,‖ MD
Investigation performed at Orthopaedic Department, University Hospital of Basel, Basel, Switzerland

Background: Magnetic resonance imaging (MRI) is the current standard in noninvasive diagnostics of osteochondral lesions (OCLs) of the talus. Single-photon emission computed tomography–computed tomography (SPECT-CT) is a new technique that displays different imaging qualities. The influence of the aforementioned diagnostic information on treatment decision making in talar OCLs is not known.

Purpose: The aim of the study was to evaluate SPECT-CT in comparison with MRI for image interpretation and decision making in OCLs of the talus.

Study Design: Case series; Level of evidence, 4.

Methods: Magnetic resonance imaging and SPECT-CT of 25 patients (average age, 32 years; range, 18-69 years) were analyzed by 3 independent orthopaedic surgeons blinded to the study. Raters had to analyze images for predefined criteria of cartilage, subchondral bone plate, and subchondral bone, including bone marrow edema on MRI and scintigraphic activity on SPECT-CT. For MRI alone, SPECT-CT alone, and their combination, the treatment decision had to be defined.

Results: In comparison with MRI alone, treatment decision making changed in 48% of the cases with SPECT-CT alone and 52% with SPECT-CT and MRI combined. While cartilage showed good correlation for interpretation between MRI and SPECT-CT, the subchondral bone plate and subchondral bone showed substantial differences. Poor intrarater correlation highlighted the different information provided by the 2 imaging techniques. Poor interrater correlation showed a high heterogeneity in the treatment decision making of OCLs.

Conclusion: Compared with MRI, SPECT-CT provides additional information and influences the decision making of OCL treatment. For thorough diagnostic evaluation in OCLs, performing both MRI and SPECT-CT is recommended. Further clinical investigation is needed to see if SPECT-CT in addition to MRI results in improved treatment outcomes.

Keywords: osteochondral lesion; talus; MRI; SPECT-CT; therapy; subchondral bone

Osteochondral lesions (OCLs) of the talus most often affect young, sports-active patients. These lesions are frequently reported in patients with sports injuries such as ankle sprains, chronic ligament instability, and fractures.[17] Patients have persistent pain, swelling, and blocking of the joint but also a reduction of sports activity and quality of life. Osteochondral lesions may develop into jointwide osteoarthritis and therefore may be considered focal osteoarthritis.[24]

Therapeutically, upon failure of nonoperative treatment, the surgeon may choose between a broad variety of reconstructive techniques.[17,30] These include excision, debridement, curettage, retrograde drilling, anterograde drilling, microfracturing, autologous chondrocyte implantation, matrix autologous chondrocyte implantation, cancellous bone grafting, osteochondral autologous transplantation/mosaicplasty, autologous matrix-induced chondrocytogenesis, and others. Reported results vary depending on techniques and authors, and success rates range from 0% to 100%.[30] As is common to medicine in general, the choice of the right surgical OCL treatment is substantially based on the diagnostics used. In talus OCL,

†Address correspondence to Victor Valderrabano, MD, PhD, Orthopaedic Department, University Hospital of Basel, Spitalstr 2, 4031 Basel, Switzerland (e-mail: vvalderrabano@uhbs.ch).
*Department of Orthopaedic Surgery, University Hospital of Basel, Basel, Switzerland.
‡Department of Nuclear Medicine, University Hospital of Basel, Basel, Switzerland.
§Department of Radiology, University Hospital of Basel, Basel, Switzerland.
‖Orthopaedic Department, Cantonal Hospital of Liestal, Liestal, Switzerland.

One or more authors has declared the following potential conflict of interest or source of funding: Independent governmental funding was provided by the Swiss Federal Council of Sports (Magglingen, Switzerland) with financial support of this study within the research concept ''Sport and Motion.''

The American Journal of Sports Medicine, Vol. 39, No. 5
DOI: 10.1177/0363546510392709
© 2011 The Author(s)

Downloaded from ajs.sagepub.com at Medizinbibliothek on April 21, 2013

radiologic treatment decision making is based on 3 factors: size, stability, and vitality of the OCL.[3,10,11] Hereby, diagnostic methods consisted of weightbearing radiographs, magnetic resonance imaging (MRI), computed tomography (CT), and ankle arthroscopy.[7,22,29] To date, MRI is widely accepted as the noninvasive standard, although Verhagen et al[29] showed equal diagnostic accuracy for both CT and MRI.

A new technique combining a SPECT (single-photon emission computed tomography) scan—a 3-dimensional scintigraphy bone scan—and a CT scan is offering new options in orthopaedic diagnostics and treatment decision making: SPECT-CT.[12,18,31] The SPECT-CT allows localization of scintigraphic osteoblastic activity in the area of interest, in combination with the anatomic resolution of a CT scan. Thus, the surgeon gets not only morphologic but also biological information on the OCL.[12] The SPECT-CT also shows excellent interobserver and intraobserver reliabilities.[18]

Varying imaging modalities, such as MRI or SPECT-CT, provide different tissue information that might influence OCL treatment decision making. So far, no study has addressed the therapeutic influence of SPECT-CT in OCL of the talus.

Therefore, the aim of the present study was to evaluate the clinical use of SPECT-CT in comparison with MRI or both. The hypotheses were as follows: (1) Different imaging information leads to different treatment decision, and (2) divergence in imaging information is found predominantly for the subchondral bone plate and the subchondral bone.

MATERIAL AND METHODS

The study cohort consisted of 25 consecutive patients (9 women and 16 men). The only selection criterion for the cohort was that of having MRI and SPECT-CT within 3 months for chronic OCL of the talus. Mean age was 32 years (range, 18-69 years). Duration of symptoms ranged from 6 months to 12 years. All patients had nonoperative treatment, and 6 had operative treatments before (arthroscopy, microfracture, drilling), without relief of symptoms and with persistent OCL. Lesions were localized according to Elias et al.[8] Of the 25 lesions, 15 were located on the medial third of talar dome (60%), 10 on the lateral third (40%), and none on the central third. Of the medial lesions, 2 were found anteromedially, 9 centromedially, and 5 posteromedially. Of the lateral lesions, 1 was found anterolaterally, 7 centrolaterally, and 2 posterolaterally. Ethical approval was obtained by the local ethical committee.

The types of OCL involved in this study were graded for MRI according to Taranow et al[26] and for the SPECT-CT scans according to the CT classification of Ferkel et al,[9] a modified version of the original Berndt/Harty classification.[1] Taranow's classification of MRI showed 10 cases with grade 1 (40%; subchondral compression), 7 cases with grade 2 (28%; subchondral cyst), 5 cases with grade 3 (20%; detached but not displaced fragments), and 3 cases with grade 4 (12%; displaced fragments). Ferkel's classification showed 10 cases with grade 1 (40%; subchondral compression), 2 cases with grade 2 (8%; partially avulsed fragment), 3 cases with grade 3 (12%; detached but not displaced fragment), 3 cases with grade 4 (12%; displaced fragments), and 7 cases with grade 5 (28%; subchondral cyst).

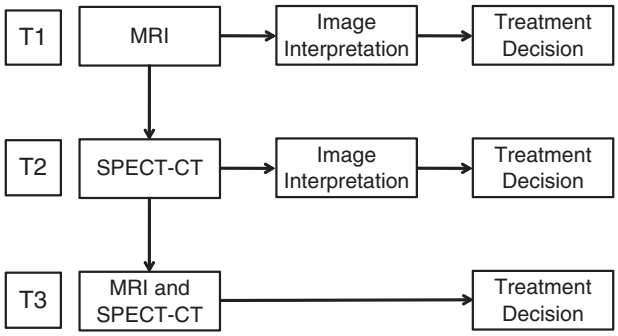

Figure 1. Flow chart showing how the analyses were done. A minimum of 5 months was set between the time points (T). Analysis was done for 1 technique per point (ie, MRI, SPECT-CT, both).

The MRI and SPECT-CT images were presented blinded and randomized to 3 independent orthopaedic surgeons (raters A-C) experienced in treating talus OCL. The raters were given 3 independent sets of diagnostic information: MRI alone, SPECT-CT alone, and MRI and SPECT-CT in combination. Sufficient time and randomly changed orders were taken between each group (>5 months) to rule out recognition. The same clinical information was added to all patients to adjust all cases: young, sports-active patient with chronic symptoms and desires to return to sports activity (Figure 1).

First, for the assessment of MRI and SPECT-CT alone, the orthopaedic surgeons had to evaluate the images according to predefined criteria (Table 1), which were established in cooperation with our musculoskeletal radiologists and according to our clinical experience. Being aware of the fact that analysis may become more difficult, we kept criteria strictly descriptive and qualitative or semiquantitative. Of these criteria for SPECT-CT, interpretation of what was considered subchondral bone and subchondral bone plate was predominantly based on the information of the CT scan, whereas size and description of the scintigraphic activity and interpretation of kissing lesions were based on the SPECT scan.

Second, the 3 raters had to make their preferred treatment decision for all 3 sets of information: MRI, SPECT-CT, and the combination thereof. Therefore, several treatment options were available. For analysis, these options were merged into 6 groups according to treatment principles: abrasion arthroplasty (excision and curettage), reconstructive techniques (microfracture, autologous chondrocyte implantation, matrix autologous chondrocyte implantation, autologous matrix-induced chondrocytogenesis, with or without cancellous bone grafting), retrograde drilling, autologous osteochondral transplantation, nonoperative treatment (physiotherapy, cast), and joint-sacrificing therapies (arthrodesis, total ankle joint replacement). The MRI examinations were performed with a 1.5-T system (Symphony, SIEMENS, Erlangen, Germany) with a special

Downloaded from ajs.sagepub.com at Medizinbibliothek on April 21, 2013

TABLE 1
Criteria and Subdivision of Criteria for Image Interpretation[a]

Cartilage	
Joint space narrowing	Not narrowed
	Partially narrowed
	Completely narrowed
Appearance	Intact
	Signal altered
	Missing
Kissing lesion	Absent
	Present
Subchondral bone plate	
Appearance	Normal
	Thinned
	Thickened
Congruency/disruption	Intact
	Discontinued
	Absent
Subchondral bone	
Sclerosis formation	Normal
	Sclerosis
	Cyst formation
Bone marrow edema/ scintigraphic activity	
Size sagittal plane	Subchondral
	¼ of talar body CSA
	½ of talar body CSA
	Total talar body CSA
Size coronal plane	Subchondral
	¼ of talar body CSA
	½ of talar body CSA
	Total talar body CSA

[a]For cartilage, SPECT-CT had to be interpreted indirectly. CSA, cross-sectional area

ankle-centered coil. Analyses were available in the axial, coronal, and sagittal planes with T1- and T2-weighted sequences, with a slice thickness of 3 mm (Figure 2A).

The SPECT-CT diagnostics were performed with a Symbia T2 device (Siemens, Erlangen, Germany) that included bone scintigraphy and CT in a 1-step procedure. Bone scintigraphy consisted of 740 MBq of 99mTc-DPD, 3.5 hours after injection, with a multiplanar 2-dimensional reconstruction in 3 phases (SPECT: 128 × 128 matrix, 32 frames, 35 seconds per frame, step and shoot). The CT consisted of multislice CT images (130 keV, 70-100 mA) of the whole foot with multiplanar reconstruction with slice thickness of 1 mm (pitch and reconstruction interval, 1 mm)[18] (Figure 2B).

Statistical analysis was performed in collaboration with a statistician using SPSS 17.0 (SPSS Inc, Chicago, Illinois). Intrarater variability was used to measure the influence of the diagnostic method (eg, MRI, SPECT-CT, or both) on the image interpretation and choice of treatment. Interrater variability was used to measure consistency of findings and rater agreement. Reliability analysis for interrater and intrarater correlations were performed with Cronbach α.[5] Results were transferred into a binary code to allow inclusion of 3 raters and several criteria

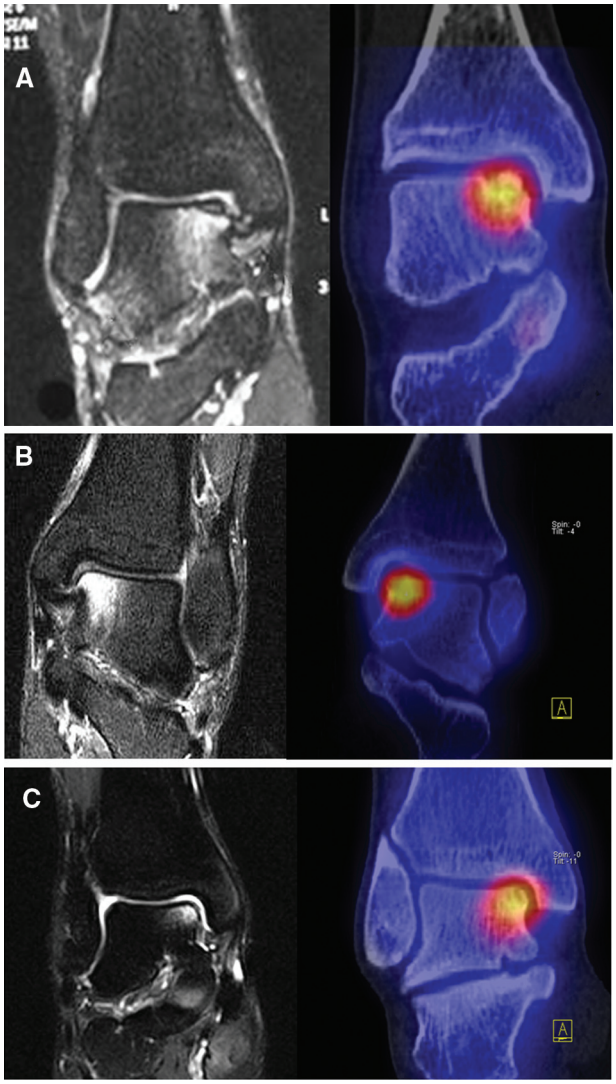

Figure 2. Osteochondral lesion of the talus. Three cases were shown by MRI and SPECT-CT. The different size of bone marrow edema and area of scintigraphic activity is evident in A and B but comparable in C. While the subchondral bone plate is continuous on MRI (A, B), it is interrupted (A) or bulky (B) on SPECT-CT, or the interruption is at another area of the lesion (C).

(eg, treatment decision, description of cartilage) in 1 step. Analysis with Cohen κ values was not applicable, because κ is not suitable for 3 and more raters while using several nominal scaled values. Cronbach α is known to show relevant results for 3 to 6 variables, and it can take every value between 0 and 1 and all negative values.[4] Because of the binary code, a large number of Cronbach α values were generated. To focus the amount of data, the Cronbach α values were graded according to Schnell et al[23] to merge them where appropriate ($\alpha \geq .70$, good; $.70 < \alpha \geq .50$, acceptable; $\alpha < .50$ and negative values, poor), thus allowing us to report the distribution of Cronbach α in percentages.

Downloaded from ajs.sagepub.com at Medizinbibliothek on April 21, 2013

TABLE 2
Intrarater and Interrater Correlations and Subsequent Change (in Percentages)[a]

	Intrarater Correlation		Interrater Correlation		
	Good/Acceptable	Poor	Good/Acceptable	Poor	Change of Interpretation/Decision[b]
Cartilage	74	26	78	22	11-19
Subchondral bone plate	44	56	67	33	40-45
Subchondral bone	55	45	17	83	38
Bone marrow edema/scintigraphic activity	25	75	60	40	24-56
Treatment decision	39	61	44	56	48-52

[a]Cronbach α values graded for good/acceptable and poor correlation. Intrarater correlation indicates the change of image interpretation between MRI and SPECT-CT. Interrater correlation indicates consistency of findings and rater agreement. Imaging interpretation per MRI and SPECT-CT alone (see Figure 1); treatment decision per MRI alone, SPECT-CT alone, and both.

[b]The percentage of cases in which the interpretation/decision was effectively changed. For values presented in a range, several comparisons were included.

RESULTS

Cartilage

Direct analyses of MRI and indirect interpretation of SPECT-CT for cartilage appearance, joint space narrowing, and kissing lesions correlated well in 10 of 27 Cronbach α values and acceptable in another 10 (together 74%) and poorly in 7 (26%). This resulted in a change of interpretation between MRI and SPECT-CT from 11% to 19%. Also, interrater variability was sufficient with good or acceptable correlation in 14 of 18 values (78%) (Table 2).

Subchondral Bone Plate and Subchondral Bone

Interpretation of subchondral bone plate appearance and disruption varied substantially between MRI and SPECT-CT. Only 8 of 18 Cronbach α values for the intrarater variability showed good or acceptable correlations, with the remaining 10 showing poor correlation only (56%). This resulted in a change of interpretation of MRI and SPECT-CT from 40% to 45% for the different criteria. That intrarater variability correlated well in 2 of 12 Cronbach α values (17%) and acceptably in another 6 (together 67%) emphasized that MRI and SPECT-CT offer different information on the subchondral bone plate.

Also, for the interpretation of the subchondral bone sclerosis, intrarater variability remained low, indicating different information between MRI and SPECT-CT, with 2 of 9 Cronbach α values correlating well (22%), another 3 acceptably (33%), and the remaining 4 poorly (45%). This resulted in a 38% change of interpretation between MRI and SPECT-CT. However, here the interrater variability was very low, with 5 of 6 values correlating poorly (83%) (Table 2).

Bone Marrow Edema Versus Scintigraphic Activity

Comparing the area of the bone marrow edema in MRI and the scintigraphic activity in SPECT-CT is interesting. In the sagittal view, the area of bone marrow edema was rated as being substantially bigger than the scintigraphic activity in 13 cases (52%), of equal size in 6 cases (24%), and smaller in another 6 (24%). In the coronal view, MRI was rated substantially bigger in 14 cases (56%), of equal size in 5 cases (20%), and smaller in 6 cases (24%). Interestingly, the smaller the bone marrow edema area, the better the correlation was found to be. Accordingly, the intrarater correlations showed poor correlation in 21 of 28 Cronbach α values (75%) and good or acceptable correlations in 25%. The consistency of these findings is evident from good interrater correlations, where 12 of 20 Cronbach α values (60%) showed good or acceptable correlation and 40% showed poor correlation (Table 2).

Treatment Decision

In comparison with MRI, treatment decisions changed in 36 of 75 cases (48%) for SPECT-CT alone and 39 (52%) for both MRI and SPECT-CT. Table 3 shows the shift of treatment decisions. The different explanatory power of MRI and SPECT-CT can be seen by the intrarater variability. Cronbach α showed good correlation in 5 of 18 values (28%), acceptable correlation in 2 other values (11%), but poor correlation in 61%.

The interrater variabilities show a good correlation in only 4 of 18 Cronbach α values (22%) and an acceptable correlation in 4 of 18. In the remaining 10 values, interrater variability was poor (56%). This showed a high heterogeneity and individuality in treatment decisions for OCLs of the talus.

DISCUSSION

Current concepts of treatment decision making in OCLs of the talus rely mainly on MRI.[3,6,26] This study evaluated the relevance and validity of a new alternative diagnostic tool, SPECT-CT, in comparison with MRI. The main findings show that SPECT-CT led to a change of treatment decision in 48% of the cases and that the combined information of SPECT-CT and MRI led to a change of 52% in

Downloaded from ajs.sagepub.com at Medizinbibliothek on April 21, 2013

TABLE 3
Treatment Decisions Shift[a]

	MRI			SPECT-CT			MRI + SPECT-CT		
	A	B	C	A	B	C	A	B	C
Abrasion arthroplasty	**0**	**9**	**0**						
Abrasion arthroplasty				*0*	*2*	*0*	*0*	*3*	*0*
Reconstructive techniques				0	3	0	0	5	0
Retrograde drilling				0	1	0	0	0	0
Osteochondral transplantation				0	2	0	0	0	0
Nonoperative treatment				0	1	0	0	1	0
Reconstructive techniques	**6**	**2**	**10**						
Reconstructive techniques				*3*	*0*	*6*	*4*	*1*	*7*
Retrograde drilling				3	0	1	1	0	2
Osteochondral transplantation				0	1	2	0	1	1
Nonoperative treatment				0	1	1	1	0	0
Retrograde drilling	**17**	**8**	**5**						
Abrasion arthroplasty				0	2	0	2	0	0
Reconstructive techniques				2	2	1	4	1	1
Retrograde drilling				*13*	*2*	*4*	*6*	*4*	*3*
Osteochondral transplantation				0	1	0	0	1	0
Nonoperative treatment				2	1	0	5	2	1
Osteochondral transplantation	**0**	**3**	**9**						
Abrasion arthroplasty				0	0	1	0	0	0
Reconstructive techniques				0	0	3	0	2	4
Retrograde drilling				0	1	1	0	0	1
Osteochondral transplantation				*0*	*2*	*3*	*0*	*1*	*3*
Joint sacrificing therapy				0	0	1	0	0	1
Nonoperative treatment	**1**	**2**	**1**						
Abrasion arthroplasty				0	0	0	0	1	0
Reconstructive techniques				0	1	0	0	1	0
Retrograde drilling				1	1	0	0	0	0
Joint sacrificing therapy				0	0	1	1	0	1
Joint sacrificing therapy	**1**	**1**	**0**						
Joint sacrificing therapy				*1*	*1*	*0*	*1*	*1*	*0*
Total									
Abrasion arthroplasty				0	4	1	2	4	0
Reconstructive techniques				5	6	10	8	10	12
Retrograde drilling				17	5	6	7	4	6
Osteochondral transplantation				0	6	5	0	3	4
Nonoperative treatment				2	3	1	6	3	1
Joint sacrificing therapy				1	1	1	2	1	1

[a]This table shows how the treatment decisions shifted from MRI alone (gold standard; values in bold) to SPECT-CT alone or MRI + SPECT-CT combined for the 3 raters: A, B, and C. Absolute numbers were given. Nonshifted numbers are italicized.

comparison with MRI only. The analyses of the different aspects of an OCL showed main differences in interpreting the subchondral bone plate and subchondral bone, especially including the disagreement of bone marrow edema in MRI versus the scintigraphic activity in SPECT-CT.

Remarkably, in 48% to 52%, the orthopaedic surgeons changed their personal strategy of treatment as a result of the different information provided by SPECT-CT or SPECT-CT and MRI combined. Magnetic resonance imaging technique is mainly based on tissue differences in hydrogen protons exhibiting different tissue water content; CT scan is based on tissue differences in attenuation coefficients for x-rays exhibiting, for example, calcification of the osseous matrix; and the SPECT scan is based on scintigraphic activity of the osteoblasts, thus providing biological information. So far, Verhagen et al[29] compared MRI and CT scans to invasive ankle arthroscopy. They found MRI to have the highest sensitivity (96%) and helical CT, the highest specificity (99%). According to the authors, CT scans showed 2 advantages: better visibility of cortical outlines and lower risk for overestimation of the lesion in comparison with the bone marrow edema in MRI.[29] However, they did not evaluate the influence of the different imaging techniques on treatment decision making. Pagenstert et al[18] showed that for osteoarthritis of small joints of the foot and ankle, interrater correlation is higher in SPECT-CT than in CT scan or bone scintigraphy alone or in combination. Unfortunately, they did not include MRI in their study, nor did they rate for treatment decision. Because of the high rater-based heterogeneity of the treatment decisions, this study cannot evaluate if the treatment results improve with extended diagnostics of SPECT-CT or

Downloaded from ajs.sagepub.com at Medizinbibliothek on April 21, 2013

the combination of MRI and SPECT-CT. The heterogeneity may be based on the fact that the level of evidence on treatment of OCLs is still very low and completely lacks Level 1 studies.[28] Furthermore, this study reports on differences between SPECT-CT and MRI; however, it does not allow one to differentiate the quantitative influence of the CT scan or the SPECT scan alone on the value of SPECT-CT and its subsequent treatment decision. Image analysis confirms the importance of both aspects; that is, subchondral bone plate and subchondral bone appearance (as related to CT and to scintigraphic activity and activity size) in comparison with that of bone marrow edema (as related to SPECT) leads to completely different interpretation.

While analyzing aspects of an OCL—cartilage, subchondral bone plate, and subchondral bone—one can see the differences found in the subchondral bone plate and subchondral bone, likely making them relevant for the change of treatment decisions. A change of interpretation was seen in 38% to 45% for these 2 tissues, while interpretation changes for the cartilage were 11% to 19%, depending on the criteria. The subchondral bone plate seems to play an important role for the osteochondral joint homeostasis. Degenerative changes can be found in an early stage on the level of the subchondral bone plate, with thickening of the subchondral bone plate and granulation tissue and small sprouting vessels on a histologic level.[25] For OCL, Levine and Kanat[14] came up with a possible pumping mechanism in the pathomechanism of cyst formation. Thus, by small disruptions of the subchondral bone plate, with every movement of the joint, joint fluid may be pumped in the subchondral zone and provoke cyst formation with reactive sclerosis. Consecutively, as shown by Qiu et al,[20] a healing process leads to an excessive bone formation. Berndt and Harty[1] have already shown that osseous changes in OCL of the talus occur in the beginning. Here SPECT-CT may show additional information, as increased osteoblastic activity can be found in advance of morphologic (eg, sclerotic) changes or cyst formation. One might expect that the additional information on the subchondral bone and subchondral bone plate may turn the treatment decision toward techniques that focus more on the osseous level—namely, retrograde drilling or osteochondral transplantation. This is not the case, because all 3 raters chose these techniques 41 times based on MRI and 39 times based on SPECT-CT. Interestingly, for the combination of MRI and SPECT-CT, these 2 techniques were chosen only 24 times; instead, the application of reconstructive techniques increased from 18 times (MRI) and 21 times (SPECT-CT) to 30 times (MRI and SPECT-CT). A possible interpretation could be that the combination, on one hand, makes the OCL look smaller because of the smaller size of scintigraphic activity in SPECT-CT and, on the other, makes the OCL look less destructive.

In evaluating the subchondral involvement in OCL, the discussion is long and unresolved on the relevance and size of bone marrow edema in MRI. Several authors believe that bone marrow edema may lead to overestimation of the lesion.[21,29] Histologically, interstitial plasma-like fluids and increased and abnormal bone formation may be found in sections of bone marrow edema in patients with avascular necrosis or osteoarthritis.[19,27] Necrotic tissue and interstitial fluid can also be found in OCL. As a consequence of a chronic inflammatory process, edema may involve not only the lesion but also its surroundings, therefore possibly making the lesion appear much larger than its actual size.[16] This is relevant to the treatment decision as well as to the clinical outcome, both of which significantly depend on lesion size.[3,11] In the present study, the area of scintigraphic activity is substantially smaller than bone marrow edema in MRI—56% in the coronal plane and 52% in the sagittal plane. Buck et al[2] compared bone marrow edema versus bone scintigraphy in patients with chronic knee pain unaware of a previous trauma. In their study, size of bone marrow edema and semiquantitative tracer uptake did not correlate. Interestingly, they found, in 28% of the patients with bone marrow edema, no tracer uptake at the same location. Similar cases were found in our study. Buck et al also showed that for the knee joint, scintigraphic activity correlates better with pain than bone marrow edema of MRI. Osteoblastic activity can be seen in the scintigraphy. It is accompanied by a release of different cytokines; among them, substance P and bradykinin seem to play an important role.[13,15] Substance P increases the proliferation of osteoblasts but also excites substance P–sensitive nociceptive nerve endings in the subchondral bone.[15] Similar results were found for bradykinin, only stimulating osteoclasts instead of osteoblasts.[13]

An inherent limitation to this study is that neither clinical results nor outcome results were given. Therefore, this study remained a theoretical approach to illuminate treatment decision making. As treatment decisions of the 3 raters could not be applied to 1 patient prospectively, this study does not report clinical data. To include that and demonstrate superiority of one or the other imaging technique on clinical results, we would need to conduct a prospective randomized trial with precisely defined treatment decision criteria and 3 arms (treatment based on MRI, SPECT-CT, or both). Instead, this study aimed to mimic, as closely as possible, the daily clinical decision making based on diagnostic information. Finally, this study concentrated on the OCL itself without addressing further accompanying pathologic abnormalities, such as ligamentous instability, tendon disorders, and hindfoot malalignment.

In conclusion, treatment of OCL of the talus depends on the diagnostic modalities used. Magnetic resonance imaging is the current standard. However, SPECT-CT may provide additional information, predominantly in the interpretation of the subchondral bone plate and the involvement of the subchondral bone. Therefore, we recommend a thorough workup that includes performing MRI and SPECT-CT to make the most well-informed decision toward a treatment plan. Also, there is need for a treatment-relevant classification system and Level 1 evidence studies to further the treatment of OCL of the talus.

REFERENCES

1. Berndt AL, Harty M. Transchondral fractures (osteochondritis dissecans) of the talus. *J Bone Joint Surg Am*. 1959;41:988-1020.

Downloaded from ajs.sagepub.com at Medizinbibliothek on April 21, 2013

2. Buck FM, Hoffmann A, Hofer B, Pfirrmann CW, Allgayer B. Chronic medial knee pain without history of prior trauma: correlation of pain at rest and during exercise using bone scintigraphy and MR imaging. *Skeletal Radiol*. 2009;38:339-347.
3. Choi WJ, Park KK, Kim BS, Lee JW. Osteochondral lesion of the talus: is there a critical defect size for poor outcome? *Am J Sports Med*. 2009;37(10):1974-1980.
4. Cortina JM. What is coefficient alpha? Examination of theory and applications. *J Appl Psychol*. 1993;78:98-104.
5. Cronbach LJ. Coefficient alpha and the internal structure of tests. *Psychometrika*. 1951;16:297-334.
6. DiPaola JD, Nelson DW, Colville MR. Characterizing osteochondral lesions by magnetic resonance imaging. *Arthroscopy*. 1991;7: 101-104.
7. Elias I, Jung JW, Raikin SM, Schweitzer ME, Carrino JA, Morrison WB. Osteochondral lesions of the talus: change in MRI findings over time in talar lesions without operative intervention and implications for staging systems. *Foot Ankle Int*. 2006;27: 157-166.
8. Elias I, Zoga AC, Morrison WB, Besser MP, Schweitzer ME, Raikin SM. Osteochondral lesions of the talus: localization and morphologic data from 424 patients using a novel anatomical grid scheme. *Foot Ankle Int*. 2007;28:154-161.
9. Ferkel RD, Sgaglione NA, DelPizzo W. Arthroscopic treatment of osteochondral lesions of the talus: long-term results. *Orthop Trans*. 1990;14:172-178.
10. Giannini S, Buda R, Vannini F, Di Caprio F, Grigolo B. Arthroscopic autologous chondrocyte implantation in osteochondral lesions of the talus: surgical technique and results. *Am J Sports Med*. 2008;36:873-880.
11. Giannini S, Vannini F. Operative treatment of osteochondral lesions of the talar dome: current concepts review. *Foot Ankle Int*. 2004;25:168-175.
12. Knupp M, Pagenstert GI, Barg A, Bolliger L, Easley ME, Hintermann B. SPECT-CT compared with conventional imaging modalities for the assessment of the varus and valgus malaligned hindfoot. *J Orthop Res*. 2009;27:1461-1466.
13. Kondo A, Togari A. Activation of osteoblastic functions by a mediator of pain, bradykinin. *Biochem Pharmacol*. 2004;68:1423-1431.
14. Levine B, Kanat IO. Subchondral bone cysts, osteochondritis dissecans, and Legg-Calvé-Perthes disease: a correlation and proposal of their possible common etiology and pathogenesis. *J Foot Surg*. 1988;27:75-79.
15. Liu G, Jiang LS, Dai LY. Substance P and its receptors in bone metabolism. *Neuropeptides*. 2007;41:271-283.
16. Nakamae A, Engebretsen L, Bahr R, Krosshaug T, Ochi M. Natural history of bone bruises after acute knee injury: clinical outcome and histopathological findings. *Knee Surg Sports Traumatol Arthrosc*. 2006;14:1252-1258.
17. O'Loughlin PF, Heyworth BE, Kennedy JG. Current concepts in the diagnosis and treatment of osteochondral lesions of the ankle. *Am J Sports Med*. 2010;38(2):392-404.
18. Pagenstert GI, Barg A, Leumann AG, et al. SPECT-CT imaging in degenerative joint disease of the foot and ankle. *J Bone Joint Surg Br*. 2009;91:1191-1196.
19. Plenk H Jr, Hofmann S, Eschberger J, et al. Histomorphology and bone morphometry of the bone marrow edema syndrome of the hip. *Clin Orthop Relat Res*. 1997;334:73-84.
20. Qiu YS, Shahgaldi BF, Revell WJ, Heatley FW. Observations of subchondral plate advancement during osteochondral repair: a histomorphometric and mechanical study in the rabbit femoral condyle. *Osteoarthritis Cartilage*. 2003;11:810-820.
21. Schimmer RC, Dick W, Hintermann B. The role of ankle arthroscopy in the treatment strategies of osteochondritis dissecans lesions of the talus. *Foot Ankle Int*. 2001;22:895-900.
22. Schmid MR, Pfirrmann CWA, Hodler J, Vienne P, Zanetti M. Cartilage lesions in the ankle joint: comparison of MR arthrography and CT arthrography. *Skeletal Radiol*. 2003;32:259-265.
23. Schnell R, Hill PB, Esser E. [Methoden der empirischen Sozialforschung]. 8th ed. Munich, Germany: Oldenourg; 2008.
24. Shearer C, Loomer R, Clement D. Nonoperatively managed stage 5 osteochondral talar lesions. *Foot Ankle Int*. 2002;23:651-654.
25. Shimizu M, Tsuji H, Matsui H, Katoh Y, Sano A. Morphometric analysis of subchondral bone of the tibial condyle in osteoarthritis. *Clin Orthop Relat Res*. 1993;293:229-239.
26. Taranow WS, Bisignani GA, Towers JD, Conti SF. Retrograde drilling of osteochondral lesions of the medial talar dome. *Foot Ankle Int*. 1999;20:474-480.
27. Thiryayi WA, Thiryayi SA, Freemont AJ. Histopathological perspective on bone marrow oedema, reactive bone change and haemorrhage. *Eur J Radiol*. 2008;67:62-67.
28. Valderrabano V, Leumann A. What is the best treatment for ankle osteochondral lesions?In: Wright JG, ed. *Evidence-Based Orthopaedics*. Philadelphia, PA: Saunders WB Co; 2008:462-472.
29. Verhagen RAW, Maas M, Dijkgraaf MGW, Tol JL, Krieps R, Van Dijk NC. Prospective study on diagnostic strategies in osteochondral lesions of the talus: is MRI superior to helical CT? *J Bone Joint Surg Br*. 2005;87:41-46.
30. Verhagen RAW, Struijs PA, Bossuyt PM, Van Dijk CN. Systematic review of treatment strategies for osteochondral defects of the talar dome. *Foot Ankle Clin*. 2003;8:233-242.
31. Wuest W, Kuwert T, Grunewald M, et al. Skeletal SPECT/CT of the peripheral extremities: interdisciplinary approach in orthopaedic disorders. First clinical results. *Cent Eur J Med*. 2007;2:499-510.

For reprints and permission queries, please visit SAGE's Web site at http://www.sagepub.com/journalsPermissions.nav

Downloaded from ajs.sagepub.com at Medizinbibliothek on April 21, 2013

Clinical Anatomy 22:261–266 (2009)

ORIGINAL COMMUNICATION

Radiographic Evaluation of Frontal Talar Edge Configuration for Osteochondral Plug Transplantation

ANDRÉ LEUMANN,[1] MARTIN WIEWIORSKI,[1] THOMAS EGELHOF,[2] HELMUT RASCH,[2] OLAF MAGERKURTH,[2] CHRISTIAN CANDRIAN,[3] DIRK JOHANNES SCHAEFER,[3] IVAN MARTIN,[3] MARCEL JAKOB,[1] AND VICTOR VALDERRABANO[1]*

[1]*Orthopedic Department, University of Basel, Basel, Switzerland*
[2]*Radiology Department, University of Basel, Basel, Switzerland*
[3]*Laboratories for Tissue Engineering, University of Basel, Basel, Switzerland*

For successful reconstruction of osteochondral lesions of the talus, the anatomic configuration of the talar edge must be respected. This study evaluated the radiographic configuration of the talar edge in the anterior-posterior (AP) view by analyzing medial and lateral talar edge angles and radii in 81 patients with a true AP view and without ankle pathology. The mean lateral talar edge angle was 91.8°, and the mean medial talar edge angle was 110.0°. The medial frontal talar edge radius was 4.8 mm and the lateral 3.5 mm, respectively. No correlation between angle and radius was found. These results revealed a significant difference between the medial and the lateral talar edge configuration. This may be due to the three-dimensional function of the human ankle joint. No study so far has addressed these differences radiologically. These differences should be addressed in the reconstruction of osteochondral lesions and be included in the preoperative planning. Clin. Anat. 22:261–266, 2009. © 2008 Wiley-Liss, Inc.

Key words: osteochondral lesion; frontal talar edge; radiologic configuration

INTRODUCTION

Osteochondral lesions (OCLs) of the talus are a frequent cause for chronic ankle pain, typically in young, sports-active patients. With an average incidence of 6.5% after severe ankle sprains, OCLs are often found in soccer, basketball, and orienteering (Verhagen et al., 2005). Besides trauma (Loren and Ferkel, 2002) and ankle ligament instability (Hintermann et al., 2002), both joint malalignment (Pagenstert et al., 2007) and avascular necrosis (Patel et al., 1998) are known to cause OCL.

Anatomically, 99% of talus OCL are located at the talar edge, either (antero)laterally (34–42%) or (postero)medially (58–63%) (Verhagen et al., 2003; Elias et al., 2007). Nowadays, the classification most used comes from Berndt and Harty (1959); Stage I is a subchondral compression, Stage II is an avulsed but attached osteochondral flake, Stage III is a detached but not dislocated osteochondral flake, and Stage IV is a detached and displaced osteochondral fragment (Berndt and Harty, 1959).

Based on these OCL stages, surgical treatment may vary (Giannini and Vannini, 2004) depending on the size of the lesion or the age of the patient. OCL smaller than 1.5 cm^2 can be treated by microfractures (Becher and Thermann, 2005) or retrograde drilling (Kono et al., 2006); lesions larger than 1.5 cm^2 can be treated by autologous chondrocyte implantation (ACI) (Whittaker et al., 2005) or mosaic-

*Correspondence to: Victor Valderrabano, Lower Extremity Orthopedics, Center for Musculoskeletal Care, University of Basel, Spitalstr. 21, 4031 Basel, Switzerland.
E-mail: vvalderrabano@ uhbs.ch

Received 22 May 2008; Revised 10 October 2008; Accepted 18 October 2008

Published online 16 December 2008 in Wiley InterScience (www.interscience.wiley.com). DOI 10.1002/ca.20740

© 2008 Wiley-Liss, Inc.

plasty (Hangody, 2003). Patients younger than 50 years can be treated by microfractures, retrograde drilling, mosaicplasty, or ACI and those older than 50 years by microfractures or, in the case of large defects, by ankle joint replacement or fusion (Giannini and Vannini, 2004). However, none of these various treatment options (Verhagen et al., 2003; Giannini and Vannini, 2004) have shown excellent evidence of efficacy in the literature and none of the treatment options have satisfactorily met all the following important goals: (i) effective pain relief, (ii) restoration of subchondral bone mass and shape, (iii) production of hyaline cartilage for prevention of osteoarthritis (OA), (iv) a graft perfectly fitting the joint contours, and (v) minimal donor-site morbidity. To achieve all of these goals (i–v), tissue engineers and orthopedic and reconstructive surgeons are currently endeavoring to create anatomically well-fitting osteochondral grafts with cultured autologous cells. By this way, joint incongruences, OCL recurrence, and early onset OA may be avoided.

To create such well-fitting, congruent, cultured autologous osteochondral grafts, it is essential to know the dimensions of the medial and lateral talar edge. Whereas the configuration of the talar edge is well described for the sagittal plane (lateral X-rays) (Frigg et al., 2007), no data are available for the even more important talar edge configuration in the coronal plane [anterior-posterior (AP) X-rays].

In view of this, the present study aims to analyze the medial and lateral angular talar edge configuration in the frontal plane (AP X-rays) and the distribution of the individual measurements.

METHODS

The present study was based on 141 consecutive healthy normal subjects who were referred as patients within a data collection period of 3 months to the Department of Radiology. These patients were scheduled for AP and lateral plain ankle radiographs because of clinical hindfoot symptoms. All patients without radiological pathologies, fully able to load the foot, and with good X-ray recording quality were included in the study (81 patients, 57%). Patients were excluded for the following reasons: poor quality of radiographs (24 patients, 17%), acute or healed fracture (21 patients, 15%), ankle or hindfoot OA (14 patients, 10%), ankle dislocation (1 patient, 1%). Finally, 81 radiographs were included for analysis: men: 51, women: 30; mean age: 40.4 years (range: 15–85 years).

Weight-bearing standard AP (exposure from anterior, film posterior) and lateral (exposure from medial, film lateral) radiographs were taken by focusing the X-ray exactly on the center of the ankle joint. Only strictly AP views were accepted, when the joint space for the talo-crural as well as the medial and lateral malleolar joint was projected maximally and symmetrically open, and the medial and lateral talar facets were well aligned and exactly superimposed (Fig. 1). A DICOM/PACS application was used to carry out standardized measurements of the ankle joints on digital X-rays as described by Frigg et al. (2007) and Magerkurth et al. (2006). All ankle radiograph measurements were performed on a radiology workstation with a digital high resolution flat panel system with flat detector technology (Aristos FX®; Siemens, Erlangen, Germany). All X-rays were analyzed by one independent radiologist blinded to all patient data using the DICOM/PACS review application E-Film (Department of Medical Imaging at the University Health Network and Mount Sinai Hospital in Toronto, Canada). All measurements were carried out in calibrated digital zoom without radiological magnification.

The measurements from the lateral X-rays (sagittal plane) have been recently reported by Frigg et al. (2007) in a recently published work.

In this study the following variables were measured in the frontal plane on the AP X-rays (coronal plane; Fig. 1):

- Medial talar edge angle (MTEA): Two lines were adjusted, one to the surface of the talar dome and one to the medial talar surface facing the medial malleolus. The angle between these two lines formed the MTEA (degrees).
- Lateral talar edge angle (LTEA): Two lines were adjusted, one to the surface of the talar dome and one to the lateral talar surface facing the lateral malleolus. The angle between these two lines formed the LTEA (degrees).
- Medial frontal talar edge radius (MFTER): A circle was digitally fitted to the medial talar edge surface. Thus the center of the circle was identified and the radius measured (mm).
- Lateral frontal talar edge radius (LFTER): A circle was digitally fitted to the lateral talar edge surface. Thus the center of the circle was identified and the radius measured (mm).

Statistical differences among both pairs of variables (MTEA vs. LTEA; MFTER vs. LFTER) were determined by the unpaired Student's *t* test. Significance was considered at $P \leq 0.05$. Correlations were determined by the correlation coefficient of Pearson with a confidential interval of 95%. All statistical calculations were performed using SPSS® software (version 12.0; SPSS, Chicago, IL).

RESULTS

Overall results are shown in Table 1. Both the talar edge angle and the frontal talar edge radius showed significant different results from medial to lateral.

At 91.8° the LTEA was nearly parallel to the body sagittal plane, whereas the MTEA was 110.0°. Accordingly, the lateral frontal talar edge is circumscribed with a smaller radius. Because of a small standard deviation, highly significant results could be found from medial to lateral, with small interindividual differences.

No correlation between angle and mortise radius (MTEA and MFTER, and LTEA and LFTER, respectively) was found (Fig. 2).

Age correlation analysis showed no significant correlation ($P > 0.05$) for all variables (Pearson correlation coefficient between 0.05 and 0.22). Analysis for

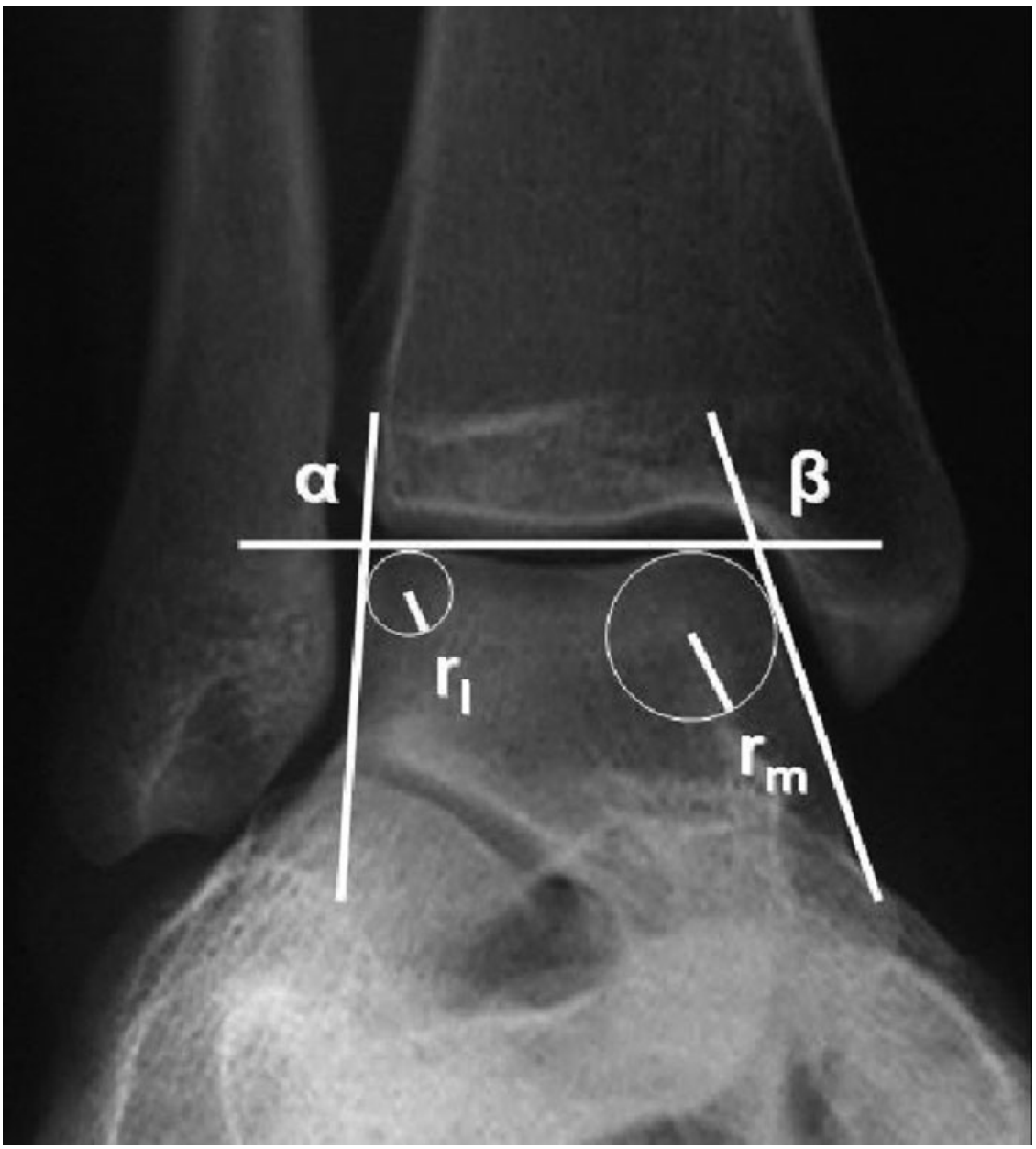

Fig. 1. An AP X-ray with the measured parameters. MTEA: medial talar edge angle (β); LTEA: lateral talar edge angle (α); MFTER: medial frontal talus edge radius (r_m); LFTER: lateral frontal talar edge radius (r_l).

TABLE 1. Results of Measured Variables

	Medial (MTEA, MFTER)		Lateral (LTEA, LFTER)		
	Mean	SD	Mean	SD	*P*
Talar edge angle (°)	110.0	±7.14	91.84	±5.56	<0.0001
Radius of the frontal talus mortise (m)	0.0048	±0.0013	0.0035	±0.0012	<0.0001

MTEA: medial talar edge angle; MFTER: medial frontal talar edge radius; LTEA: lateral talar edge angle; LFTER: lateral frontal talar edge radius; SD: standard deviation.

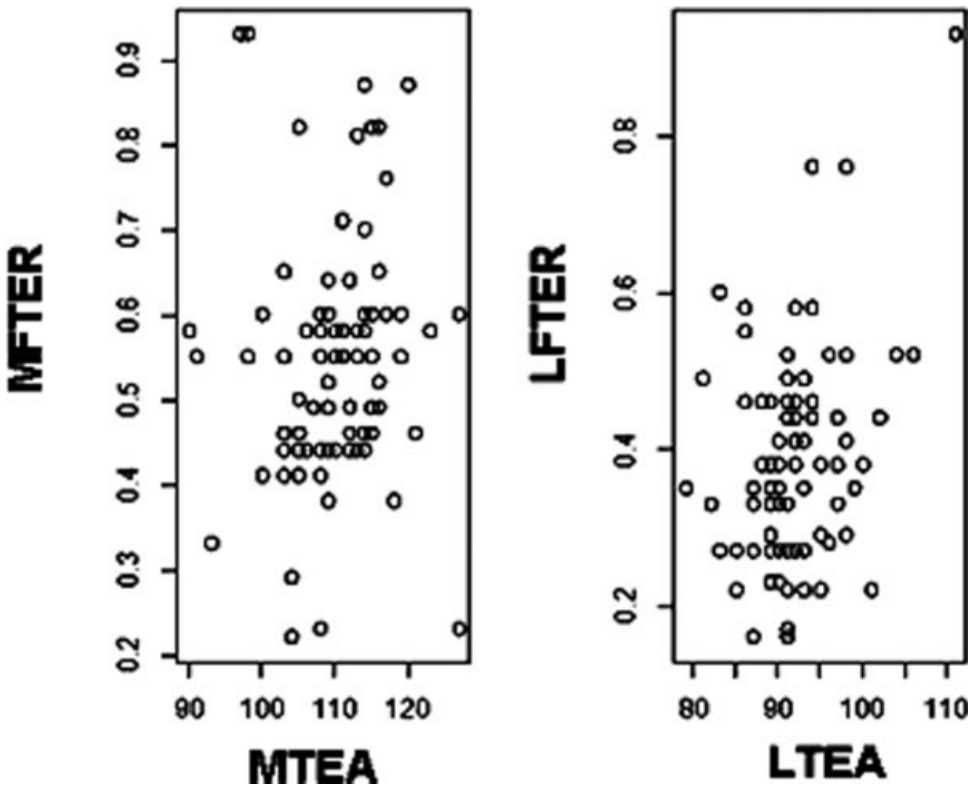

Fig. 2. The relationship of talar edge angle and edge radius. No correlation was found. MTEA: medial talar edge angle; LTEA: lateral talar edge angle; MFTER: medial frontal talus edge radius; LFTER: lateral frontal talar edge radius.

gender differences showed no significant difference for all variables between male and female ($P > 0.05$).

DISCUSSION

OCLs of the talus are common in athletic patients and often located on the medial and lateral talar edge. With the evolving efforts of culturing engineered osteochondral autografts for the treatment of OCL, knowledge about the exact talar edge dimensions is crucial. In summary, the present study provides the exact values for these dimensions. Furthermore, this study showed that there is a significant difference between the medial (MTEA) and lateral (LTEA) talar edge angles as well as between the medial (MFTER) and lateral (LFTER) frontal talar edge radii.

Stagni et al. (2005) evaluated 36 plain radiographs for different biomechanical parameters. They precisely defined the talo-crural joint in the sagittal and frontal planes but did not discuss the MTEA, LTEA, MFTER, and LFTER. They pointed out the importance of semiautomated measurement techniques to improve on older investigations relying on ''free-hand'' measurements (Stagni et al., 2005). Accordingly, our study was performed on fully digitized radiographs in order to minimize measurement mistakes.

All anatomic or radiographic studies so far considered the medial and lateral talus edge as a sharp edge (Reimann et al., 1986; Fessy et al., 1997; Stagni et al., 2005). Obviously, as shown in this study, this is not the case. Mortise radius is found to be 3.5 mm on the lateral side and 4.8 mm on the medial side, respectively. A sharp edge to the talus dome would not be ideal biomechanically. One of the main functions of hyaline cartilage is to provide joint movement with minimal resistance and shear forces. A sharp edge would accumulate shear forces at a high level and lead to early cartilage degeneration. Furthermore, the ankle joint has been described as having a three-dimensional movement (Konradsen and Voigt, 2002; Valderrabano et al., 2003). With sharp edges, this function would be diminished.

Reimann et al. (1986) evaluated 20 ankle specimens postmortem. They did not measure the MTEA and LTEA, but measured the frontal angle between tibial ankle joint surface and the medial malleolar joint surface. Schmidt (1981) found the angle between tibial crural joint facet and medial malleolar joint facet to be 110° (range: 105–113°). Given a constant cartilage layer, this value can be applied to the MTEA. These results concur exactly with our radiological results of a mean of 110.0°. Consistently to the reported mean LTEA of 91.8°, Schmidt (1981) measured the angle between tibial crural joint facet and lateral medial malleolar joint facet to be 91° (range: 88–93°).

Additionally they showed that the medial tibiocrural-malleolar angle (and therefore also the medial and lateral frontal mortise angle) was a constant value along the whole sagittal mortise. This finding allows a two-dimensional measurement in a three-dimensional joint. This will also later simplify preoperative diagnostics and planning.

The present study found significant differences between the medial and lateral talus edge configurations. The explanation for these differences may be seen in the biomechanical function of the ankle joint. Movement of the ankle joint is found to be three-dimensional: dorsiflexion/plantar flexion, inversion/eversion, and internal/external rotation (Konradsen and Voigt, 2002; Valderrabano et al., 2003). In dorsiflexion, the talus is fixed in the malleolar pincette; in plantar flexion, the talus is loose and a spacing of 2–3-mm gaps appear in the ankle joint gutters (Reimann et al., 1986). Therefore, strong ligamentous guidance is important. As the deltoid ligament is stronger than the lateral ligaments, movement of the talus is known to be more fixed on the medial side (Arndt et al., 2004). With a larger MTEA on the medial side, the talus is able to manage a smoother fit to the medial edge of the tibia, and thus there are less joint peak pressures during walking. By this way, the talus can better perform the small but important inversion movement within the ankle joint (Konradsen and Voigt, 2002; Valderrabano et al., 2003).

The treatment of OCLs (e.g., on the talar mortise) can focus on either cartilage repair (Brittberg et al., 1994) or osseous correction (Kono et al., 2006; Pagenstert et al., 2007). Only one technique offers the possibility of performing osteochondral therapy. With the mosaicplasty or the osteochondral autologous transfer system (OATS) technique, a bone plug with hyaline cartilage is harvested from a healthy joint and transferred to the talar mortise (Hangody, 2003). As the knee cartilage has different biomechanical and biochemical properties to the ankle cartilage, limited clinical results have been reported for knee-to-ankle mosaicplasty (Reddy et al., 2007; Haasper et al., 2008). Furthermore, a high donor-site morbidity in the knee has been reported (Reddy et al., 2007). It is known that a difference of 1 mm in joint surface levels is enough to affect clinical outcome adversely and leads to greater local cartilage degeneration (McKinley et al., 2006). Recently, many tissue engineering groups have been trying hard to provide cultured osteochondral autografts for surgeons. Constructing an osteochondral autograft means in vitro rebuilding of an integrated plug of bone and cartilage either by using stem cells or by extracting autologous chondrocytes and osteocytes and transforming them into regrowing cells (Martin et al., 2007). In such constructs a perfect fit is mandatory. This study provides important data (MTEA, LTEA, MFTER, LFTER) for precisely fitting tissue-engineered talar edge osteochondral grafts. In designing osteochondral grafts the question arises whether customized grafts fit the surgeon's need or individual reconstructions are needed. To meet the exact anatomy by customized grafts, based on the results of this study, different sizes have to be claimed, i.e., different sizes in radius for the lateral and medial edges and different sizes in angles for the lateral and medial edges, because these two factors are shown to be independent. In this case, X-ray evaluation may be exact enough for preoperative planning. In the case of individual 3D reconstruction, a 3D preoperative planning tool by CT-scan or MRI is mandatory.

This study may have certain limitations. The evaluation was performed in the frontal plane only. Measurements of the sagittal mortise radius have already been published by Frigg et al. (2007). These authors evaluated lateral radiographs of chronic ligamentous instability of the ankles and of a matched control group. The talar mortise radius was 17.7 mm in the control group.

In this study the mean age of the patients was 40.4 years. This is significantly more than that in a normal osteochondral patient cohort. Verhagen et al. (2003) found a mean age of 28 years. But once adolescence and osseous growth is finished, no changing of the osseous talus shape under physiologic conditions has been reported. The advantages of this study are the large number of patients who are healthy and uninjured, and a consistent quality of recording and data analysis.

REFERENCES

Arndt A, Westblad P, Winson I, Hashimoto T, Lundberg A. 2004. Ankle and subtalar kinematics measured with intracortical pins during the stance phase of walking. Foot Ankle Int 25:357–364.

Becher C, Thermann H. 2005. Results of microfracture in the treatment of articular cartilage defects of the talus. Foot Ankle Int 26:583–589.

Berndt AL, Harty M. 1959. Transchondral fractures (osteochondritis dissecans) of the talus. J Bone Joint Surg Am 41:988–1020.

Brittberg M, Lindahl A, Nilsson A, Ohlsson C, Isaksson O, Peterson L. 1994. Treatment of deep cartilage defects in the knee with autologous chondrocyte transplantation. N Engl J Med 331:889–895.

Elias I, Zoga AC, Morrison WB, Besser MP, Schweitzer ME, Raikin SM. 2007. Osteochondral lesions of the talus: localization and morphologic data from 424 patients using a novel anatomical grid scheme. Foot Ankle Int 28:154–161.

Fessy MH, Carret JP, Bejui J. 1997. Morphometry of the talocrural joint. Surg Radiol Anat 19:299–302.

Frigg A, Magerkurth O, Valderrabano V, Ledermann HP, Hintermann B. 2007. The effect of osseous ankle configuration on chronic ankle instability. Br J Sports Med 41:420–424.

Giannini S, Vannini F. 2004. Operative treatment of osteochondral lesions of the talar dome: Current concepts review. Foot Ankle Int 25:168–175.

Haasper C, Zelle BA, Knobloch K, Jagodzinski M, Citak M, Lotz J, Krettek C, Zeichen J. 2008. No mid-term difference in mosaicplasty in previously treated versus previously untreated patients with osteochondral lesions of the talus. Arch Orthop Trauma Surg 128:499–504.

Hangody L. 2003. The mosaicplasty technique for osteochondral lesions of the talus. Foot Ankle Clin 8:259–273.

Hintermann B, Boss A, Schäfer D. 2002. Arthroscopic findings in patients with chronic ankle instability. Am J Sports Med 30:402–409.

Kono M, Takao M, Naito K, Uchio Y, Ochi M. 2006. Retrograde drilling for osteochondral lesions of the talar dome. Am J Sports Med 34:1450–1456.

Konradsen L, Voigt M. 2002. Inversion injury biomechanics in functional ankle instability: A cadaver study of simulated gait. Scand J Med Sci Sports 12:329–336.

Loren GJ, Ferkel RD. 2002. Arthroscopic assessment of occult intraarticular injury in acute ankle fractures. Arthroscopy 18:412–421.

Magerkurth O, Knupp M, Ledermann H, Hintermann B. 2006. Evaluation of hindfoot dimensions: a radiological study. Foot Ankle Int 27:612–616.

Martin I, Miot S, Barbero A, Jakob M, Wendt D. 2007. Osteochondral tissue engineering. J Biomech 40:750–765.

McKinley TO, Rudert MJ, Tochigi Y, Pedersen DR, Koos DC, Baer TE, Brown TD. 2006. Incongruity-dependent changes of contact stress rates in human cadaveric ankles. J Orthop Trauma 20:732–738.

Pagenstert GI, Hintermann B, Barg A, Leumann A, Valderrabano V. 2007. Realignment surgery as alternative treatment of varus and valgus ankle osteoarthritis. Clin Orthop Relat Res 462:156–168.

Patel DV, Breazeale NM, Behr CT, Warren RF, Wickiewicz TL, O'Brien SJ. 1998. Osteonecrosis of the knee: current clinical concepts. Knee Surg Sports Traumatol Arthrosc 6:2–11.

Reddy S, Pedowitz DI, Parekh SG, Sennett BJ, Okereke E. 2007. The morbidity associated with osteochondral harvest from asymptomatic knees for the treatment of osteochondral lesions of the talus. Am J Sports Med 35:80–85.

Reimann R, Anderhuber F, Gerold J. 1986. The geometry of the human trochlea tali. Acta Anat (Basel) 127:271–278.

Schmidt HM. 1981. Die Artikulationsflächen der Sprunggelenke. Adv Anat Embryol Cell Biol 66:1–79.

Stagni R, Leardini A, Ensini A, Cappello A. 2005. Ankle morphometry evaluated using a new semi-automated technique based on X-ray pictures. Clin Biomech (Bristol, Avon) 20:307–311.

Valderrabano V, Hintermann B, Nigg BM, Stefanyshyn D, Stergiou P. 2003. Kinematic changes after fusion and total replacement of the ankle, Part 1: Range of motion. Foot Ankle Int 24:881–887.

Verhagen RA, Struijs PA, Bossuyt PM, van Dijk CN. 2003. Systematic review of treatment strategies for osteochondral defects of the talar dome. Foot Ankle Clin 8:233–242.

Verhagen RA, Maas M, Dijkgraaf MG, Tol JL, Krips R, van Dijk CN. 2005. Prospective study on diagnostic strategies in osteochondral lesions of the talus. Is MRI superior to helical CT? J Bone Joint Surg Br 87:41–46.

Whittaker JP, Smith G, Makwana N, Roberts S, Harrison PE, Laing P, Richardson JB. 2005. Early results of autologous chondrozyte implantation in the talus. J Bone Joint Surg Br 87:179–183.

Scand J Med Sci Sports 2012: 22: 776–782
doi: 10.1111/j.1600-0838.2011.01309.x

© 2011 John Wiley & Sons A/S

SCANDINAVIAN JOURNAL OF
MEDICINE & SCIENCE
IN SPORTS

Altered cell metabolism in tissues of the knee joint in a rabbit model of Botulinum toxin A-induced quadriceps muscle weakness

A. Leumann[1,2], D. Longino[1], R. Fortuna[1], T. Leonard[1], M. A. Vaz[1,3], D. A. Hart[4], W. Herzog[1]

[1]Human Performance Laboratory, Faculty of Kinesiology, University of Calgary, Alberta, Canada, [2]Orthopaedic Department, University Hospital of Basel, Basel, Switzerland, [3]Exercise Research Laboratory, School of Physical Education, Federal University of Rio Grande do Sul, Rio Grande do Sul, Brazil, [4]McCaig Institute for Bone and Joint Health, Faculty of Medicine, University of Calgary, Alberta, Canada

Corresponding author: Walter Herzog, PhD, Human Performance Laboratory, Faculty of Kinesiology, University of Calgary, 2500 University Drive NW, Calgary, Alberta, Canada T2N 1N4. Tel: +403 220 8525, Fax: +403 284 3553, E-mail: walter@kin.ucalgary.ca

Accepted for publication 27 January 2011

Quadriceps muscle weakness is frequently associated with knee injuries in sports. The influence of quadriceps weakness on knee joint homeostasis remains undefined. We hypothesized that quadriceps weakness will lead to tissue-specific alterations in the cell metabolism of tissues of the knee. Quadriceps weakness was induced with repetitive injections of Botulinum toxin A in six 1-year-old New Zealand White rabbits for 6 months. Five additional animals served as controls with injections of saline/dextrose. Muscle weakness was assessed by muscle wet mass, isometric knee extensor torque, and histological morphology analysis. Cell metabolism was assessed for patellar tendon, medial and lateral collateral ligament, and medial and lateral meniscus by measuring the total RNA levels and specific mRNA levels for collagen I, collagen III, MMP-1, MMP-3, MMP-13, TGF-β, biglycan, IL-1, and bFGF by reverse transcription and polymerase chain reaction. While the total RNA levels did not change, tissue-specific mRNA levels were lower for relevant anabolic and catabolic molecules, indicating potential changes in tissue mechanical set points. Quadriceps weakness may lead to adaptations in knee joint tissue cell metabolism by altering a subset of anabolic and catabolic mRNA levels corresponding to a new functional and metabolic set point for the knee that may contribute to the high injury rate of athletes with muscle weakness.

The knee is one of the most frequently affected joints in sports injuries. Soccer, skiing, American football, volleyball, and ice hockey as well as many other sports have been reported to represent high-risk activities for knee-specific injuries. Kujala et al. (1995) surveyed more than 50 000 sports injuries, and found that 11–22% occurred at the knee, another 2–11% were located in the thigh, and a further 2–6% in the lower leg. Other authors report a range of approximately 25–46% of all sports injuries located at the knee (Chan et al., 1993; Lindenfeld et al., 1994).

Etiologically, several risk factors for knee injuries have been identified including previous injuries, altered kinematics, and proprioception, genetics, muscle weakness, and instability, to name but the most important (Walden et al., 2006). Among these factors, muscle weakness is probably the least understood. Muscle weakness is of primary importance for performance in strength and endurance sports. Furthermore, the focus in the prevention and rehabilitation of sports injuries is based on limiting muscle weakness (Tsepsi et al., 2006). Muscle contraction and activity loads joints, and altered loading caused by muscle weakness might affect all structures of the joint and may hold the key to understanding the relationship between muscle weakness and joint injury. Therefore, this study was aimed at elucidating the influence of Botulinum toxin type-A (BTX-A)-induced quadriceps muscle weakness on knee joint homeostasis.

As it is not easy to address this question in a non-invasive human model, we chose to work with an animal model. The BTX-A-induced muscle weakness model in the rabbit is a well-described and accepted model of chronic muscle weakness (Longino et al., 2005a ,b). BTX-A is a protein that blocks the release of acetylcholine from the pre-synaptic terminal at the neuromuscular junction (Kao et al., 1976). The decrease of excitation leads to a loss of force that is dose-dependent and can be regulated easily (Longino et al., 2005a, b).

To the best of our knowledge, the influence of muscle weakness on joint structures such as tendons, ligaments, and menisci has not been studied systematically. We hypothesized that muscle weakness leads

to changes in knee joint homeostasis evidenced by alterations to cellular metabolism for tissue-specific genes. These alterations may ultimately lead to weakened joint structures and their responses to mechanical stresses, and place them at an increased risk for knee injuries.

Therefore, we examined the effects of quadriceps weakness on adaptive responses of knee tissues by assessing mRNA levels for a number of relevant molecules in the patellar tendon (PT), the medial (MCL) and lateral (LCL) collateral ligament, and the medial (MM) and lateral menisci (LM) in a BTX-A-induced muscle weakness model in the rabbit.

Methods

Animals and animal injections

Eleven 1-year-old female New Zealand White rabbits (weight: average, 5.1 kg, range, 4.9–5.5 kg; Riemen's Furriers, St. Agatha, Ontario, Canada) were used for this study; six animals served as experimental animals and received unilateral injections of BTX-A. Five age- and sex-matched rabbits served as controls and received a sham injection using the same injection protocol as the test group rabbits. Experiments were approved by the local Animal Care Committee. Housing and nutrition were provided in accordance with the Canadian Council on Animal Care Guidelines and allowing for normal activity.

For the study duration of 6 months, the experimental hindlimb was injected monthly with BTX-A (BOTOX, Allergan Inc., Toronto, Ontario, Canada). Each month, 3.5 U/kg were injected in three different lines along the thigh – medial, central, and lateral – corresponding to the vastus medialis muscle, rectus femoris muscle, and vastus lateralis muscle. Before injection, rabbits were sedated with a 0.18 mL subcutaneous injection of Atravet (10 mg/mL) (acepromazine, Ayerst Laboratories, Montreal, Quebec, Canada). For the control rabbits, sham injections of equal volumes of a 0.9% sodium/5% dextrose solution were performed. The results for the contralateral limb of the BTX-A-treated animals were not included in the analysis, as the literature would suggest that the contralateral side is not an appropriate normal control as it may be affected by the intervention (Radhakrishnan et al., 2003; Lee et al., 2009).

Muscle assessments

For the final tests at the end of the 6-month experimental period, a nerve cuff electrode was implanted under general anesthesia on the femoral nerve of the experimental and control animals to allow for maximal electrical stimulation of the knee extensors. Pelvis and femoral condyles were fixed with bone pins to a stereotaxic frame and the tibia was restrained to an instrumented bar anterior to the ankle at angles of 80°, 100°, and 120°, using a custom-built force sensor (Vishay 2100 amplifier, Vishay Intertechnology, Malvern, Pennsylvania, USA). Information was recorded using Windaq data collection software (collection card, DI-400, 12 bit; Dataq Instruments, Akron, Ohio, USA). Maximal isometric measurements were achieved by stimulating the femoral nerve supra-maximally (frequency, 100 Hz, stimulation duration, 500 ms, individual pulse duration, 0.1 ms, rectangular square wave, Grass 8800 stimulator; Astro-Med Inc., Longueil, Quebec, Canada). Between contractions, rest periods of at least 1 min were given to prevent fatigue. Torque results were normalized by the weight of the rabbits.

Following torque measurements, rabbits were euthanized with Euthanyl (MTC Pharamceuticals, Cambridge, Ontario, Canada). The individual heads of the quadriceps were dissected (rectus femoris, vastus medialis, small vastus lateralis, large vastus lateris, and vastus intermedius muscle) and wet mass was measured using a commercial balance with a resolution of 0.001 g. The large vastus lateralis muscle was then embedded in paraffin for histological analysis (Leica TP 1020, Leica Microsystems, Heerbrugg, Switzerland) and cut cross-sectionally with a microtome (Leica RM 2165, Leica Microsystems) into 0.8 μm sections. Every 16 μm, a 0.8 μm section was used for staining with hematoxylin–eosin (Fisher Scientific, Wohlen, Switzerland), digitized by × 5 magnification using an Axionstar *plus* (Carl Zeiss, Jena, Germany) microscope, and analyzed using a customized Matlab program (Matlab 7.6.0, R2009a) to calculate the relative area of the contractile and non-contractile materials.

Total RNA isolation

For molecular analysis, tissues were immediately harvested, weighed, flash-frozen in liquid nitrogen, and subsequently stored at − 80 °C. The tissues harvested were the PT, MCL, LCL, MM, and LM. All tissues were subjected to RNA isolation using the TRIspin method and total RNA was quantified using the SYBR Green reagent (Molecular Probes, Eugene, Oregon, USA) (Reno et al., 1997).

Reverse transcription (RT) and polymerase chain reaction (PCR)

Total RNA (1 μg) of each sample was initially reverse transcribed RT with random RT primers using a Qaigen Omniscript kit (Qaigen Inc., Mississauga, Ontario, Canada). All samples for a given tissue were subjected to RT at the same time to avoid potential variability. mRNA levels for specific molecules were assessed using validated primer sets for rabbits (Hart & Achari, 2010). All samples for a given tissue were subjected to optimized PCR conditions at the same time to avoid potential variability. Assessments of all no RT controls were negative for genomic DNA contamination of RNA preparations. A subset of RNA samples from each tissue was subjected to RT a second time and re-analysis confirmed the original findings. The mRNA levels for the following molecules were assessed: biglycan, collagen I, collagen III, MMP-1, MMP-3, MMP-13, bFGF, TGF-β1, and IL-1. All results were normalized to the housekeeping gene 18S as described previously (Hart & Achari, 2010). We considered these molecules a subset of anabolic and catabolic/inflammatory molecules that are relevant for the maintenance of the mechanical properties of the tissues.

Statistical methods

In order to detect differences between experimental and control tissues, Student's *t*-tests and one-way analysis of variances were used. The level of significance was set at $\alpha < 0.05$. Analysis was performed using Microsoft Office Excel 2007 and SPSS 12.0.

Results

Quadriceps muscle weakness

The administration of BTX-A led to significant muscle weakness in all the parameters assessed: muscle wet mass, isometric knee extensor torque, and contractile area. Therefore, we were successful in creating a chronic muscle weakness model.

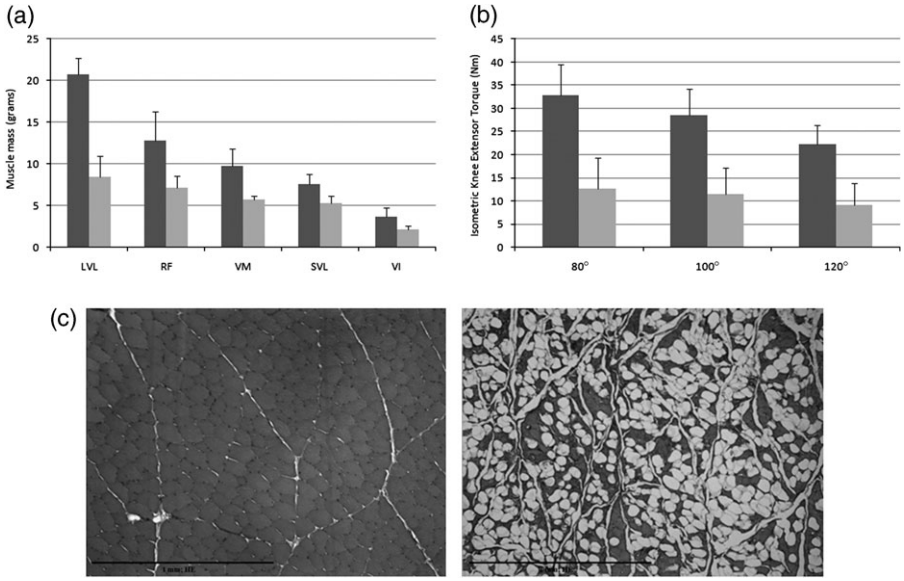

Fig. 1. (a) Muscle wet mass. Absolute values (g) and standard deviation are shown for control animals (dark bars) and Botulinum toxin type-A (BTX-A) animals (bright bars). All differences were found to be significant ($P<0.01$). LVL, large vastus lateralis; RF, rectus femoris; VM, vastus medialis; SVL, small vastus lateralis; VI, vastus intermedius. (b) Isometric knee extensor torque. Absolute values corrected for the rabbit total weight (N m/kg) are shown for control animals (dark bars) and BTX-A animals (bright bars) for three different knee joint angles (extended leg = 180°). All differences were found to be significant ($P<0.001$). (c) Histological muscle morphology of the large vastus lateralis. The left picture (control muscle) shows predominantly contractile material (red staining) while the right picture (experimental muscle, BTX-A injected) shows substantial loss of contractile material that is replaced primarily by fat tissue (white). Hematoxylin–eosin staining, × 5 magnification.

The mean wet mass for the total quadriceps group (-47.3%; $P<0.01$), as well as for each individual quadriceps muscle ($P<0.01$), was significantly smaller for the experimental compared with the control group rabbits [Fig. 1(a)].

The isometric knee extensor torques were significantly ($P<0.001$) reduced for each knee joint angle for the experimental compared with the control group animals [Fig. 1(b)].

Histological analysis of the vastus lateralis revealed that it consisted of 96.9% contractile material for the control group animals, while it only contained 43.7% contractile material after 6 months of muscle weakness in the experimental group animals [$P<0.001$; Fig. 1(c)]. The non-contractile material in the experimental muscles consisted of dense connective tissue and fat.

Total RNA yields and specific mRNA levels

The total RNA levels in tendons, ligaments, and menisci did not decrease in general, but mRNA levels for specific molecules were significantly decreased [Fig. 2(a)].

Experimental group rabbits showed significantly reduced mRNA levels for specific anabolic and catabolic molecules [Fig. 2(b) and (c)].

The mRNA alterations detected in the PT, which is directly influenced by quadriceps muscle weakness, were similar to those in the indirectly affected tissues of the knee for the major anabolic (collagen I, collagen III, TGF-β) and the major catabolic (MMP-1, MMP-3, MMP-13) molecules assessed.

Discussion

In this study, we induced long-term quadriceps weakness in a rabbit model to simulate the loss of force associated with a muscle injury or with aging. Weakening the quadriceps muscle with BTX-A led to changes in cellular metabolism (e.g. mRNA levels) for specific genes that are relevant for the mechanical properties of the tissues, but did not change the general metabolism of cells (e.g. total RNA levels). These results indicate that athletes experiencing muscle weakness may be potentially more susceptible to knee injuries due to such changes as several studies suggest a correlation of both mRNA levels to protein translation and biomechanical properties (Rowe et al., 1978; Sun & Yokota, 2002).

Muscle weakness is a frequent associate of muscle injury (Stauber, 2004), muscular imbalance (Myer et al., 2009), knee joint injuries [e.g. anterior cruciate ligament (ACL) rupture] (Hart et al., 2010), and aging. Muscle weakness induced by repetitive BTX-A injections was confirmed in this study. Muscle mass diminished by 47%, and maximal knee extensor

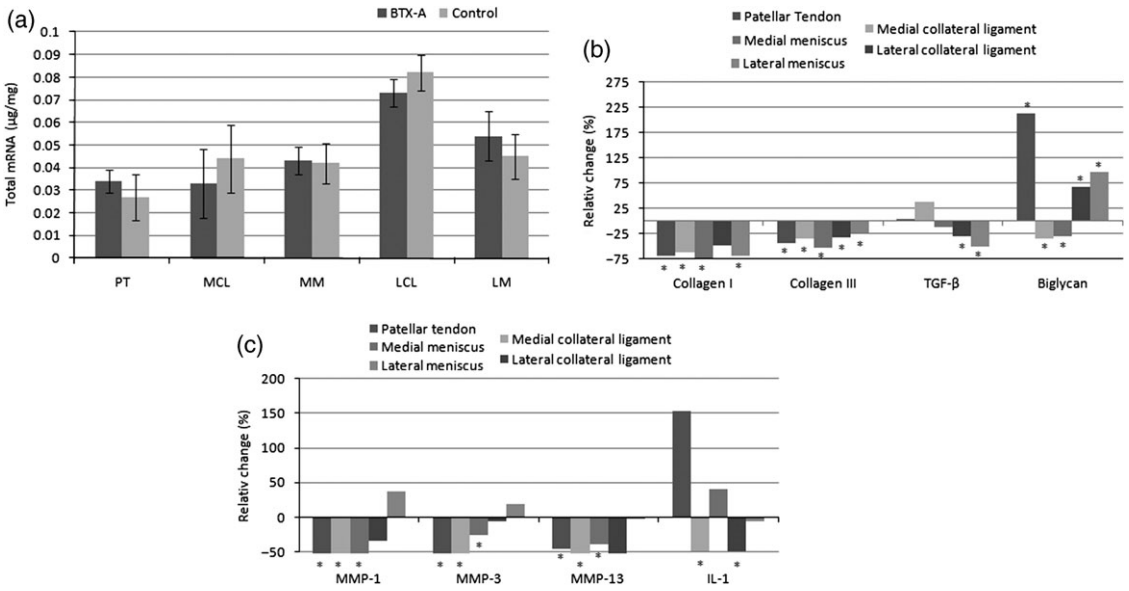

Fig. 2. (a) Total mRNA levels. Total mRNA (µg/mg) levels for Botulinum toxin type-A (BTX-A) and control animals. No significant differences ($P > 0.05$) were found for general cell metabolism. PT, patellar tendon; MCL, medial collateral ligament; MM, medial meniscus; LCL, lateral collateral ligament; LM, lateral meniscus. (b) mRNA levels of anabolic factors. Relative changes (%) of BTX-A animals in comparison with the control animals are shown. Significant differences are indicated with $^*P < 0.05$. (c) mRNA levels of catabolic factors. Relative changes (%) of BTX-A animals in comparison with the control animals are shown. Significant differences are indicated with $^*P < 0.05$.

torques decreased 59–61%. It has been shown previously that BTX-A-induced muscle weakness is approximately constant after 1 month (Longino et al., 2005a, b; Rehan Youssef et al., 2009). However, little is known regarding histological changes in the target muscles. We found that part of the muscle weakness was likely a result of a loss of contractile material in the target muscles. The present results imply that BTX-A treatment does not only lead to blockage of the pre-synaptic exocytosis of acetylcholine storing vesicles (Kao et al., 1976) but also results in long-term structural changes in BTX-A-treated muscles. In the absence of muscle contraction, the contractile material disappears and the tissue undergoes fatty and fibrous degeneration.

To our knowledge, no studies have reported on the adaptation of joint tissues in humans or animal models to chronic *in vivo* muscle weakness. In contrast, several studies analyzed adaptations of joint tissues to increased muscle load or increased muscle strength. After an acute bout of exercise, mRNA levels for collagen I and collagen III are rapidly down-regulated in tendon tissue (Sullivan et al., 2009). In short-term recurrent or cyclic loading, it was found that protein synthesis was up-regulated (Miller et al., 2005; Heinemeier et al., 2007), while mRNA levels for catabolic factors, such as collagenase I (MMP-I), were down-regulated in tendons (Wren et al., 1998; Arnoczky et al., 2007). Finally, chronic loading resulted in an up-regulation of both anabolic and catabolic factors in tendons, indicating that chronic loading produces a new steady-state homeostasis that is characterized by an increase in tissue turnover (Archambault et al., 2001).

The current results suggest a response that is opposite to that associated with chronic loading of connective tissues. Repetitive injections of BTX-A led to prolonged muscle weakness and to depressed mRNA levels for both anabolic and catabolic factors in the PT, the MCL and LCL, and the MM and LM. Such down-regulation of mRNA levels for a subset of anabolic and catabolic factors indicates that prolonged muscle weakness may produce a selective depression in structural tissue homeostasis leading to a new integrated set point while the total cell metabolism remains unchanged. The fact that the adaptations of the PT, whose mechanical environment may be directly related to muscle strength, are not overtly different from those of the ligaments and menisci, may require invoking alternative hypotheses, including that the detected changes may be due to an adaptive alteration in joint homeostasis and not muscle weakness directly (Frank et al., 2004).

The results of this study suggest a potential explanation for the increased risk of knee injury associated with muscle weakness (Fig. 3). Muscle weakness may be induced by many factors such as persistent weakness after muscle injury, muscular imbalance, knee joint injuries, arthrogenic muscle inhibition, neuromuscular dysfunction, and aging (Lewek et al., 2002; Palmieri-Smith et al., 2008). As a result of chronic muscle weakness, matrix and cell regulatory molecules may be depressed. Such selective decreases in cell metabolism could lead to

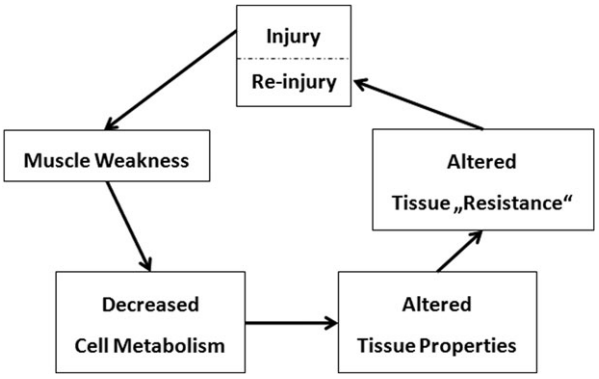

Fig. 3. New pathomechanism of injury proneness. For details, see text.

decreased tissue properties such as reduced failure strain and strength, and decreased rates of tissue adaptation and regeneration (Rowe et al., 1978; Sun & Yokota, 2002). Therefore, the prevention and rehabilitation of muscle weakness should not only include muscle strength training but also address the affected joints in order to facilitate adaptation to a new level of joint homeostasis.

A weakness of the present study is that we cannot unequivocally relate the loss of muscle strength to the changes in knee tissue cell metabolism. Variables other than muscle weakness may have influenced the results. For example, BTX-A could have affected the tissues of the knee directly and acted intraarticularly or in the peri-articular tissues either by direct diffusion of BTX-A (Yaraskavitch et al., 2008) or by neuronal transport (Antonucci et al., 2008). BTX-A may then have acted either as a direct signaling molecule for tenocytes and fibrocytes or as a toxin. However, if this scenario had occurred, it would be difficult to explain why tissue-specific mRNA levels were altered, but the total cell metabolism was not overtly affected. Also, there are no studies reporting the direct effects of BTX-A on tenocytes or fibrocytes, thereby further eliminating this possibility.

A second possibility is that BTX-A affects knee joint proprioception by altering afferent information from the muscle spindles of the quadriceps muscle. The magnitude of this effect would be questionable as proprioception of other knee joint muscles, as well as cutaneous, ligamentous, and capsular proprioceptive inputs, would likely have remained unaffected. Furthermore, the importance of afferent joint feedback to the maintenance of normal joint homeostasis is not known.

Finally, BTX-A-induced muscle weakness may promote disuse due to inactivity. This mimics the situation of an injured athlete where the injury itself leads to loss of strength (in this study produced by BTX-A injections), but the reduction of training because of the injury may lead to another muscular disuse. In this study, we measured the direct loss of strength. However, we did not measure activity in the experimental animals nor did we perform gait analyses. However, gait analyses on identically treated animals have been performed before (Longino et al., 2005a) and showed loss of push off force in the vertical ground reaction forces correlating to the reduced quadriceps muscle strength, but no changes in the horizontal ground reaction forces, indicating that no additional instability or disuse occurred, thus suggesting that the remnant forces in the quadriceps muscles using our BTX-A injection protocol and all the other muscles controlling the knee joint were sufficient to allow animals to locomote essentially unimpeded. Furthermore, the constant body weight of the experimental animals and the lack of signs of illness provide further evidence that an overt disuse did not occur during the treatment protocol. It is fairly well accepted among veterinary doctors that animals that are restricted in their daily life (e.g. less hopping activity) show changes of body weight. On the other hand, Fortuna et al. (2011) showed that BTX-A injections in one hindlimb also led to changes in muscular strength and contractile properties in the contralateral hindlimb either by direct action of the BTX-A or by atrophy-induced muscle disuse. Therefore, in order to exclude the ''contralateral limb effect,'' they did not serve as controls in this study, but a separate set of animals injected with saline/dextrose were used as sham controls. Summarizing, it remains unknown whether the observed effects on knee tissue mRNA levels were due to a general change in knee joint homeostasis associated with disuse or were directly caused by changes in muscle tension due to the BTX-A-induced muscle weakness. It is important to note that ultimately disuse and loss of muscle strength will cause reduced joint loading.

The current study has additional limitations. The number of subjects was low. Nevertheless, statistical significance was reached, thereby avoiding possible type II statistical errors. The range of molecules assessed at the mRNA level was broad, but not expansive. Further characterization of a more complete set of molecules is required, perhaps using a rabbit-specific gene array that would provide conclusions to be drawn regarding how extensive the mRNA changes were following BTX-A treatment. Also, a longer time course of muscle weakness may be needed to establish whether the set point reached after 6 months is indeed stable or whether the alterations become more severe over time. Furthermore, an assessment of changes in mRNA levels without a parallel assessment of structural and biomechanical changes is a limitation that will have to be addressed in the future. However, a main thrust of this work will be to link the findings of this animal model to muscle weakness in athletes. In addition, the reduction of muscle strength by 60% is severe. It

remains unknown whether the same changes to knee tissues would occur following a less severe strength reduction. Also, it would be important to determine whether the changes in tissue response can be reversed by rehabilitation and training.

Perspectives

In conclusion, the present study showed that BTX-A-induced muscle weakness leads to altered cell regulation in the PT, MCL and LCL, and the MM and LM, leading to depressed mRNA levels for a subset of anabolic and catabolic molecules. These findings suggest that chronic muscle weakness that is frequently associated with muscle injuries, muscular imbalance, knee joint injuries (e.g. ACL rupture), and aging may lead to a new steady state for joint homeostasis and potentially weakens the mechanical properties of these structures. Therefore, adaptations of knee joint tissues secondary to muscle weakness must be addressed in the rehabilitation of athletes and in the prevention of knee joint injuries.

Key words: Botulinum toxin A, quadriceps muscle weakness, joint homeostasis, molecular metabolism, re-injury in sports.

Acknowledgements

This work was supported by the CIHR, the Canada Research Chair Program (W. H.), the Alberta Heritage Foundation for Medical Research, and the AHFMR Team Grant for Osteoarthritis. Financial support was provided by the Swiss National Foundation (PBBEP3-125614) and the Swiss Orthopaedic Society (A. L.), by the Calgary Foundation-Grace Glaum Professorship (D. A. H.), and by CAPES-Brazil and UFRGS-Brazil (R. F. and M. V.). The authors thank Carol Reno for excellent technical assistance in the RT-PCR aspects of the study.

Disclosures: None.

References

Antonucci F, Rossi C, Gianfranseschi L, Rossetto O, Caleo M. Long-distance retrograde effects of Botulinum neurotoxin A. J Neurosci 2008: 28: 3689–3696.

Archambault JM, Hart DA, Herzog W. Response of rabbit Achilles tendon to chronic repetitive loading. Connect Tissue Res 2001: 42: 13–23.

Arnoczky S, Lavagnino M, Egerbacher M, Caballero O, Garner K. Matrix metalloproteinase inhibitors prevent a decrease in the mechanical properties of stress-deprived tendons. Am J Sports Med 2007: 35: 763–769.

Chan KM, Yuan Y, Li CK, Chien P, Tsang G. Sports causing most injuries in Hong Kong. Br J Sports Med 1993: 27: 263–267.

Fortuna R, Aurelio Vaz M, Rehan Youssef A, Longino D, Herzog W. Changes in contractile properties of muscles receiving repeat injections of Botulinum toxin (Botox). J Biomech 2011: 44: 39–44.

Frank CB, Shrive NG, Boorman RS, Lo IK, Hart DA. New perspectives on bioengineering of joint tissues: joint adaptation creates a moving target for engineering replacement tissues. Ann Biomed Eng 2004: 32: 458–465.

Hart DA, Achari Y. Alterations to cell metabolism in connective tissues of the knee after ovariohysterectomy in a rabbit model: are there implications for the post-menopausal athlete? Br J Sports Med 2010: 44: 867–871.

Hart JM, Pietrosimone B, Hertel J, Ingersoll CD. Quadriceps activation following knee injuries: a systematic review. J Athl Train 2010: 45: 87–97.

Heinemeier KM, Olesen JL, Haddad F, Langberg H, Kjaer M, Baldwin KM, Schierling P. Expression of collagen and related growth factors in rat tendon and skeletal muscle in response to specific contraction types. J Physiol 2007: 582: 1303–1316.

Kao I, Drachman DB, Price DL. Botulinum toxin: mechanism of presynaptic blockade. Science 1976: 193: 1256–1258.

Kujala UM, Taimela S, Antti-Poika I, Orava S, Tuominen R, Myllynen P. Acute injuries in soccer, ice hockey, volley-, basketball, judo, and karate: analysis of national registry data. Br Med J 1995: 311: 1465–1468.

Lee M, Gandevia SC, Carroll TJ. Unilateral strength training increases voluntary activation of the opposite untrained limb. Clin Neurophysiol 2009: 120: 802–808.

Lewek M, Rudolph K, Axe M, Snyder-Mackler L. The effect of insufficient quadriceps strength on gait after anterior cruciate ligament reconstruction. Clin Biomech 2002: 17: 56–63.

Lindenfeld TN, Schmitt DJ, Hendy MP, Mangine RE, Noyes FR. Incidence of injury in indoor soccer. Am J Sports Med 1994: 22: 364–371.

Longino D, Frank C, Herzog W. Acute Botulinum toxin-induced muscle weakness in the anterior cruciate ligament-deficient rabbit. J Orthop Res 2005a: 23: 1404–1410.

Longino D, Frank C, Leonard TR, Vaz MA, Herzog W. Proposed model of Botulinum toxin-induced muscle weakness in the rabbit. J Orthop Res 2005b: 23: 1411–1418.

Miller BF, Olesen JL, Hansen M, Dossing S, Crameri RM, Welling RJ, Langberg H, Flyvberg A, Kjaer M, Babraj JA, Smith K, Rennie MJ. Coordinated collagen and muscle protein synthesis in human patella tendon and quadriceps muscle after exercise. J Physiol 2005: 567: 1021–1033.

Myer GD, Ford KR, Barber Foss KD, Liu C, Nick TG, Hewett TE. The relationship of hamstrings and quadriceps strength to anterior cruciate injury in female athletes. Clin J Sports Med 2009: 19: 3–8.

Palmieri-Smith RM, Thomas AC, Wojtys EM. Maximizing quadriceps strength after ACL reconstruction. Clin Sports Med 2008: 27: 405–424.

Radhakrishnan R, Moore SA, Sluka KA. Unilateral carrageenan injection into muscle or joint induces chronic bilateral hyperalgesia in rats. Pain 2003: 104: 567–577.

Rehan Youssef A, Longino D, Seerattan R, Leonard T, Herzog W. Muscle weakness causes joint degeneration in rabbits. Osteoarthritis Cartilage 2009: 17: 1228–1235.

Reno C, Marchuk L, Sciore P, Frank CB, Hart DA. Rapid isolation of total RNA from small samples of hypocellular, dense connective tissue. Biotechniques 1997: 22: 1082–1086.

Rowe DW, Moen RC, Davidson JM, Byers PH, Bornstein P, Palmiter RD. Correlation of procollagen mRNA levels in normal and transformed chick

embryo fibroblasts with different rates of procollagen synthesis. Biochemistry 1978: 17: 1581–1590.
Stauber WT. Factors involved in strain-induced injury in skeletal muscles and outcomes of prolonged exposures. J Electromyogr Kinesiol 2004: 14: 61–70.
Sullivan BE, Carroll CC, Jemiolo B, Trappe SW, Magnusson SP, Dossing S, Kjaer M, Trappe TA. Effect of acute resistance exercise and sex on human patellar tendon structural and regulatory mRNA expression. J Appl Physiol 2009: 106: 468–475.
Sun HB, Yokota H. Reduction of cytokine-induced expression and activity of MMP-1 and MMP-13 by mechanical strain in MH7A rheumatoid synovial cells. Matrix Biol 2002: 21: 263–270.
Tsepsi E, Vagenas G, Ristanis S, Georgoulis AD. Thigh muscle weakness in ACL-deficient knees persist without structured rehabilitation. Clin Orthop Relat Res 2006: 450: 211–218.
Walden M, Haegglund M, Ekstrand J. High risk of new knee injury in elite footballers with previous anterior cruciate ligament injury. Br J Sports Med 2006: 40: 158–162.
Wren TAL, Beaupre GS, Carter DR. A model for loading-dependent growth, development, and adaptation of tendons and ligaments. J Biomech 1998: 31: 107–114.
Yaraskavitch M, Leonard T, Herzog W. Botox produces functional weakness in non-injected muscles adjacent to the target muscle. J Biomech 2008: 41: 897–902.

4 Zusammenfassung und Ausblick

Zusammenfassung

Die vorliegende Arbeit befasst sich mit anatomischen, biomechanischen und klinischen Aspekten von osteochondralen Läsionen (OCL) am Talus. Diese stellen eine grosse klinische Herausforderung dar, betreffen sie doch junge, sportlich aktive Patienten. Chronische Schmerzen, eine eingeschränkte Belastbarkeit des Fusses bis hin zum Karriereende eines Sportlers sind die Konsequenzen. Ein besseres Verständnis von Pathomechanismen, insbesondere den anatomischen Verhältnissen und der Gelenksbiomechanik, aber auch eine verbesserte Diagnostik sollen dazu beitragen, die Therapiewahl besser auf jeden einzelnen Patienten zu individualisieren, um damit ein besseres Outcome zu erzielen. Die Gelenksbiomechanik ist die zentrale Regelgrösse in der Homöostase eines Gelenks, weshalb das Gelenk funktionell als Organ betrachtet werden kann („joint as an organ concept"). Dies ist für das Verständnis der Komplexität einer osteochondralen Läsion wichtig.

Die vorliegende Arbeit ist in 4 Originalartikel gegliedert. *Im ersten Artikel* wurde die Dichteverteilung der subchondralen Platte (Grenzlamelle) verglichen mit deren mechanischer Indentationskraft und die typischen Verteilungsmuster analysiert. Dabei zeigten sich zwei typische Verteilungsmuster, welche entweder mono- oder bizentrische Maxima zeigten. Diese korrelieren mit den Lokalisationen osteochondraler Läsionen. *Im zweiten Artikel* wurde die Talusdomkonfiguration radiologisch analysiert, um ein Grundlage zu schaffen für die Produktion möglicher Knorpel-Knochen-Ersatzkonstrukte als Therapie von OCL. Dabei zeigte sich wenig Variabilität interindividuell, aber signifikante Unterschiede der medialen zur lateralen Talusdomkante. *Im dritten Artikel* wurde das SPECT-CT (Single photon emission computed tomography,-computed tomography) als neues Diagnostikum bei OCL dem MRI (magnet resonance imaging) gegenübergestellt und es konnte gezeigt werden, dass die Interpretation der Läsion vor allem bezüglich des subchondralen Knochens und der Grenzlamelle deutlich variierte. Dies führte in über 50% der Fälle zu einem Wechsel der Therapiestrategie. *Im vierten Artikel* wurde dem Joint as an Organ-Konzept weiter auf den Grund gegangen. Hierbei wurde im Kaninchenmodell eine Muskelatrophie induziert und molekularbiologisch die Veränderungen im mRNA steady state anderer gelenksbeteiligter Gewebe bestimmt. Dabei konnte gezeigt werden, dass in einem chronischen Modell ein neuer steady state erreicht werden kann. Eine ähnliche Situation findet sich auch bei OCL, bei denen eine ligamentäre Instabilität sehr oft miteinhergeht, welche wieder eine Muskelatrophie induzieren kann.

Ausblick

Diese Arbeit soll zum Verständnis osteochondraler Läsionen beitragen, wird aber mit Sicherheit auch die Grundlage für weitere anatomische, biomechanische und klinische Forschungsarbeiten darstellen. Osteochondrale Läsionen stellen nach wie vor eine grosse medizinische Herausforderung dar. Die perfekte Therapie – eine restitutio ad integrum – ist bislang nicht möglich. Dies hat vielleicht einerseits damit zu tun, dass die therapeutischen Möglichkeiten noch nicht vollständig ausgeschöpft wurden. Insbesondere aus dem Bereich Tissue Engineering können in den nächsten Jahren sicherlich weitere Entwicklungen und Verbesserungen erwartet werden. Und sind auch dringend notwendig. Aber auch über die Pathomechanismen, die Aetiologie und den Krankheitsverlauf ist viel zu wenig bekannt. Im Laufe dieser Arbeit wurden diese „schwarzen Wissenslöcher" immer grösser. Und auch wenn die vorliegende PhD-Arbeit versuchte einigen dieser Fragen nachzugehen, so bleiben viele Fragen unbeantwortet.

1) Wir konnten zeigen, dass sich die subchondrale Platte (Grenzlamelle) an die biomechanische Langzeitbelastung anpasst und spezifische Dichteverteilungsmuster zeigt, die mit der Lokalisation von OCL korrelieren.
- Doch wir wissen nicht, welches dieser Dichteverteilungsmuster für eine osteochondrale Verletzung prädisponiert.
- Wir wissen nicht, wie diese Dichteverteilungsmuster oder die osteochondralen Läsionen mit dem Rückfussalignement oder der Beinachsenbelastung in statischer Hinsicht zusammenhängt. Hiermit beschäftigt sich die Dissertation von Carla Bricker unter meiner Betreuung.
- Wir wissen nicht, ob diese Dichteverteilungsmuster mit Gangmustern in der dynamischen Analyse korrelieren.
- Inwieweit diese Dichteverteilungsmuster durch chirurgische Massnahmen (z.B. Korrekturosteotomie) am oberen Sprunggelenk verändert werden können.

2) Wir konnten zeigen, dass das SPECT-CT zum MRI zusätzliche Informationen über Morphologie und Biologie der osteochondralen Läsion zeigt und dies die Therapiewahl des Orthopäden massgeblich beeinflusst.
- Doch wir wissen nicht, ob diese Therapie auch tatsächlich das bessere klinische Resultat zeigt.
- Wir wissen nicht, wie sich das SPECT-CT im Verlauf postoperativ verhält. Hiermit beschäftigt sich die Masterarbeit von Geneviève Hassink.
- Wir wissen nicht, ob andere, nicht Osteoblasten-bezogene Tracer noch weitere Informationen liefern könnten, z.B. Chondroblasten-Tracer, Angiogenese-Tracer.

- Wir wissen nicht, ob ein SPECT-MRI als Fusionsprodukt noch bessere Informationen liefern könnte.

3) Wir konnten zeigen, dass die Konfiguration des Talus radiologisch wenig Variabilität zeigt. Dies könnte die Voraussetzung sein, vorgefertigtes Ersatzgewebe züchten zu können, z.B. tissue engineered Knorpel-Knochen Grafts.

- Doch wir wissen nicht, ob die Gewebe besser durch eine Matrix alleine oder mit einer Zellbesiedelten Matrix versehen werden sollten (Lee et al., 2010).
- Wir wissen nicht, ob Erkenntnisse von kleinen Läsionen auf grosse, das ganze Gelenk betreffende Läsionen (joint-wide Arthrose) und vice versa übertragen werden können. Damit beschäftigt sich die Masterarbeit von Davide Croci.
- Wir wissen nicht, wie die verschiedenen Gewebe idealerweise miteinander gekoppelt werden, um die Funktion der subchondralen Platte erreichen zu können.
- Wir wissen nicht, wie ein solches Konstrukt idealerweise verankert werden sollte, ohne darauf besiedelte Zellen zu zerstören. (Candrian et al., 2009)
- Wir wissen nicht, ob Zellen auf einem solchen Konstrukt (2cm Durchmesser) eine Chance haben, zu überleben, z.B. aufgrund von fehlender Mikrovaskularität, katabolem Gelenksmilieu, Störung der Gelenkshomöostase durch den chirurgischen Eingriff, biomechanische Belastbarkeit des TE-Konstrukts etc.

4) Wir konnten zeigen, dass die Gelenkshomöstase einem Steady State folgte. Durch die Induktion einer Muskelatrophie kam es zu Anpassungsveränderungen in Sehnen, Ligamenten und Menisken (Chondrocyte-like cells).

- Wir wissen zwar, dass Gelenksverletzungen wie osteochondrale Läsionen auch zu Veränderungen wie einer Muskelatrophie führen können (nachgewiesen für OSG-Arthrose (Valderrabano et al., 2007) oder untersucht für ligamentäre OSG-Instabilität (EMG-basierte Masterarbeit von Lukas Ebneter)). Aber wir wissen nicht, inwieweit diese Veränderungen beim Menschen auch reversibel sind.
- Wir wissen nicht, inwieweit eine Veränderung der Gelenkshomöostase auch zu einer Veränderung der Synovialflüssigkeit führt und damit ein kataboles Milieu kreieren kann.
- Obwohl sich diese Modelle im Tiermodell sehr genau messen lassen, wissen wir nicht, ob die Prozesse beim Menschen genau gleich ablaufen. Auch wenn davon ausgegangen werden muss, dass dies beim Menschen analog ist, so fällt doch immer wieder auf, dass das Heilungs- und Regenerationspotential beim Menschen in vieler Hinsicht kleiner ist. Verschiedene Knorpelersatztherapien zeigen bei Tieren viel bessere klinische und histologische Resultate als beim Menschen.

Deshalb steht die Forschung über die osteochondralen Läsionen zum einen, aber auch das Verständnis der Gelenksfunktion (Joint as an Organ) zum anderen erst in den Kinderschuhen. Verbessertes Verständnis kombiniert mit weiteren Meilensteinen in der Gewebsersatzforschung wird hoffentlich dazu beitragen, dass die Therapie von osteochondralen Läsionen am Talus erfolgreicher wird.

5 Literaturverzeichnis

Anderson IF, Crichton KJ, Grattan-Smith T, Cooper RA, Brazier D. Osteochondral fractures of the dome of the talus. J Bone Joint Surg Am. 1989;71:1143-1152.

Archambault J.M., Hart D.A., Herzog W. Response of rabbit Achilles tendon to chronic repetitive loading. Connect Tissue Res. 2001;42: 12-23.

Berndt AL, Harty M. Transchondral fractures (osteochondritis dissecans) of the talus. J Bone Joint Surg Am. 1959;41:988-1020.

Boocock M., McNair P., Cicuttini F., Stuart A., Sinclair T. The short-term effects of running on the deformation of knee articular cartilage and its relationship to biomechanical loads of the knee. Osteoarthritis Cartilage. 2009;17:883-890.

Candrian C, Barbero A, Bonacina E, Francioli S, Hirschmann MT, Milz S, Valderrabano V, Heberer M, Martin I, Jakob M. A novel implantation technique for engineered osteo-chondral grafts. Knee Surg Sports Traumatol Arthrosc. 2009;17:1377-1383.

Couppé C., Kongsgaard M., Aagaard P., Hansen P., Bojsen-Moller J., Kjaer M., Magnusson S.P. Habitual loading results in tendon hypertrophy and increased stiffness of the human patellar tendon. J Appl Physiol. 2008;105:805-810.

Dipaola JD, Nelson DW, Colville MR. Characterizing osteochondral lesions by MRI. Arthroscopy. 1991;7:101-104.

Elias I, Zoga AC, Morrison WB, Besser MP, Schweitzer ME, Raikin SM. Osteochondral lesions of the talus: localization and morphologic data from 424 patients using a novel anatomical grid scheme. Foot Ankle Int. 2007;28:154-161.

Ferkel RD, Zanotti RM, Komenda GA, Sgaglione NA, Cheng MS, Applegate GR, Dopirak RM. Arthroscopic treatment of chronic osteochondral lesions of the talus: long-term results. Am J Sports Med. 2008;36:1750-1762.

Giannini S, Vannini F. Operative treatment of osteochondral lesions of the talar dome: current concepts review. Foot Ankle Int. 2004;25:168-175.

Han S.K., Wouters W., Clark A., Herzog W. Mechanically induced calcium signaling in chondrocytes in situ. J Orthop Res. 2012;30:375-381.

Hart D.A., Achari Y. Alterations to cell metabolism in connective tissues of the knee after ovariohystererctomy in a rabbbit model: are there implications for the post-menopausal athlete? Br J Sports Med. 2010;44:867-871.

Heinemeier K.M., Olesen J.L., Haddad F., Langberg H., Kjaer M., Baldwin K.M., Schierling P. Expression of collagen and related growth factors in rat tendon and skeletal muscle in response to specific contraction types. J Physiol. 2007;582:1303-1316.

Hepple S, Winson IG, Glew D. Osteochondral lesions of the talus: a revised classification. Foot Ankle Int. 1999;20:789-793.

Herzog W., Longino D., Clark A. The role of muscles in joint adaptation and degeneration. Langenbecks Arch Surg. 2003;388:305-315.

Krampla W.W., Newrkla S.P., Kroener A.H., Hruby W.F. Changes on magnetic resonance tomography in knee joints of marathon runners: a 10-year longitudinal study. 2008;37:619-626.

Lee C, Cook JL, Mendelson A, Moioli KE, Yao H, Mao JJ. Regeneration of the articular surface of the rabbit synovial joint by cell homing: a proof of concept study. Lancet. 2010;376:440-448.

Leumann A, Engelhardt M, Greitemann B, Freiwald J, Schmitt H. Begleitverletzungen und Langzeitschäden bei OSG-Instabilität – GOTS Expertenmeeting Spreewald 2012. Sportortho Sporttrauma. 2013; in press.

Leumann A, Longino D, Fortuna R, Leonard T, Vaz MA, Hart DA, Herzog W. Altered cell metabolism in tissues of the knee joint in a rabbit model of Botulinum toxin A-induced quadriceps muscle weakness. Scand J Med Sci Sport. 2012;22:776-782.

Leumann A, Horisberger M, Valderrabano V. Mechano-Biologische Verknüpfung: The joint as an organ-Konzept. Schweiz Z Sportmed Sporttraumatol. 2011a;59:161-164.

Leumann A, Valderrabano V, Plaass C, Rasch H, Studler U, Hintermann B, Pagenstert GI. A novel imaging method for osteochondral lesions of the talus – comparison of SPECT-CT with MRI. Am J Sports Med. 2011b;39:1095-1101.

Leumann A, Wiewiorski M, Egelhof T, Rasch H, Magerkurth O, Candrian C, Schaefer DJ, Martin I, Jakob M, Valderrabano V. Radiographic Evaluation of Frontal Talar Edge Configuration for Osteochondral Plug Transplantation. Clin Anat; 2009;22:261-266.

Leumann A, Plaass C, Pagenstert G, Büttner O, Hintermann B, Valderrabano V. State of the art in der Behandlung osteochondraler Läsionen am Talus. Sportortho Sporttrauma. 2008; 24:84-90.

Loomer R, Fisher C, Lloyd-Smith R, Sisler J, Cooney T. Osteochondral lesions of the talus. Am J Sports Med. 1993;21:13-19.

Luke A.C., Stehling C., Stahl R., Li X., Kay T., Takamoto S., Ma B., Majumdar S. , Link T. High-field magnetic resonsance imaging assessment of articular cartilage before and after marathon running: does long-distance running lead to cartilage damage? Am J Sports Med. 2010;38:2273-2280.

Madry H, Van Dijk CN, Mueller-Gerbl M. The basic science of the subchondral bone. Knee Surg Sports Traumatol Arthrosc. 2010;18:419-433.

Miller B.F., Olesen J.L., Hansen M., Dossing S., Crameri R.M., Welling R.J., Langberg H., Flyvberg A., Kjaer M., Babraj J.A., Smith K., Rennie M.J. Coordinated collagen and muscle protein synthesis in human patella tendon and quadriceps muscle after exercise. J Physiol. 2005; 567:1021-1033.

Millington SA, Li B, Tang J, Trattnig S, Crandall JR, Hurwitz SR, Acton ST. Quantitative and topographical evaluation of ankel articular cartilage using high resolution MRI. J Orthop Res. 2007;25:143-151.

Pan J, Zhou X, Li W, Novotny JE, Doty SB, Wang L. In situ measurement of transport between subchondral bone and articular cartilage. J Orthop Res. 2009;27:1347-1352.

Racunica T.L., Teichtahl A.J., Wang Y., Wluka A.E., English D.R., Giles G.G., O'Sullivan R., Cicuttini F.M. Effect of physical activity on articular knee joint structures in cummunity-based adults. Arthritis Rheum. 2007;57:1261-1268.

Rehann Youssef A., Longino D., Seerattan R., Leonard T., Herzog W. Muscle weakness causes joint degeneration in rabbits. Osteoarthritis Cartilage. 2009;17:1228-1235.

Sullivan B.E., Carroll C.C., Jemiolo B., Trappe S.W., Magnusson S.P., Dossing S., Kjaer M., Trappe T.A. Effect of actue exercise and sex on human patellar tendon structural and regulatory mRNA expression. J Appl Physiol. 2009;106:468-475.

Taranow WS, Bisignani GA, Towers JD, Conti SF. Retrograde drilling of osteochondral lesions of the medial talar dome. Foot Ankle Int. 1999;20:474-80.

Valderrabano V, Miska M, Leumann A, Wiewiorski M. Reconstruction of osteochondral lesions of the talus with autologous spongiosa grafts and autologous matrix-induced chondrogenesis. Am J Sports Med. 2013;41:519-527.

Valderrabano V, Leumann A, Rasch H, Egelhof T, Hintermann B, Pagenstert G. Knee-to-ankle mosaicplasty for the treatment of osteochondral lesions of the ankle joint. Am J Sports Med. 2009;37:105S-111S.

Valderrabano V, Leumann A. What is the best treatment for ankle osteochondral lesions? Chapter 66, pp:464-474. In: Evidence-based orthopaedics. Elsevier. 2008.

Valderrabano V., Nigg B.M., Von Tscharner V., Frank C.B., Hintermann B. J. Leonard Goldner Award 2006. Total ankle replacement in ankle osteoarthritis: an analysis of muscle rehabilitation. Foot Ankle Int. 2007;28:281-291.

Verhagen RA, Maas M, Dijkgraaf MG, Tol JL, Krips R, Van Dijk CN. Prospective study on diagnostic strategies in osteochondral lesions of the talus. Is MRI superior to helical CT? J Bone Joint Surg Br. 2005;87:41-46.

Verhagen RA, Struijs PA, Bossuyt PM, Van Dijk CN. Systematic review of treatment strategies for osteochondral defects of the talar dome. Foot Ankle Clin. 2003;8:233-242.

6 Danksagung

Als Prof. Walter Dick 2008 an mich herantrat und mir vorschlug, einige meiner Forschungsideen im neu angebotenen PhD-Programm für Biomedical Engineering umzusetzen, war es schwierig vorherzusehen, was dies alles bedeuten würde. Doch Prof. Victor Valderrabano begleitete und führte mich als Supervisor von A-Z durch das gesamte Projekt, öffnete Türen, gab mir Freiheiten im Klinikbetrieb und ermöglichte mir so, die Arbeit voranzutreiben. Ihm gebührt ein ganz grosses Dankeschön!

Meine experimentellen Arbeiten durfte ich im Labor von Frau Prof. Magdalena Müller-Gerbl, welche meine Arbeit auch als Co-Supervisorin betreute, und in Calgary bei Prof. Walter Herzog absolvieren. An beiden Orten wurde ich in verschiedene biomechanische Forschungsmethoden eingeführt und erhielt die Möglichkeit, diese mit eigenen Ideen anzupassen und umzusetzen. Hierfür möchte ich mich sehr herzlich bedanken.

Bei den externen Gutachtern, Prof. Stefan Nehrer und Prof. Peter Federolf, möchte ich mich für Ihre Unterstützung und Ihr Wohlwollen herzlich bedanken.

Als ich 2012 längere Zeit krank war, war unklar, ob ich dieses PhD –Projekt je werde fertigstellen können. Doch meine Betreuer und Mentoren haben immer an mich geglaubt und mir die notwendige Zeit gegeben. Ich weiss dies nicht hoch genug einzuschätzen! Vielen Dank!

Viele verschiedene Personen haben weiter dazubeigetragen: Roger Kurz, Peter Zimmermann, Tim Leonard, Rafael Fortuna, Mireille Toranelli, David Hart, Corinne Wiederkehr, Hoa Nguyen, Azim Jinha, Olaf Büttner, Martin Wiewiorski und viele mehr. Danke vielmals! Thank you! Merci beaucoup!

Zuletzt, doch am allerwichtigsten, steht der Dank an meine Frau Anke und meine Kinder Valentin und Dominic, ohne deren Unterstützung diese Arbeit nie möglich gewesen wäre! Ich liebe Euch über alles!

7 Schriftliche Erklärung

Ich erkläre, dass ich die Dissertation

Osteochondrale Läsionen am Talus: Anatomische, biomechanische und klinische Analyse

nur mit der darin angegebenen Hilfe verfasst und bei keiner anderen Universität und keiner anderen Fakultät der Universität Basel eingereicht habe.

Ich bin mir bewusst, dass eine unwahre Erklärung rechtliche Folgen haben kann.

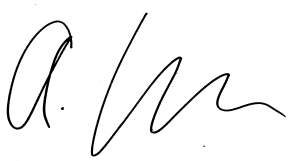

Basel, 28. Juli 2013 André Leumann

8 Anhang

8.1 Auszeichnungen

Mehrere dieser Arbeiten wurden prämiert:

Dirk-Schäfer Forschungspreis 2012 für die am höchsten publizierte Forschungsarbeit des Departements Chirurgie der Universität Basel im Jahre 2011. (Artikel 3.2)

1. Preis der Schweizerischen Gesellschaft für Sportmedizin (SGSM) für die beste wissenschaftliche Arbeit am Jahreskongress 2009. (Artikel 3.4)

3. Posterpreis der Gesellschaft für orthopädisch-traumatologische Sportmedizin (GOTS) am Jahreskongress 2008 (Artikel 3.3)

8.2 Zusätzliche Publikationen

Aufgrund meiner wissenschaftlichen Arbeiten zum Thema „Osteochondrale Läsionen am Talus“ und meiner Forschungsaufenthalte im Anatomischen Institut der Universität Basel und im Human Performance Laboratory der Universität Calgary, Canada, sowie meiner wissenschaftlichen Tätigkeit im Rahmen meiner klinischen Arbeit auf der Orthopädischen Klinik am Universitätsspital Basel sind zusätzliche Arbeiten entstanden, welche hier der Vollständigkeit halber aufgeführt werden. Die Vorträge an Kongressen sind ca. 25 an der Zahl und beinhalten sowohl an Kongressen eingereichte und akzeptierte Vorträge als auch Vorträge auf Einladung des Veranstalters.

Peer-reviewed Originalarbeiten

Anatomie

Histomorphometric, CT Arthrographic, and Biomechanical Mapping of the Human Ankle. Buettner O, **Leumann A,** Lehner R, Dell-Kuster S, Rosenthal R, Mueller-Gerbl M, Valderrabano V.
Foot Ankle Int. 2013 PMID:23396179

Micro CT analysis of the subarticular bone structure in the are of the talar trochlea. Nowakowski AM, Deyhle H, Zander S, **Leumann A,** Müller-Gerbl M.
Surg Radiol Anat 2013 PMID:23307423

Computer tomographic evaluation of talar edge configuration for osteochondral graft transplantation.
Wiewiorski M, Hoechel S, Wishart K, **Leumann A,** Müller-Gerbl M, Valderrabano V, Nowakowski AM.
Clin Anat 2013;25:773-780.

Biomechanik

Dynamic in-vivo force transfer in the lapine knee loaded by quadriceps muscle contraction
Leumann A, Fortuna R, Leonard T, Valderrabano V, Herzog W.
Clin Biomech 2013 PMID:23312211

Computed tomography analysis of knee pose and geometry before and after total knee arthroplasty.
Ho KC, Saevearsson SK, Ramm H, Lieck R, Zachow S, Sharma GB, Rex EL, Amiri S, Wu BC, **Leumann A,** Anglin C.
J Biomech 2013;45:2215-2221.

A novel method for determining articular cartilage chondrocyte mechanics in vivo.
Abusara Z, Seerattan R, **Leumann A,** Thompson R, Herzog W.
J Biomech 2011;44:940-934.

Klinik

Reconstruction of osteochondral lesions of the talus with autologous spongiosa grafts and autologous matrix-induced chondrogenesis
Valderrabano V, Miska M, **Leumann A,** Wiewiorski M.
Am J Sports Med 2013;41:519-527.

Knee-to-ankle mosaicplasty fort he treatment of osteochondral lesions of the ankle joint.
Valderrabano V, **Leumann A,** Rasch H, Egelhof T, Hintermann B, Pagenstert G.
Am J Sports Med 2009;37:105S-111S.

8.3 Weitere Arbeiten

Übersichtsarbeiten

Mechano-Biologische Verknüpfung: The joint as an organ-Konzept.
Leumann A, Horisberger M, Valderrabano V.
Schweiz Zeitschrift Sportmed Sporttraumatol 2011;59:161-164.

Osteochondrale Läsionen am Talus im Sport
Wiewiorski M, **Leumann A**, Pagenstert G, Valderrabano V.
Schweiz Zeitschrift Sportmed Sporttraumatol 2011;59:174-179.

Osteochondral Lesions of the Talus – Etiology, Pathomechanisms, and Classifications.
Horisberger M, **Leumann A,** Walcher M, Pagenstert GI, Valderrabano V.
Tech Foot Ankle Surg. 2011;10:134-138.

Computertomography/Robot-assisted retrograde drilling of osteochondral lesions of the ankle joint.
Wiewiorski M, **Leumann A,** Pagenstert GI, Frigg A, Valderrabano V.
Tech Foot Ankle Surg. 2011;10:139-143.

Autologous Tissue-engineered osteochondral graft for talus osteochondral lesions: state-of-the-art and future perspectives.
Scotti C, **Leumann A,** Candrian C, Barbero A, Croci D, Schaefer D, Jakob M, Valderrabano V, Martin I.
Tech Foot Ankle Surg. 2011;10:163-168.

Autologous Matrix-induced Chondrogenesis-aided repair of osteochondral lesions of the talus.
Valderrabano V**, Leumann A,** Frigg A, Pagenstert GI, Wiewiorski M.
Tech Foot Ankle Surg. 2011;10:159-162.

SPECT-CT: Diagnostik im Zusammenspiel von Morphologie und Biologie.
Leumann A, Pagenstert G, Wiewiorski M, Pansini M, Valderrabano V.
Sportortho Sporttrauma. 2011;26:152-157.

State of the art in der Behandlung osteochondraler Läsionen am Talus.
Leumann A, Plaass C, Pagenstert G, Büttner O, Hintermann B, Valderrabano V.

Sportortho Sporttrauma. 2008; 24:84-90.

Fallberichte (Peer-reviewed)

Autologous matrix-induced chondrogenesis aided reconstruction of a large focal osteochondral lesion of the talus
Wiewiorski M, **Leumann A,** Buettner O, Pagenstert G, Horisberger M, Valderrabano V.
Arch Orthop Trauma Surg 2011;131:293-296.

CT-gesteuerte roboter-assistierte retrograde Anbohrung osteochondraler Läsionen des oberen Sprunggelenks.
Wiewiorski M, Jacob AL, Rasmus M, Buettner O, **Leumann A,** Kretzschmar K, Rasch H, Markus T, Dziergwa S, Bilecen D, Valderrabano V.
Sportortho Sporttrauma 2009;25: 280-5.

Buchkapitel

Mosaicplasty with bone-periosteum graft from the iliac crest.
Leumann A, Valderrabano V, Kilger R, Plaass C, Pagenstert P, Hintermann B.
Buchkapitel in „AAOS Techniques in F&A". AAOS. 2009

Osteochondrale Läsionen am Sprunggelenk.
Leumann A, Pagenstert G, Valderrabano V.
Buchkapitel (9.3.7) in „Essentials in Orthopädie", Editoren: Ruchholtz S, Wirtz DC. Thieme Verlag. 1. Auflage 2010, 2. Auflage 2013

Knorpelverletzungen und osteochondrale Läsionen
Leumann A, Büttner O, Valderrabano V
Buchkapitel in „Fuss und Sport"; Editoren: Valderrabano V, Engelhardt M, Küster HH. Deutscher Ärzteverlag 2009.

What is the best treatment for ankle osteochondral lesions
Valderrabano V**, Leumann A**
Buchkapitel in „Evidence-based Orthopaedics". Elsevier 2009.

Curriculum vitae

Leumann, André Georges

Date of birth: February 14th, 1978
Nationality: Swiss
Marital status: married to Dr. Anke Leumann-Runge PhD MBA
Children: Valentin (2010), Dominic (2011), and Marius (2013)

Mail Address:

Private
Chrischonastr. 19
79540 Lörrach, Germany
leumanna@uhbs.ch
Mobile: +4179 657 4168

Hospital
Orthopaedic Department
University Hospital of Basel
4031 Basel, Switzerland
leumanna@uhbs.ch
Call-Center: +4161 265 2525

Language: German (Mother tongue), English and French (fluent)

Diploma

- 2011 **Medical Board Licence Orthopaedics and Traumatology**
  Swiss Society for Orthopaedics and Traumatology (SGOT)
- 2011 **Medical Board Licence Sports Medicine**
  Swiss Society for Sports Medicine (SGSM)
- 2013 **Medical Board Licence Internventional Pain Management**
  Swiss Society for Interventional Pain Management (SSIPM)
- 2006 **Medical Doctor Thesis, University of Basel**
  „Chronic Ankle Instability in the Swiss Orienteering National Team“,
- 2014 **Philosophical Doctor Thesis Biomedical Engineering, University of Basel**
  „Osteochondral Lesions of the Talus: Anatomical, biomechanical and clinical analysis“
  Prof. V. Valderrabano MD PhD, Prof. M. Müller-Gerbl MD

Current Positions

- Since 01/2011 **Oberarzt, Orthopaedic Department, University Hospital of Basel**
  Team Leader for Sports Orthopaedics
- Since 06/2012 **Executive Board, Gesellschaft für orthopädisch-traumatologische Sportmedizin GOTS)**
- Since 10/2011 **Executive Board, Swiss Society of Sports Medicine (SGSM)**
- Since 10/2007 **Team Physician, Swiss Orienteering National Team**

Education

- 1998-2994 **Medical School University of Berne, Switzerland**
- 07/1998 **Swiss Entry Exam for the Medical School**
- 1993-1998 **High School, Kreuzlingen, Switzerland** (Type B, with latin)

Orthopaedic, Traumatologic and Sports Medicine Training

- 07-12/2012 **Oberarzt, Department of Traumatology, University Hospital of Basel**
  Prof. M. Jakob MD
- 07/2005 - 12/2010 **Resident Orthopaedic Surgery**
  University Hospital of Basel
  Prof. W. Dick MD, Prof. B. Hintermann MD, Prof. V. Valderrabano MD PhD
- 01-12/2009 **Post-doctoral fellow, Human Performance Laboratory**
  Faculty of Kinesiology, University of Calgary (Canada)
  Prof. W. Herzog PhD
- 07/2008- 12/2008 **Scientific Post-doctoral researcher, Institute of Anatomy**
  Department of Biomedicine, University of Basel (Switzerland)
  Prof. M. Müller-Gerbl MD
- 07/07-06/08 **Traumatology and Orthopaedics, Hospital of Davos (Switzerland)**
- 01-06/2007 **Pediatric Orthopaedics, Children University Hospital of Basel**
- 01-06/2005 **Resident General Surgery, Regional Hospital Thun**

Awards

- 11/2012 **Dirk Schäfer Forschungspreis**
- 06/2011 **Michael Jaeger Preis 2011, 2nd prize**
- 06/2011 **GOTS Best paper 2011, 2nd prize**
- 10/2009 **SGSM Poster Award 2009, 1st prize**
- 02/2009 **Novartis Research Foundation – Scholarship**
- 11/2008 **SNF Scholarship Swiss National Foundation 2009**
- 10/2008 **Research Grant of the Swiss Orthopaedic Society (SGOT)**
- 06/2008 **GOTS Poster Award 2008, 3rd prize**
- 06/2007 **GOTS Young Investigators Award 2007, 3rd prize**
- 12/2006 **Research Grant of the Swiss Federal Council of Sports 2007-2009**
- 05-06/2006 **GOTS Traveling Fellowship South Korea / Japan**
- 10/2005 **EFSMA Young Investigators Award**

Basel, February 20th 2014

Dr. André Leumann